Molecular Architecture of the Octopus bimaculoides Central Nervous System

by

Jeremea Ocampo Songco

A dissertation accepted and approved in partial fulfillment of the

requirements for the degree of

Doctor of Philosophy

in Biology

Dissertation Committee:

Dr. Chris Q. Doe, Chair

Dr. Cristopher M. Niell, Advisor

Dr. Adam C. Miller, Core Member

Dr. Emily L. Sylwestrak, Core Member

Dr. Matthew C. Smear, Institutional Representative

University of Oregon

Summer 2024

DISSERTATION ABSTRACT

Jeremea Ocampo Songco

Doctor of Philosophy in Biology

Title: Molecular Architecture of the Octopus bimaculoides Central Nervous System

Interacting with our environments requires that we appropriately integrate sensory information and convert these inputs into a perception of our surroundings to generate basic and complex behaviors. Traditionally, model organisms, such as nematodes, flies, zebrafish, or even mice, have been used in the laboratory setting to investigate neural circuit formation and function. While these organisms have furthered our understanding of how different cell types wire up to drive complex behavior, there is much to be learned from exploring the brain of non-traditional organisms.

Cephalopods have the largest brain among invertebrates and have a rich catalog of behaviors, including navigating complex underwater environments and rapid body-patterning known as camouflage. While seminal work during the 1960s revealed cellular properties of neurons using the giant squid axon, recent advancements in technology have permitted further characterization of cell types and circuits in a species that is unlike many of those used traditionally in the field of neuroscience. By investigating the brain of these animals, we can begin to understand fundamental mechanisms involved in the formation and function of complex neural circuits.

Unlike model organisms, there are limited tools in genetic manipulation and the field has yet to produce a comprehensive brain atlas bridging anatomical, molecular, and functional properties of cell types in these animals. Therefore, my dissertation sought to develop key resources that will serve as a foundation for such studies once it becomes technically possible. I first contributed to the optimization and usage of functional imaging in an ex vivo preparation of the octopus brain in order to characterize response properties of visually responsive cells in the optic lobe, the main visual center which is a paired brain region that comprises 2/3 of the central nervous system of octopuses. We found evidence for retinotopic organization of responses to light (ON) and dark (OFF) spots, including spatial tuning properties that may be suggestive of

environmental demands.

To begin elucidating the diversity of unit responses we revealed in this initial study, I focused on developing a single-cell molecular atlas of the *Octopus bimaculoides* optic lobe by combining single cell RNA-sequencing (scRNA-seq) with multiplexed fluorescence in situ hybridization (FISH). We identified six classes of mature neuronal cell types in addition to a large population of immature neurons. Our FISH revealed sublaminar organization across the optic lobe, further characterizing the cell types that were initially identified in the 1960s based on morphology. An octopus' ability to engage in a wide range of visually guided behaviors rests upon the various inputs and outputs the optic lobes have to other structures in the central nervous system. However, there has yet to be published a mapping of these structures as well as an in-depth understanding of the molecular landscape across the central nervous system. Therefore, I sought to develop the first brain-wide gene expression resource for cephalopods by characterizing all of the structures in this species through Hematoxylin & Eoisin (H&E) staining of serial sections of the brain, and I quantified expression for 40 genes, including functional and developmental determinants, across 20 identified brain regions. Together, this work reveals functional and molecular organization in the optic lobe as well as other brain regions, furthering our understanding of how a completely different organism can carry out complex behaviors.

This dissertation includes previously published and unpublished co-authored material.

CURRICULUM VITAE

NAME OF AUTHOR: Jeremea Ocampo Songco-Casey

GRADUATE AND UNDERGRADUATE SCHOOLS ATTENDED:

University of Oregon, Eugene
San Diego State University, San Diego, California

DEGREES AWARDED:

Doctor of Philosophy, Biology, 2024 University of Oregon
Master of Science, Biology, 2021 University of Oregon
Bachelor of Arts, Psychology, 2018 San Diego State University

AREAS OF SPECIAL INTEREST:

Neuroscience
Molecular Biology
Developmental Neurobiology

PROFESSIONAL EXPERIENCE:

Graduate Researcher, University of Oregon, 2018-24
Laboratory of Dr. Cristopher Niell

Graduate Teaching Assistant, University of Oregon, 2018-20

Undergraduate Research Assistant, San Diego State University, 2015-18
Laboratory of Dr. Claire Murphy

Summer Undergraduate Research Assistant, University of Washington, 2017
Laboratory of Dr. David Gire

GRANTS, AWARDS, AND HONORS:

NIH BRAIN Initiative Grant Diversity Supplement, University of Oregon, 2021-23
National Institutes of Health, Brain Research Through Advancing Innovative Neurotechnologies Initiative

Science Coalition's "Fund It Forward" Student Video Challenge Winner, 2022

Department of Biology Diversity, Equity, & Inclusion Grant, submitted on behalf of Womxn in Neuroscience, Anti-Racism Training, University of Oregon, 2021

ARCS Scholar Award, University of Oregon, 2018-21
Achievement Rewards for College Scientists, Oregon Chapter

HHMI Gilliam Fellowship Nomination, University of Oregon, 2020
Howard Hughes Medical Institute

Graduate Research Fellowship Program Honorable Mention, University of Oregon, 2020
National Science Foundation

WiN Scholarship, University of Oregon, 2019
Womxn in Neuroscience

CMiS Travel Award, University of Oregon, 2019
A Community for Minorities in STEM

Promising Scholars Award, University of Oregon, 2018

Maximizing Access to Research Careers Scholar, San Diego State University, 2016-18
Funded by the National Institutes of General Medical Science

SACNAS Travel Award, San Diego State University, 2016
Society of Advancing Chicanos/Hispanics and Native Americans in Science

Cox Cares Scholarship, San Diego State University, 2014-15
Funded by the San Diego Scholarship Foundation

Lehman Family Scholarship, San Diego State University, 2014-15
Funded by the San Diego Scholarship Foundation

PUBLICATIONS:

Coffing, G. C., Tittes, S., Small, S. T., **Songco-Casey, J. O.**, Piscopo, D. M., Pungor, J. R., Miller, A. C., Niell, C. M., & Kern, A. D. (2024). Cephalopod Sex Determination and its Ancient Evolutionary Origin Revealed by Chromosome-level Assembly of the California Two-Spot Octopus. bioRxiv.

Pungor, J.R., Allen, V.A., **Songco-Casey, J.O.**, and Niell, C.M. (2023). Functional organization of response properties in the octopus optic lobe. Curr. Biol. *33*, 2784-2793.e3.

Baden, T., Briseño, J., Coffing, G., Cohen-Bodénès, S., Courtney, A., Dickerson, D., Dölen, G., Fiorito, G., Gestal, C., Gustafson, T., Heath-Heckman, E., Hua, Q., Imperadore, P., Kimbara, R., Król, M., Lajbner, Z., Lichilín, N., Macchi, F., McCoy, M. J., … **Songco-Casey, J.O.**, … Albertin, C. B. (2023). Cephalopod-omics: Emerging Fields and Technologies in Cephalopod Biology. Integrative And Comparative Biology, 63(6), 1226–1239.

Songco-Casey, J.O., Coffing, G.C., Piscopo, D.M., Pungor, J.R., Kern, A.D., Miller, A.C., and Niell, C.M. (2022). Cell types and molecular architecture of the Octopus bimaculoides visual system. Curr. Biol. *32*, 5031–5044.e4.

Findley, T. M., Wyrick, D. G., Cramer, J. L., Brown, M. A., Holcomb, B., Attey, R., Yeh, D., Monasevitch, E., Nouboussi, N., Cullen, I., **Songco, J. O.**, King, J. F., Ahmadian, Y., & Smear, M. C. (2021). Sniff-synchronized, gradient-guided olfactory search by freely moving mice. eLife, 10, e58523.

ACKNOWLEDGMENTS

I would like to express sincere appreciation to Dr. Cristopher Niell for his mentorship and guidance on the work presented in this dissertation. His enthusiasm for science and out-of-the-box thinking has been inspiring to witness and learn from. His encouragement to pursue the "weird" questions in science played a large role in cultivating my curiosity about the brain and is a major factor for why cephalopod neuroscience will always hold a special place in my heart.

I am equally thankful to Dr. Adam Miller. Our 1:1 meetings were truly impactful, especially earlier on in my career, as he helped me understand what I know and what I don't know in the fields of molecular and developmental biology. He imparted wisdom onto me—both with respect to scientific projects and outside. He is truly dedicated to the growth of trainees in and outside of his lab in a way I hope to emulate in the next stages of my career as well.

I extend deep gratitude to my DAC as a whole – Dr. Chris Doe, Dr. Cristopher Niell, Dr. Adam Miller, Dr. Emily Sylwestrak, and Dr. Matt Smear. They challenged me in ways that allowed me to grow as a rigorous and detail-oriented scientist earlier on. They provided a welcoming space for cultivating both personal and professional growth and were supportive in all of my endeavors.

To members of the Niell Lab – past and present: I am sincerely grateful for all of the mentorship and support I received from you all, in and outside of lab. Despite entering the ION program as a cohort of 1, all of you were quick to welcome me into the lab and helped me feel like part of the community. To Dr. Denise Niell, without you, I would not have learned as much as I did about molecular biology. Your rigorous approach to research has critically taught me to become a better scientist as well. I especially need to thank Dr. Angie Michaiel, Dr. Elliot Abe and Dr. Philip Parker, who have provided endless support for my research and professional goals and continue to do so to this day. Thank you all for being excellent mentors and friends.

I wish to express my sincere appreciate to many of my peers within the graduate program, including Dr. Rachel Lukowicz Bedford, Alyssa Quiogue, and Lucy Moholt-Siebert. In each of you, I have found unwavering support and scientific inspiration. Your approaches to research and mentoring have shown me alternate ways of thinking and inspired creativity in my work as a result. Thank you for accepting me.

I am also thankful for the friends I've kept and made during the last six years. Despite our varied interests, I am grateful for the friends I have in San Diego. Equally so, I am thankful for the friends I've made since starting grad school, especially those who have served as examples for science advocacy. Despite not being at the same institution and having only met briefly, each of you were impactful on my journey to graduating.

I would also like to thank peers I've met outside of the program – specifically, those that I played soccer alongside as well as those that I've had the pleasure to learn from while at Thermo Fisher Scientific for an internship. All of my soccer teammates have provided a much-needed reprieve from science when experiments weren't going as planned. To the friends I've made through my internship: thank you for welcoming me and relying on me as one of your own. I grew so much in my short time at Thermo Fisher Scientific and gained both technical and organizational skills in my experience. To Dr. Scott Clarke and Dr. Leticia Montoya: thank you for teaching me to be a better and more efficient scientist. I am especially grateful to Dr. Alexia Bachir. Your trust in me reminded me of how capable I am, and your mentorship leaves a lasting impact on me.

To the MARC program at SDSU: this is where the journey started, and I need to share my deep gratitude for the support I received from all of my peers and mentors in the program. Thank you for supporting my goals then and now. To the ARCS Foundation, thank you for believing in my ability to be a great scientist even before meeting me. I am especially grateful for Caron, Larry, and Lara, whom I have grown close to over the last six years and always feel supported by in my research and professional goals.

Lastly, I would like to thank the University of Oregon G3 Core, Imaging Core, including Adam Fries and Leah DeBlander, and histology support provided by Dr. Poh-Keng Loi and Brandon Wiskow, and the Marine Biological Laboratories for our animals. I acknowledge support by the ARCS Foundation and University of Oregon Promising Scholars Award. The investigations outlined in this dissertation were supported in part by the National Institutes of Health Brain Research Through Advancing Innovative Neurotechnologies Initiative R01NS118466-01S1 as well as from the following grants to Dr. Cristopher Niell (NIH R01NS118466-01, Office of Naval Research N00014-21-1-2426) and jointly to Dr. Cristopher Niell and Dr. Adam Miller (University of Oregon Renee James Seed grant).

DEDICATION

This work is dedicated to my loving family and husband.

To my parents, Federico and Eva Songco: thank you for teaching me the value of education when I was still young; for reminding me that an education is a privilege – one that cannot be taken away once you've obtained it. The sacrifices you made to come to the United States and give us a better life do not go unnoticed, and I am proud to be your daughter.

To my sisters, Ferjea Sahagun and Redjean Songco: thank you for being sisters by blood, best friends by choice. Thank you for your support in this journey and for reminding me of my best qualities during the roughest of times.

To my late grandma, Clarita Ocampo. Memories of your selflessness, happiness, and strength inspire me to remain resilient, light, and hopeful. Thank you for guiding me from afar.

To my husband, Nathan Michael Casey: I am at this finish line because of you. Thank you for believing in me from the beginning, for making my life easier, and for all of the sacrifices you've made to support me in this goal. Your strength, resilience, and wisdom inspire me to be better, every day. Your unconditional love fuels me. Thank you for being a light in my life.
I am here because of you.

To our boys: I am thankful to have had the opportunity to spend these last few months with each of you. Theo Alexander, you will always be in our hearts. Baby A, thank you for the little taps reminding me I have you keeping me company while writing. We can't wait to meet you soon.

LIST OF FIGURES

LIST OF TABLES

Table Page

CHAPTER I
INTRODUCTION

The ability to interact with our rich environments requires that our brain convert sensory information into a perception of our surroundings. Tasks we likely engage in every day without giving it a single thought utilize rapid computations carried out by intricate neural circuits shaped by our biology and our experiences. To understand how these basic and complex behaviors are carried out, it is critical to understand the components that contribute to their underlying circuitry.

Often, investigations into neural circuit formation and function utilize traditional model organisms, which are defined by their short, closed lifespan, ability to reproduce many offspring and generations, and the availability of genetic tools[1]. Through using model organisms in the laboratory setting, we have learned about critical features of neural circuits – from development to function, behavior, and, even, pathology (Reviewed in[2–6]). However, investigating different embodiments of advanced neural processing can facilitate our understanding of the fundamentals of how these circuits form and function, therefore elucidating, for simplicity's sake, "how to build a complex brain". Due to their large brains, complex nervous systems, and advanced behaviors, cephalopods are an intriguing emerging model system for expanding our understanding of how a completely different brain executes dynamic computations.

Octopus Brains as a Model for Understanding Complexity

Cephalopods, which includes squid, cuttlefish, and octopuses, have the largest brain among invertebrates[7–10], with their central nervous system—as well as each of their arms—serving as a rich network of neuronal communication[11]. The cephalopod central nervous system is located at the base of the mantle, between the eyes of the animal (Figure 1). It is characterized by two masses, one that sits above the esophagus, termed the supraesophageal mass (SEM), while the other sits right below the esophagus (subesophageal mass; SUB)[11]. These masses are in between the two large optic lobes, which comprise ⅔ of the entire central nervous system and are considered to be the main visual processing areas[12,13]. In reference to the body-axis, the SEM is

considered dorsal and contains brain areas responsible for mantle control and regulation of visceral organs, whereas the SUB is ventral and comprises brain areas responsible for controlling the arms[14–16].

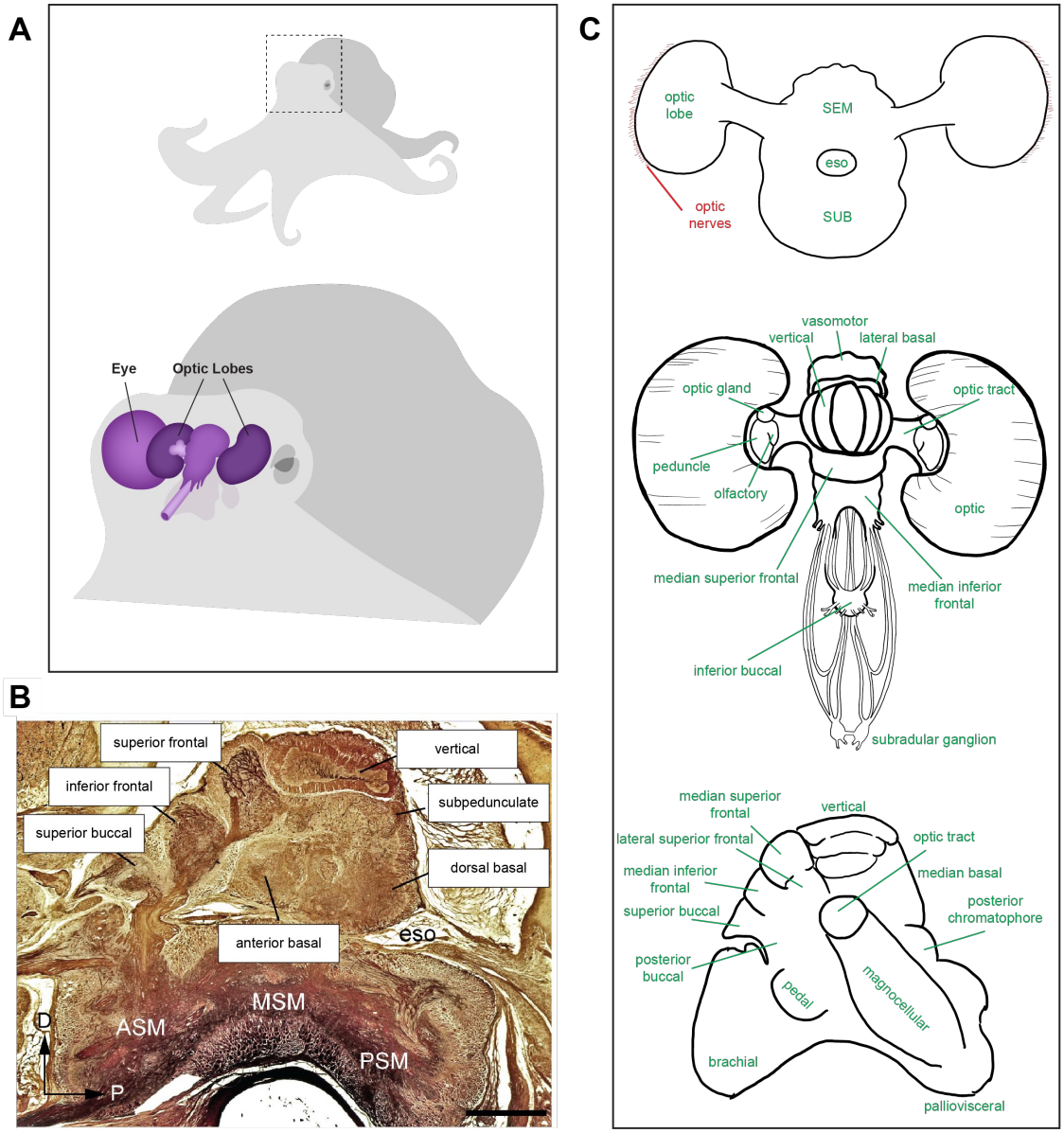

Figure 1. Overview of cephalopod brain anatomy organization.
A) Location and 3D rendering of major structures in the Octopus brain.
B) Sagittal section displaying lobes of the SEM and SUB, from [17].
C) Diagram of major structures in the octopus brain, viewed from the front. Modified from [18] (top). Diagram of octopus brain organization seen from above, adapted from [11] (middle). Diagram of central nervous system lobes in octopus, viewed from the right side (bottom). Adapted from [11].

The cephalopod nervous system contains approximately 25 differentiated lobes which can be grouped into systems based on their specialized functions[10,11,17,19,19–22,22–25,25]. In octopuses, these functional systems are: 1) learning and memory (vertical and superior frontal lobe), 2) chemosensory and tactile learning and memory (inferior frontal lobe), visual processing (optic lobes), lower visuo-motor control (peduncle lobes), higher motor control for sensory processing and behavior (SEM), and lower motor control for funnel, arm, and mantle movement (SUB). From hatching to adulthood, the number of neurons in the central brain grow exponentially from 200,000 to 200 million[26,27], with morphological changes in the brain reflecting their adaptive behavior[28].

For example, the vertical and subvertical lobes are part of tactile and visual learning[11] and increases from hatching to adult, and the subfrontal lobe, which is involved in tactile learning[29] also increases in size from hatching to juvenile and adult, reflecting the growth and usage of the arms. The optic lobes remain the largest structures of the central nervous system and, while it continues to grow through the lifespan of the animal, at hatching its parts and organization resemble what would be expected in the adult[13]. At hatching, the anterior basal and peduncle lobes, both of which fall within the cerebellum-like visuo-motor control functional system, are proportionally larger, given demands for prey capture along the water column. Specifically, the anterior basal regulates posture and movement of head and eyes while swimming[11], while the peduncle lobes are involved in locomotion based on visual cues[11,23]. In the SUB, the buccal lobe, which is involved in prey capture and feeding[30] and grows from 8% of total volume of the hatching to 18% in the adult as it is involved in lower motor control of the arms[28], while the chromatophore lobes are not differentiated at hatching[31], despite forming 5% of total brain volume in later development, similar to what has been described as a "metamorphosis"[32–34].

Like vertebrates, octopuses utilize many visually guided behaviors in their everyday life, such as navigating their environments and engaging in prey capture and predator avoidance (Reviewed in [35]). Octopus vision is often referred to as a textbook example of convergent evolution, since both vertebrates and octopuses developed camera-type eyes[36–38], which focus light through a lens onto a layer of cells called the retina[13,39], despite these two lineages diverging over 500 million years ago. Uncannily, the anatomical resemblances of their camera eye propagate to the cellular

level as well—to the extent that the term "deep retina" was coined by Santiago Ramon y Cajal in reference to the octopus visual system. While the morphology and presumed synaptic connections, based on histology, of the octopus central nervous system has been described[11,13], technical limitations have prevent a thorough deconstruction of other critical features that define neural circuits in the octopus visual system and across the rest of their brain.

Goals of Dissertation

In this dissertation, I will describe the work that I have done to characterize the functional identities of cells in the octopus visual system as well as the molecular architecture of the entire octopus central nervous system. In Chapter II, I will describe a protocol established to obtain the first calcium-evoked unit responses from the octopus visual system by applying two-photon imaging on an ex vivo preparation of the brain. We found evidence of retinotopic organization of responses to light (ON) and dark (OFF) spots as well as identified spatial tuning properties to ON and OFF that may be suggestive of environmental demands. In Chapter III, I will characterize the molecular identities of cells found in the octopus visual system by combining single cell RNA-sequencing (scRNA-seq) with multiplexed RNA fluorescence in situ hybridization (FISH) of top differentially expressed genes from each of the cell type clusters. We identified six major cell classes based on neurotransmitter and neuropeptide usage as well as a large population of immature neurons, which is unsurprising given that the octopus brain continues to grow throughout its lifespan. In Chapter IV, I expand our understanding of molecular architecture beyond the visual areas of the octopus brain by analyzing gene expression across each of the lobes found in the central nervous system. We generate the first mapping of brain organization in this species using serial sections stained with Hematoxylin & Eoisin (H&E), and we further characterize these regions by performing RNA FISH on 40 genes, including classical neurotransmitters, neuropeptides, and developmental markers. As a result, we produce the first brain-wide gene expression mapping in octopuses. Together, this work reveals an initial account of functional response properties and molecular identities in the octopus visual system and across the central nervous system, providing a foundation for future studies to bridge anatomical, molecular, and functional characteristics of neural circuits in cephalopods.

References

1. Ankeny, R.A., and Leonelli, S. (2011). What's so special about model organisms? Stud. Hist. Philos. Sci. Part A *42*, 313–323. https://doi.org/10.1016/j.shpsa.2010.11.039.

2. Kandel, E.R. (2001). The Molecular Biology of Memory Storage: A Dialogue Between Genes and Synapses. Science *294*, 1030–1038. https://doi.org/10.1126/science.1067020.

3. Churchland, A., and Lisberger, S. (2015). Contributions from different model organisms to brain research: Introduction. Neuroscience *296*, 1–2. https://doi.org/10.1016/j.neuroscience.2015.03.058.

4. Jeibmann, A., and Paulus, W. (2009). Drosophila melanogaster as a Model Organism of Brain Diseases. Int. J. Mol. Sci. *10*, 407–440. https://doi.org/10.3390/ijms10020407.

5. Joshua, M., and Lisberger, S.G. (2015). A tale of two species: Neural integration in zebrafish and monkeys. Neuroscience *296*, 80–91. https://doi.org/10.1016/j.neuroscience.2014.04.048.

6. Bollmann, J.H. (2019). The Zebrafish Visual System: From Circuits to Behavior. Annu. Rev. Vis. Sci. *5*, 269–293. https://doi.org/10.1146/annurev-vision-091718-014723.

7. Packard, A. (1972). CEPHALOPODS AND FISH: THE LIMITS OF CONVERGENCE. Biol. Rev. *47*, 241–307. https://doi.org/10.1111/j.1469-185x.1972.tb00975.x.

8. Williamson, R., and Chrachri (2004). Cephalopod neural networks. Neurosignals *13*, 87–98. https://doi.org/10.1159/000076160.

9. Budelmann, B.U. (1995). The cephalopod nervous system: What evolution has made of the molluscan design. In The Nervous Systems of Invertebrates: An Evolutionary and Comparative Approach Experientia Supplementum., O. Breidbach and W. Kutsch, eds. (Birkhäuser Basel), pp. 115–138. https://doi.org/10.1007/978-3-0348-9219-3_7.

10. Nixon, M., and Young, J.Z. (2003). The brains and lives of cephalopods (Oxford University Press).

11. Young, J.Z. (1971). The anatomy of the nervous system of Octopus vulgaris (Clarendon Press).

12. Hanlon, R.T., and Messenger, J.B. (2008). Cephalopod behaviour 6. print. (Cambridge University Press).

13. Fernald, R.D. (2006). Casting a Genetic Light on the Evolution of Eyes. Science *313*, 1914–1918. https://doi.org/10.1126/science.1127889.

14. Yoshida, M., and Ogura, A. (2011). Genetic mechanisms involved in the evolution of the

cephalopod camera eye revealed by transcriptomic and developmental studies. BMC Evol. Biol. *11*, 180. https://doi.org/10.1186/1471-2148-11-180.

15. Yoshida, M.A., Ogura, A., Ikeo, K., Shigeno, S., Moritaki, T., Winters, G.C., Kohn, A.B., and Moroz, L.L. (2015). Molecular Evidence for Convergence and Parallelism in Evolution of Complex Brains of Cephalopod Molluscs: Insights from Visual Systems. Integr. Comp. Biol. *55*, 1070–1083. https://doi.org/10.1093/icb/icv049.

16. Young, J.Z. (1963). THE NUMBER AND SIZES OF NERVE CELLS IN *OCTOPUS*. Proc. Zool. Soc. Lond. *140*, 229–254. https://doi.org/10.1111/j.1469-7998.1963.tb01862.x.

17. Young, J.Z. (1962). The Optic Lobes of Octopus vulgaris. Philos. Trans. R. Soc. Lond. B. Biol. Sci. *245*, 19–58. https://doi.org/10.1098/rstb.1962.0005.

18. Young, J.Z. (1961). Learning and discrimination in the octopus. Biol. Rev. Camb. Philos. Soc. *36*, 32–95. https://doi.org/10.1111/j.1469-185x.1961.tb01432.x.

19. Buresi, A., Andouche, A., Navet, S., Bassaglia, Y., Bonnaud-Ponticelli, L., and Baratte, S. (2016). Nervous system development in cephalopods: How egg yolk-richness modifies the topology of the mediolateral patterning system. Dev. Biol. *415*, 143–156. https://doi.org/10.1016/j.ydbio.2016.04.027.

20. Shigeno, S., Sasaki, T., Moritaki, T., Kasugai, T., Vecchione, M., and Agata, K. (2008). Evolution of the cephalopod head complex by assembly of multiple molluscan body parts: Evidence from Nautilus embryonic development. J. Morphol. *269*, 1–17. https://doi.org/10.1002/jmor.10564.

21. Shigeno, S., Sasaki, T., and Von Boletzky, S. (2010). The origins of cephalopod body plans: a geometrical and developmental basis for the evolution of vertebrate-like organ systems. In Cephalopods – Present and Past. *1,* 23-34.

22. Boycott, B.B. (1965). LEARNING IN THE OCTOPUS. Sci. Am. *212*, 42–51.

23. Boycott, B.B., and Young, J.Z. (1955). A memory system in *Octopus vulgaris* Lamarck. Proc. R. Soc. Lond. Ser. B - Biol. Sci. *143*, 449–480. https://doi.org/10.1098/rspb.1955.0024.

24. Gray, E.G., and Young, J.Z. (1997). The fine structure of the vertical lobe of Octopus brain. Philos. Trans. R. Soc. Lond. B Biol. Sci. *258*, 379–394. https://doi.org/10.1098/rstb.1970.0040.

25. Maddock, L., and Young, J.Z. (1987). Quantitative differences among the brains of cephalopods. J. Zool. *212*, 739–767. https://doi.org/10.1111/j.1469-7998.1987.tb05967.x.

26. Messenger, J.B. (1967). The peduncle lobe: a visuo-motor centre in octopus. Proc. R. Soc. Lond. B Biol. Sci. *167*, 225–251. https://doi.org/10.1098/rspb.1967.0025.

27. Shigeno, S., Andrews, P.L.R., Ponte, G., and Fiorito, G. (2018). Cephalopod Brains: An Overview of Current Knowledge to Facilitate Comparison With Vertebrates. Front. Physiol. *9*. https://doi.org/10.3389/fphys.2018.00952.

28. Shomrat, T., Zarrella, I., Fiorito, G., and Hochner, B. (2008). The Octopus Vertical Lobe Modulates Short-Term Learning Rate and Uses LTP to Acquire Long-Term Memory. Curr. Biol. *18*, 337–342. https://doi.org/10.1016/j.cub.2008.01.056.

29. Wells, M.J. (2013). Octopus: physiology and behaviour of an advanced invertebrate (Springer-Science+Business Media, B.V).

30. Giuditta, A., Libonati, M., Packard, A., and Prozzo, N. (1971). Nuclear counts in the brain lobes of*octopus vulgaris* as a function of body size. Brain Res. *25*, 55–62. https://doi.org/10.1016/0006-8993(71)90566-X.

31. Packard, A., and Albergoni, V. (1970). Relative Growth, Nucleic Acid Content and Cell Numbers of the Brain in Octopus Vulgaris (Lamarck). J. Exp. Biol. *52*, 539–552. https://doi.org/10.1242/jeb.52.3.539.

32. Nixon, M., and Mangold, K. (1996). The early life of Octopus vulgaris (Cephalopoda: Octopodidae) in the plankton and at settlement: a change in lifestyle. J. Zool. *239*, 301–327. https://doi.org/10.1111/j.1469-7998.1996.tb05453.x.

33. Wells, M.J., and Young, J.Z. (1965). Split-Brain Preparations and Touch Learning in the Octopus. J. Exp. Biol. *43*, 565–579. https://doi.org/10.1242/jeb.43.3.565.

34. Young, J.Z. (1965). The Buccal Nervous System of Octopus. Philos. Trans. R. Soc. Lond. Ser. B *249*, 27–44. https://doi.org/10.1098/rstb.1965.0007.

35. Hanlon, R.T., and Messenger, J.B. (1988). Adaptive Coloration in Young Cuttlefish (Sepia Officinalis L.): The Morphology and Development of Body Patterns and Their Relation to Behaviour. Philos. Trans. R. Soc. Lond. B Biol. Sci. *320*, 437–487. https://doi.org/10.1098/rstb.1988.0087.

36. Packard, A. (1985). SIZES AND DISTRIBUTION OF CHROMATOPHORES DURING POST-EMBRYONIC DEVELOPMENT IN CEPHALOPODS. Vie Milieu Life Environ., 285.

37. Packard, A. (1988). The Skin of Cephalopods (Coleoids): General and Special Adaptations. In, pp. 37–67. https://doi.org/10.1016/B978-0-12-751411-6.50010-2.

38. Packard, A., and Sanders, G. (1969). What the octopus shows to the world. Endeavour *28*, 92–99.

FUNCTIONAL ORGANIZATION OF VISUAL RESPONSES IN THE OCTOPUS OPTIC LOBE

* This chapter contains previously published co-authored material.

JR Pungor, VA Allen, JO Songco-Casey, and CM Niell. Current Biology, Volume 33, Issue 13, 10 July 2023.

Author contributions: J.R.P. and C.M.N. conceived the project and designed experiments. J.R.P. led the project and performed experiments. V.A.A. and J.O.S.-C. both optimized the experimental protocol and performed experiments, contributing equally. C.M.N. and J.R.P performed data analysis. All authors contributed to the writing of the manuscript.

Introduction

Cephalopods evolved large and complex brains independently from the rest of the animal kingdom. Like vertebrates, cephalopods also evolved camera-type eyes that focus a high resolution image onto a retina[1]. Together, their large brain and camera-type eyes implement a sophisticated visual system, which mediates a wide range of advanced visually-based behaviors[2], including prey capture and predator avoidance[3,4], identifying mates[5,6], spatial navigation[7,8], and a remarkable ability to rapidly camouflage to their surroundings[9–12]. However, because the cephalopod brain evolved independently from that of other highly visual species, the neural organization of their visual system is dramatically different.

Anatomical studies have delineated the morphology and structural connectivity of neurons in the cephalopod retina and optic lobes[13–20]. Unlike vertebrates, the cephalopod retina contains only photoreceptors, which send axons out of the retina into the optic lobes of the brain (Figure 1A, C). The optic lobes comprise roughly two thirds of the centralized nervous system and are where most of the visual processing in the cephalopod brain is thought to occur[12]. The outer optic lobe is a layered structure (Figure 1D, E), with two cell body layers, termed the outer granular (OGL) and inner granular layer (IGL), surrounding a layer of processes, the plexiform layer (Plex),

where photoreceptor axons terminate. Together these were termed the “deep retina” due to their resemblance to the layers of the vertebrate retina[13,15]. The center of the optic lobe, the medulla (Med), consists of clusters of cell bodies arranged in a tree-like structure surrounded by neuropil[21]. Recent transcriptomic studies have revealed a rich diversity of cell types within the optic lobe, as well as extensive sub-laminar organization[22–25].

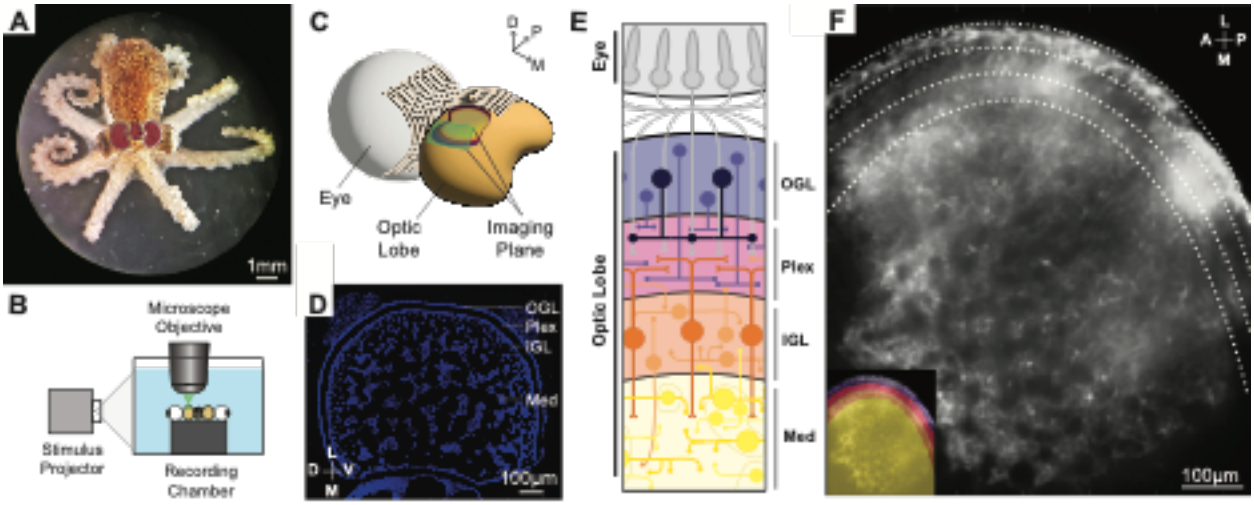

Figure 1. Experimental paradigm for calcium imaging of visual responses in the optic lobe
A) Image of a juvenile *Octopus bimaculoide*s. The central brain is shown in burgundy, and one optic lobe is outlined in white.
B) Schematic of the experimental set-up. A projector is used to present visual stimuli on the side of the recording chamber, with the preparation underneath the objective of a two-photon microscope on an adjustable platform.
C) Illustration of octopus visual system anatomy. Bundles of photoreceptor projections exit the back of the eye (left), decussate vertically, and enter the optic lobe (right) in a retinotopic manner. In the cutaway, the layered structure of the optic lobe can be seen, as it is in our imaging planes. Dorsal, posterior, and medial axes are shown in the key.
D) Coronal section of the center of the octopus optic lobe, stained with DAPI to illustrate the overall anatomy of the layers, which are labeled as in Figure 1E. Dorsal-ventral and lateral-medial axes are shown in the key.
E) Simplified illustration of the anatomy of the layers of the optic lobe. Color code for layers also applies to Figure 1C, F.
F) Mean fluorescence image of calcium indicator loading across a horizontal optical section of the optic lobe, as shown in the green square in 1C, with layers delineated by dotted lines. Inset shows layers in color overlay. Lateral-medial and anterior-posterior axes are shown in the key.

Early studies of photoreceptors in the cephalopod eye provided an initial description of visual processing at the input stage[26,27]. Like most other invertebrates[28], cephalopods have rhabdomeric photoreceptors that depolarize in response to increases in light (ON responses)[29], in contrast to vertebrate photoreceptors that depolarize in response to decrements in light (OFF responses).

Nearly all species of cephalopods, including octopuses, only express one type of opsin in their photoreceptors and are therefore thought to be monochromats[26,30], consistent with behavioral findings[31,32]. Electrophysiological recordings from the retina have demonstrated ON-center receptive fields and indications of lateral inhibition[33–36]. However, little is known regarding neural responses beyond the photoreceptors[35,37,38].

In the visual system of many species, responses to increments and decrements of light are processed in separate ON and OFF pathways[39], although the neural circuit mechanisms that give rise to these pathways, as well as their functional properties, can vary[40,41]. Likewise, many visual systems, though not all[42], exhibit a topographic organization of visual space within the brain, known as retinotopy. However, no studies have addressed the neural representation of ON and OFF visual stimuli within the cephalopod optic lobe, or how this is organized topographically and transformed across the optic lobe layers.

Here we developed techniques for two-photon calcium imaging of visually evoked responses in *Octopus bimaculoides*[43], a promising model species for studying cephalopod vision[44]. We used this calcium imaging approach to measure how spatial and luminance information are represented in large-scale neural responses, and to determine how these responses are organized within the optic lobe.

Results

Calcium Imaging of Stimulus-Specific Visual Responses in the Optic Lobe

Historically, electrophysiological recordings in the cephalopod brain have been technically challenging, and methods to express genetically encoded calcium indicators are not yet available in cephalopods. Here we employed a calcium imaging approach using an injection of a synthetic calcium indicator, Cal-520 AM-ester, to measure large-scale neural activity in the octopus optic lobe. Our general approach was adapted from techniques previously used to measure visual responses in the zebrafish optic tectum[45], and the bolus loading method established for acetoxymethyl (AM) ester calcium indicators[46]. In this method, a membrane-permeable AM-ester form of a calcium indicator dye is injected into the brain, where it is taken up by cells and rendered fluorescent based on cleavage of the AM moiety by endogenous esterases. This

typically leads to dye loading across a region of 500-1000μm in the intact brain in zebrafish and mouse[46].

We injected Cal-520 AM-ester into one optic lobe of an ex vivo preparation comprised of the eyes and central brain of an octopus (Figure 1A) and imaged neural responses with a two-photon microscope, which provided optical access for recording across the optic lobe to a depth of up to 200μm (Figure 1B). The small sizes of the juvenile octopuses allowed us to image a large cross-section of their optic lobes spanning multiple layers, providing a view across both its tangential and laminar organization (Figure 1C-E), similar to how a cross-section of the top of the earth would both span longitude and latitude (tangential organization), as well as reveal the layers of the earth's crust and mantle (laminar organization). Figure 1F shows loading of the fluorescent indicator across an optic lobe, with its different layers readily discernible. The full field of view of the microscope was 0.64mm^2, but measurable fluorescent loading typically only covered 0.35 +/- 0.05mm^2 (n=6 animals). The radius of the optic lobe at this age is roughly 1mm, with an approximately 4mm^2 surface area, indicating we were imaging ~1/10th of the optic lobe area in a given experiment.

Visual stimuli were displayed via a LCD projector onto a white diffusion filter mounted on the side of the chamber containing the preparation (Figure 1B). An adjustable platform allowed us to align the precise orientation of the eye so that receptive fields for a given imaging region were centered on the screen. This approach allowed us to present high-resolution stimuli across the visual field of one eye while simultaneously recording the responses across a region of the optic lobe.

To obtain visually evoked responses, we initially used a stimulus of individual full contrast ON (light) and OFF (dark) rectangular spots (24x18deg) tiling the projection screen, presented in a random order on a 50% luminance gray background for 1sec duration. This stimulus elicited fluorescence responses in the optic lobe dependent on the location of the spot in the visual field (Figure 2, Video S1). ON and OFF responses were based directly on the activity during the stimulus duration for light and dark spots, rather than comparing onset and offset transients for

ON stimuli as is done when light stimuli are presented on a dark background. Figure 2A shows the mean response, measured as the change in fluorescence divided by mean fluorescence (dF/F0) at each pixel across the optic lobe, over five repeated presentations of an ON spot at one location. The evoked activity, locked to stimulus onset, persisted throughout the one second stimulus period and was followed by a decay, consistent with calcium indicator dynamics. This activation map also suggests a temporal sequence of activity, with fluorescence signal first increasing rapidly in the superficial optic lobe, followed by more gradual and sustained response in the medulla. Figure 2B shows the mean response across the optic lobe during the stimulus presentation for ON spots in three neighboring locations. We found activation of distinct regions within the optic lobe to each location, indicating specificity for the location of the stimulus in visual space in a retinotopic manner. Finally, Figure 2C shows the response to an OFF spot at the same recording location as Figure 2B (middle), responding in approximately the same region, but deeper in the laminar structure of the optic lobe, in the IGL and medulla.

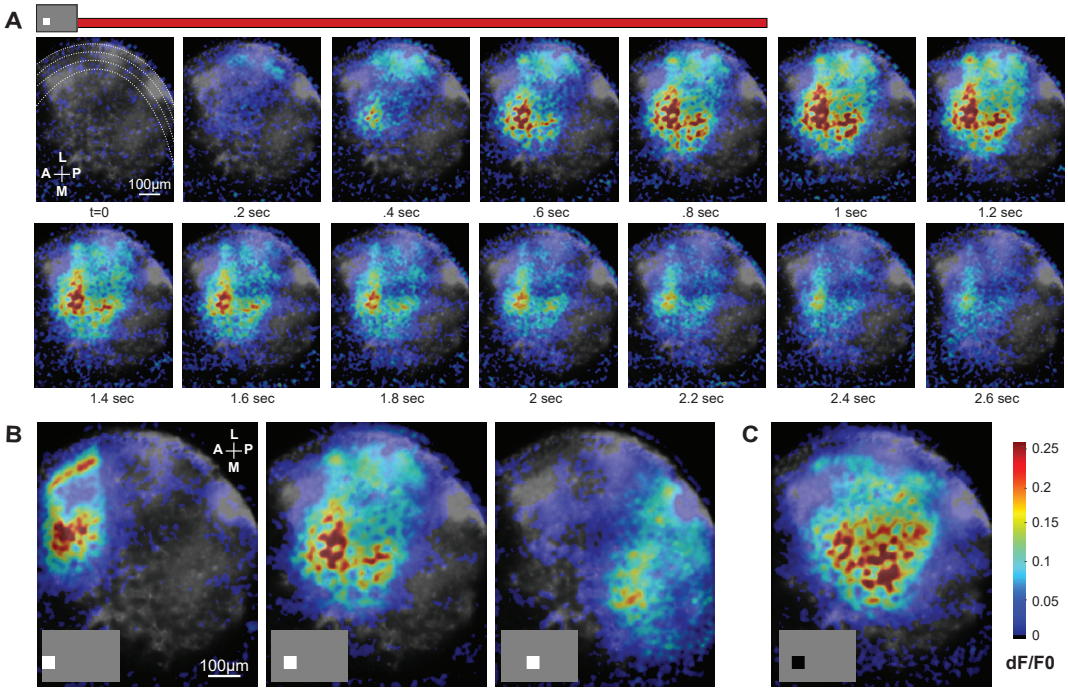

Figure 2. Visually evoked responses in the optic lobe
A) Mean timecourse of fluorescence response to a flashed ON spot at one location in the visual field (averaged over five stimulus repetitions), showing spatial organization and temporal dynamics. Duration of stimulus presentation is indicated by the red bar above the frames. Individual imaging frames are shown at 0.2sec intervals.
B) Mean fluorescence response across the optic lobe to ON stimuli at three different horizontal locations, averaged across the stimulus duration for five repetitions.

C) Mean fluorescence response to an OFF stimulus at the same location as H (middle), averaged across the stimulus duration for five repetitions.

These results demonstrate that our calcium imaging approach allowed us to measure stimulus-specific visual responses, and provide initial support for both retinotopic and laminar organization of responses. To probe the specificity and spatial organization of visual responses more systematically, we next performed mapping of spatial receptive fields using a sparse noise stimulus.

Spatially Localized ON and OFF Receptive Fields

We used a sparse noise stimulus adapted from[47] to calculate ON and OFF receptive fields. The stimulus consisted of frames of ON and OFF circular spots of three different sizes (radius = 3, 6, 12deg) in a randomly distributed pattern, along with randomly interleaved ON or OFF full-field frames (Figure 3A). Each frame was presented for 1sec over a total recording time of 10mins. This sparse noise stimulus elicited robust and spatially localized fluorescence responses across the optic lobe, as demonstrated in Figure 3B and Video S2.

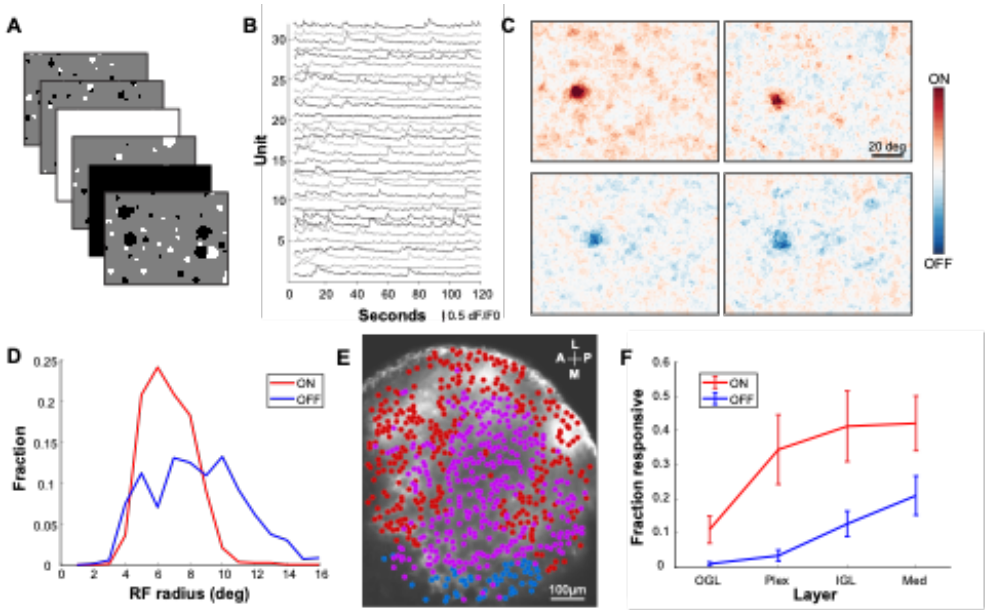

Figure 3. ON and OFF receptive fields mapped with a sparse noise stimulus
A) Example frames from the sparse noise stimulus used to map receptive fields. Frames were presented consecutively in a randomized order for 1sec each.
B) Traces of fluorescence activity at 32 locations across the optic lobe in response to the sparse noise stimulus.

C) RFs from four example units, two each for ON (top) and OFF (bottom) components of the stimulus. Note that because these units are from within a single imaging field of view, the RFs are in the same vicinity of visual space, consistent with retinotopic organization.
D) Histogram of RF sizes for ON and OFF stimuli (n=6 animals).
E) Location of units with RFs for ON (red), OFF (blue), or both (magenta) in one session across the optic lobe.
F) Fraction of units overall with significant RFs for ON and OFF across the layers of the optic lobe (n=6 animals).

For analysis, we selected individual regions of interest (ROIs), 20x20μm, centered on peaks in the mean fluorescence image above a baseline fluorescence threshold, to exclude regions that were not loaded with calcium indicator. This identified ~500-1000 ROIs spaced across each of the multiple layers of the optic lobe captured within each imaging field (e.g Figure 3E). We selected this approach, rather than extracting responses specifically from cell bodies as typically performed for calcium imaging in vertebrates, both due to the challenge in localizing signals to individual cells in tightly packed cell body layers and the fact that, in invertebrates, much of the neural signal is localized to processes within the neuropil. We refer to each ROI as a unit, denoting a specific location within the optic lobe, rather than a single neuron. This analysis allowed us to map how visual information is represented at locations across the optic lobe. As noted in the Discussion, single-cell or cell-type specific recordings will likely be needed to directly probe individual cell tuning properties.

We computed receptive fields (RFs) for each unit using reverse correlation based on the evoked dF/F0 fluorescence signal for each frame of the sparse noise stimulus, excluding the full-field flashes (see Methods). We performed this separately for the ON (light) and OFF (dark) components of the stimulus to avoid cancelation of positive and negative stimulus contrast for units that responded to both polarities. This revealed spatially localized RFs for both ON and OFF stimuli, as shown by examples in Figure 3C. RFs were generally circularly symmetric by visual inspection, so we fit RFs to a Gaussian model to determine their size and location within visual space. Across experiments, 59 +/- 26% of all units had a RF significantly above background as determined by their z-scored response. The Gaussian model provided a good fit to the RFs, with a pixel-wise correlation between the measured RF and model fit of 0.85 +/- 0.07 for ON RFs and 0.74 +/- 0.14 for OFF (mean +/- s.d.) The lower correlation for OFF response likely reflects noisier RF estimates due to the lower response amplitude in OFF units (see Figure

4 below), but in both cases the vast majority of variance in the RF was explained by the Gaussian model. The RF radius, based on sigma of the Gaussian fit, was 5.7 +/- 0.6deg for ON, and 7.4 +/- 0.6deg for OFF (p=0.31 for ON vs OFF) (Figure 3D). Note that this is likely an overestimate of the RF size of individual neurons, since the response of each unit within the lobe represents the summed response of a number of individual neurons.

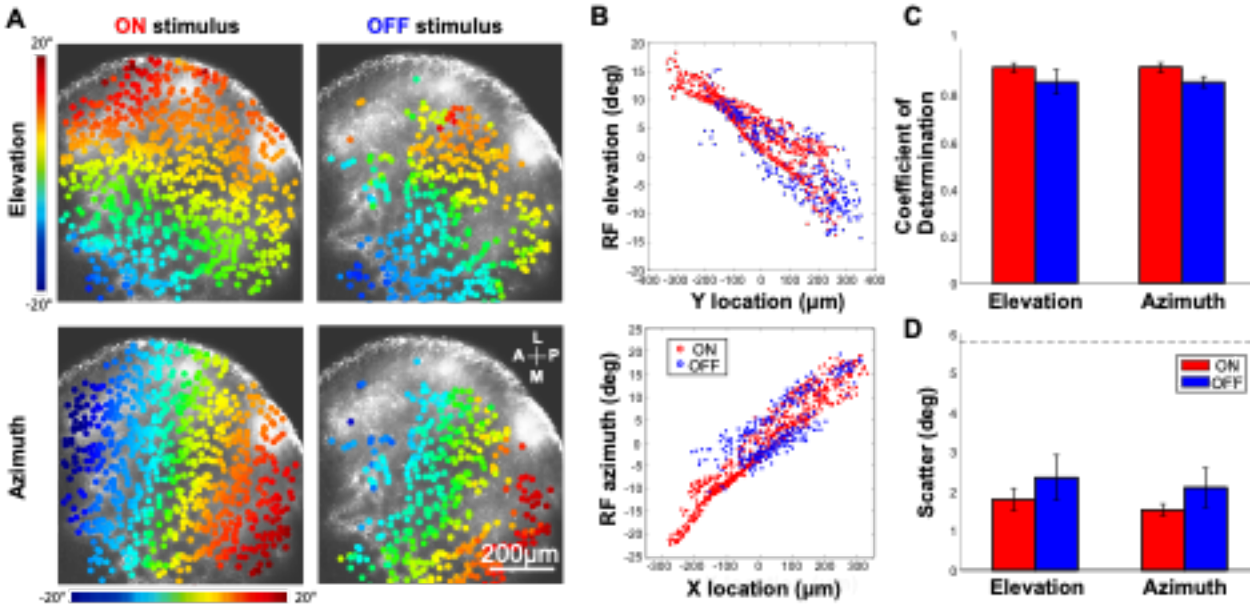

Figure 4. Retinotopic organization of visual responses in the octopus optic lobe
A) Example mapping of RFs in the optic lobe of responses to both ON (left) and OFF (right) stimuli. Areas are colored by the position of their RFs along the elevation (top) and azimuth (bottom) as shown by the color scale bars (degrees of visual space). Based on the position of the octopus eyes, elevation corresponds to the dorsal-ventral axis of the animal's body, and azimuth corresponds to the anterior-posterior axis of the animal's body.
B) Scatter plot of RF location for elevation (top) and azimuth (bottom) versus unit location within the optic lobe, for both ON and OFF responses. Adjacent groups of cells responded to adjacent areas of the visual field.
C) Mean coefficient of determination for elevation and azimuth maps across all recordings (n=6 animals).
D) Mean scatter in RF location for elevation and azimuth, across all recordings (n=6 animals). Dashed line shows chance level based on a shuffle control.

In each experiment, the measured RFs only subtended a restricted region of the visual field, consistent with a retinotopic organization and the fact that we are only imaging a limited extent of the optic lobe area (roughly 1/10th, as described above). We calculated that an area of 430 +/- 290deg^2 (mean +/- s.d.) of the visual field that was covered by the RFs in each experiment. For context, the projection screen was 5400deg^2 (90x60deg), so the fraction of visual space represented (~1/12th) corresponds well to the fraction of the optic lobe imaged.

We next examined the distribution of ON and OFF responses across the optic lobe to determine where the pathway for processing each arises. Figure 3E shows all units in an example recording labeled based on whether they had a RF for only ON (red), only the OFF (blue) component, or for both components of the stimulus (magenta). While ON responses are distributed throughout the lobe, OFF responses are largely restricted to the deeper layers of the IGL and medulla. To quantify this, we calculated the fraction of ON and OFF RFs in each layer across recordings (Figure 3F), confirming that OFF responses primarily emerge in the IGL and are strongest in the medulla. The sequential emergence of OFF responses relative to ON is consistent with the fact that photoreceptor axons in cephalopods, which mainly terminate in the superficial layers of the optic lobe (Plex), respond to increments of light, and demonstrates that the OFF processing pathway originates in neurons further along the visual processing pathway.

We found both ON and OFF responses within the same fields of view, corresponding to the same region of visual space, suggesting that variations are primarily due to depth. However it remains possible that there could also be variations in the ON/OFF distribution across the visual field in other regions of the optic lobe.

Retinotopic Organization of the Optic Lobe

To determine if there was a retinotopic organization of visually evoked responses in the octopus optic lobe, we labeled each unit according to the location of its RF, based on the center of the Gaussian fit described above. As shown in Figure 4A, we found clear retinotopic progression for ON and OFF responses, along both the elevation and azimuth of the visual field, resulting in a map of visual space across the optic lobe. This is further demonstrated in Figure 4B, which shows the high degree of correlation between the unit's physical location across the optic lobe with its RF location in visual space. The retinotopic maps of ON and OFF RFs were also aligned in regions of the lobe that were responsive to both (Figure 4B). Note that, as described above, the imaged retinotopic map does not span the full visual space of the projector screen, but is typically restricted to roughly 20x20deg (mean 430deg^2), due to the fact that we were only imaging a subregion of the optic lobe.

We next quantified the retinotopic organization in each experiment by performing a linear regression between the RF elevation/azimuth in the visual space of all responsive units and their x/y location within the optic lobe. We used both the x and y location of the units to predict each RF parameter, since the visual axes were not always aligned to the x and y axes of the imaging plane depending on the orientation of the preparation. This fit resulted in a mean coefficient of determination greater than 0.8 for both ON and OFF maps across experiments (Figure 4C), confirming robust retinotopy. We also computed the scatter of RF locations (i.e. how much RF locations deviate from a linear retinotopic progression), based on the residuals from the fit, which demonstrated that individual unit's RFs have scatter of less than 2 degrees (Figure 4D). Finally, the slope of the RF fit determines the magnification factor of the map (i.e. how much the RF location changes for a given distance in the brain), with a mean progression of 21.9 +/- 1.4 μm/deg in elevation and 25.0 +/- 3.0 μm/deg in azimuth. Together, these data provide the first functional demonstration of a retinotopic organization of visual information within the cephalopod brain.

Size Selectivity in ON and OFF Pathways Across Layers of the Optic Lobe

To further examine visual response properties and their organization within the octopus optic lobe, we next calculated size tuning of units based on their evoked responses to spots of different sizes in the sparse noise stimulus. For each unit with a significant RF, we determined the center of its ON or OFF RF from the Gaussian fit, and computed the mean dF/F0 response timecourse when spots of different sizes appeared in this RF. We limited this analysis to units with significant RFs, based on z-score as described above, because it is only meaningful for units that have a defined RF location.

Figure 5A shows the mean timecourse of response during the 1sec stimulus presentation for each size stimulus, including full-field flash, for all units across experiments, divided into their layer within the optic lobe. In order to accurately represent the relative magnitude of responses across layers, given the differential distribution of ON and OFF units (Figure 3E), we weighted these mean traces by the respective fraction of responsive units within each layer. All responsive

populations showed sustained activity throughout the 1sec stimulus presentation, although with diverse temporal dynamics. We note that because our measurements represent the activity of multiple neurons in each unit, these dynamics could also represent the summation of populations with heterogeneous temporal responses, for example both transient and sustained responses.

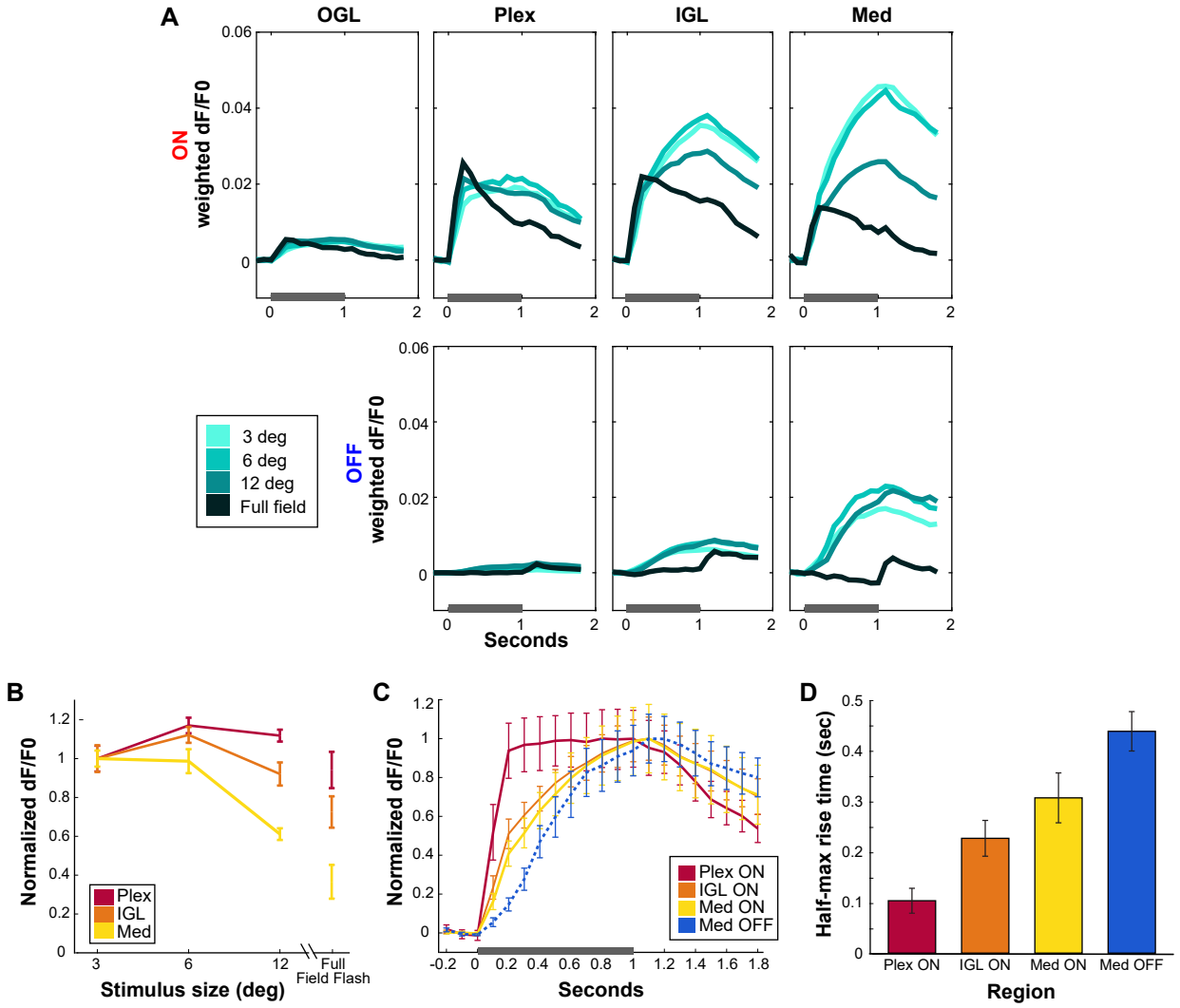

Figure 5. Size selectivity and temporal dynamics across the layers of the optic lobe
A) Mean timecourse of ON (top) and OFF (lower) responses for each stimulus size, separated by layers of the optic lobe. Response for each layer and luminance are weighted by fraction of units responsive. OGL did not show a significant response to OFF, and was omitted from this figure. Stimulus onset is at t=0 and each frame was presented for 1sec, as shown by gray bars on the x axis (n=6 animals).
B) Mean size tuning curves for ON responses in each layer, normalized to the response to the smallest stimulus (n=6 animals).
C) Mean timecourse of unit responses, averaged across the three sizes of stimulus spots and normalized to the maximum response, for ON (Plex, IGL, Med) and OFF (Med) (n=6 animals).
D) Mean rise time to half-maximum response from data in C.

For ON stimuli (Figure 5A, top), there was a strong and rapid response in the Plex, which was approximately equal in amplitude for all stimulus sizes, as well as to the full-field flashes. However, as responses progressed deeper into the IGL and medulla, the sustained response increased for small stimuli but decreased for larger spots and full-field flashes, indicating size selectivity. Interestingly, the initial onset responses were similar across sizes, with the responses to different sizes diverging only after ~200msec. Figure 5B shows the size tuning curve of ON responses for each layer, based on the mean dF/F0 across stimulus duration, normalized to the response to the smallest stimulus size. These show a decrease in the relative response to larger stimuli in the IGL and medulla. Together, the responses to ON stimuli showed an emergence of size selectivity, both over time and across layers.

In contrast, responses to OFF stimuli (Figure 5A, bottom) only appeared in deeper layers of the optic lobe (IGL and Med). There was no size suppression across different sized spots, in contrast to what was seen in the ON. Rather, responses to OFF spots of all sizes were roughly equal, leading to a relative bias toward large stimuli in OFF compared to ON. Strikingly, there was no response at all to the full-field OFF stimulus, despite responses to the range of OFF spot sizes and to full-field ON. These differences in spatial integration for ON and OFF suggest different processing pathways exist for these two luminance modalities, even in these early visual processing stages.

Finally, we examined the mean timecourse of response onset to ON and OFF spots across the layers of the optic lobe (Figure 5C, D), revealing distinct temporal dynamics. ON responses increased rapidly in the plexiform layer, and then spread into the deeper regions of the IGL and Med. On the other hand, OFF responses were first seen predominantly in the medulla (Figure 5A, bottom panels), and had a slower rise time (Figure 5C, blue trace). We quantified this difference in timecourse based on the mean rise time to half-maximum response (Figure 5D). It should be noted that this metric represents the rate of increase of response rather than latency to first response, which was faster than our framerate as clear responses were already seen in the first frame following stimulus onset (Figure 5C). There was an approximately 100msec

difference in rise time for ON responses from Plex to IGL and medulla, and an additional 100msec difference within the medulla from ON responses to OFF responses (Figure 5D), consistent with a later emergence in the visual processing circuit.

Discussion

Octopuses represent an intriguing independent evolution of a complex nervous system. However, relatively little is known about how their brain functions at the neural level. Combining large scale two-photon calcium imaging with controlled visual stimuli, we were able to overcome technical challenges that previously hindered recordings of neural activity in cephalopods. The establishment of such recording techniques, and future improvements, will be essential for elucidating the computations performed in their visual system, as well as other aspects of sensory processing, cognition, and behavior in cephalopods.

Using this calcium imaging approach, we measured response properties of populations of neurons within the octopus optic lobe, and began to identify what fundamental features of the visual world they encode, and how these emerge in the early stages of visual processing. We found similarities in visual processing between octopus and other species, such as a retinotopic organization of responses, highlighting potential fundamental principles for the organization of visual systems across the animal kingdom. We also identified unique organization of ON/OFF pathways and size selectivity, that may have arisen due to these animals' environmental constraints[48] or distinct evolutionary trajectories[49]. These findings are the first to show visual processing dynamics across the layers of the octopus optic lobe and provide a foundation for studying the processing of more complex visual features.

Spatial Organization of Response Properties in the Optic Lobe

Although there have been previous studies of the anatomical organization of the octopus visual system, little is known about its functional organization. Based on the fashion in which the optic nerves from the eye were found to enter the optic lobe[16,50,51], it was predicted that visual information would be retinotopically organized within the lobe, as it is in many, though not all[42], visual systems across the animal kingdom. However, studies in the motor system of cephalopods

demonstrated a surprising lack of somatotopy in their central brain, suggesting they may have evolved alternative, non-topographic architectures for representing spatial information[52]. In this study, we found that neural coding in the visual system of the octopus is indeed organized retinotopically, with aligned maps for responses to ON and OFF stimuli, demonstrating that the lack of topographic mapping previously observed in the motor system is not a general feature of cephalopod brain organization.

Previous anatomical studies had suggested potential neural circuits across the layers of the octopus optic lobe that could implement sequential processing of visual input[13,14,16], as in the vertebrate retina or fly visual system[53]. Our findings support these predictions, demonstrating that the temporal dynamics of visual responses in octopuses do in fact proceed sequentially across the laminar organization of their brain. This is accompanied by a transformation of the visual input, including the emergence of the OFF pathway, as well as an increase in size selectivity in the ON pathway. Our findings of differential response dynamics across distinct layers provide an initial framework for understanding the functional computations performed by the cephalopod visual system.

Comparative Aspects of ON/OFF Pathways and Spatial Processing

A key computation for any visual system is the ability to respond to both light and dark stimuli within a scene. Given that photoreceptors depolarize to only ON (invertebrates) or OFF (vertebrates) stimuli, there is a necessary computation to invert the polarity of the photoreceptor signal within the subsequent visual circuitry to achieve this. For vertebrates it is known that this inversion occurs at the photoreceptor to bipolar cell synapse[54], while in Drosophila segregated ON and OFF responses emerge one synapse further from the photoreceptors, between the lamina and medulla[55].

Here we found that ON responses dominate in the primary input layer of the octopus optic lobe, the plexiform layer, corresponding to the fact that cephalopod photoreceptors depolarize to light increments. OFF responses only emerge initially in the IGL and are greatly increased in the medulla, suggesting a potential site for the sign inversion circuitry. We also found that OFF

responses have a strikingly different profile from ON. Despite prominent responses to full-field ON stimuli across layers, there is a complete lack of response to full-field OFF stimuli. This suggests that the OFF pathway may emerge through a different mechanism than direct inversion of the photoreceptor input, which would yield responses to a full-field OFF stimulus. One possibility is that the OFF pathway receives input from a subset of ON neurons that have completely suppressed the response to a full-field stimulus. A more intriguing possibility is that the mechanisms that generate OFF responses may rely directly on boundaries between light and dark regions, which would explain why OFF responses are driven by localized dark stimuli (i.e. spots) that contain such edges, but not full-field stimuli, which do not.

Additionally, we found differences in size selectivity for spots in the ON and OFF pathways (Figure 5A). While responses in the ON pathway decreased for larger spots, the responses to spots in the OFF pathway were roughly equal across the sizes of stimuli we measured. This implies a net bias toward the enhancement of responses to smaller stimuli in the ON pathway. Asymmetries in ON/OFF visual processing have been found in other species across the animal kingdom, and are thought to enhance ethologically relevant visual features to meet each animals' specific visual demands[56–60]. The enhancement of responses to smaller stimuli in the ON pathway that we observed may be beneficial when processing visual scenes underwater, where light intensity is greatly attenuated by both absorption and scatter[61]. As a result, nearby objects, like potential prey, would tend to appear bright against a large, dark background. An OFF pathway biased towards larger stimuli might also aid in the detection of large, looming objects, which often represent predators. It will be interesting to see if such ON/OFF processing differences exist more broadly across cephalopods that occupy other ecological niches, particularly as these vary greatly in luminance levels and visual scene statistics[62].

Implications for Future Studies

Our findings provide initial insight into how luminance and size information are processed within the different layers of the octopus optic lobe. However, both anatomical and

transcriptomic studies[22,24,25,63] have revealed a high degree of cell type diversity within these layers, so the bulk response properties we examined here undoubtedly mask a high degree of underlying functional diversity. Identifying more detailed response properties within the parallel pathways of diverse cell types in this system will likely benefit from methods to record using genetically encoded calcium indicators, not yet available in cephalopods to date. Such an approach would also help address the challenge in associating activity in neural processes, which often dominate in invertebrate neurons, with individual neurons or populations of neurons[64].

More broadly, future studies based on these findings and methodology could explore the range of feature selectivity in the visual system of octopuses, as has been studied in other species, such as motion processing, orientation selectivity, object recognition, and lateralization of visual responses[65,66]. Additionally, this approach can be used to study aspects of visual responses that may be specific to cephalopods, such as the ability to detect stimuli based on the polarization angle of light[67], or to extract information from the visual scene for camouflage[11]. Further studies may continue to reveal how the cephalopod brain performs the computations that enable the remarkable visual capabilities of these enigmatic creatures.

Methods

Experimental Model and Subject Details

All studies were conducted with approved protocols from the University of Oregon Animal Care Services, in compliance with the Association for Assessment and Accreditation of Laboratory Animal Care International guidelines. Animal husbandry and protocols were carried out in accordance with published guidelines for the care and welfare of cephalopods in the laboratory[68,69].

Octopus bimaculoides were obtained from the Cephalopod Culture Program at the Marine Biological Laboratory (Woods Hole, MA) and from Aquatic Research Consultants (Dr. Charles Winkler, San Pedro, CA). Animals used were 4-8 weeks old and of indeterminate gender. Octopuses were kept in a 250 gallon closed circulating seawater system, held at 22°C and illuminated on a 12/12hr day/night light cycle. Each animal was kept in an isolated enclosure

within the system, allowing for ample freedom to roam, while keeping them isolated from potential cannibalism from counterparts. Each enclosure contained items that provided shelter (large shells, tubes) and environmental enrichment (smaller shells, Legos, beads, rotated weekly). Animals were fed a mixed diet of frozen shrimp, clams, and fish, offered daily.

Method Details

Calcium Imaging

Animals were deeply anesthetized in artificial seawater (ASW) (460mM NaCl2, 10mM KCl, 10mM glucose, 10mM HEPES, 55mM MgCl2, 11mM CaCl2, 2mM glutamine, pH 7.4) supplemented to contain 110mM MgCl2 at 13-15°C. When the animal was no longer responsive to a firm pinch test of the mantle, it was transferred to an oxygenated dish of a 30:70 mix of isotonic 370mM MgCl2 with ASW that was held between 13-15°C. Animals were then rapidly euthanized via decapitation and removal of the arm crown. A solution to dilate their pupils (10% phenylephrine HCl in ASW) was manually applied to the eyes. Dissection was performed to expose the brain and remove surrounding musculature and skin in order to reduce motion artifacts and increase optical access for recording.

The ex vivo preparation of the central brain and both eyes was secured to a coverslip using cyanoacrylate (Vetbond, 3M). A dye solution of 1mM Cal-520 AM (AAT Bioquest), 2.5% Alexa Fluor™ 568 Hydrazide (Thermo Fisher), 8% dimethylsulfoxide, and 2% pluronic acid (AAT Bioquest) in ASW was injected into one of the optic lobes via a glass micropipette needle (Harvard Apparatus Cat. Num. 30-0038) using a pressure injector (ASI, Inc). Micropipettes with a tip diameter of 9µm were back filled with the dye solution via capillary loading. For each animal, three individual injection sites were used. Three 1sec pulse injections at 5PSI pressure, with a constant 1PSI back pressure, were performed along the track of each injection site, with each injection done closer to the surface of the lobe than the last by retracting the needle ~50µm between each. Injections were targeted to the superficial layers (IGL and superficial medulla) of the optic lobe to optimize dye delivery to areas that were optically accessible in the imaging set-up. After injection, the preparation was covered in a thin layer of 4% low melt agarose in ASW

(Sigma) to secure it and to minimize movement. This paradigm was adapted from previous work in zebrafish[45], see also[70].

The preparation was kept in a recording chamber filled with ASW and continuously oxygenated via an airstone to maintain tissue viability[71]. The recording chamber consisted of a 7.6cmx7.6cmx5cm plastic box (TAP Plastics) where one side was replaced with a white diffusing glass (Edmund Optics, Cat. Num. 02-149) to serve as a projection screen for visual stimuli. The coverslip with the mounted preparation attached was secured to a custom-built rotatable platform within the recording chamber to allow for alignment of the preparation to the stimulus screen. The eye ipsilateral to the loaded dye was placed 2cm from the screen for recordings, with the contralateral eye facing away from the screen. The chamber temperature was monitored and held between 17-22°C.

Due to the need for the calcium indicator to be taken up into cells and then for the AM moiety to be cleaved, resulting in fluorescence, the preparation was kept in the dark under the two-photon microscope for 30-45 minutes before recording began. During this time we periodically examined the preparation for fluorescence and visual responses using a brief (<1sec) presentation of a flashing full field white stimulus. Experiments began after ~30-45 minutes, when the fluorescent loading had plateaued and visual responses were apparent.

Calcium imaging was performed with a two-photon microscope (Neurolabware Inc.), using a 16X Nikon CFI75 LWD objective, via the Scanbox software package for Matlab (MATHWORKS). Data were acquired at a 10Hz framerate, with an 800x800μm (796x796 pixel) field of view. Recordings were taken at 90 to 170μm depths from the dorsal surface of the optic lobe.

Visual Stimuli

Custom generated visual stimuli, rendered using the PsychToolbox package for Matlab[72], were displayed with a pico LCD projector (AAXA Technologies) onto the diffusing glass on the side of the recording chamber. To avoid light from the stimulus entering the two-photon detection

pathway, the projected light was passed through a 450/50 bandpass filter (Chroma Technology Corporation), avoiding overlap with the emission spectrum of the Cal-520 calcium dye and the bandpass 525/50 emission filter of the microscope. The stimulus bandpass filter also restricted the stimulus light to be within the known absorption spectrum of cephalopod photopigments[26]. Stimuli were gamma-corrected in software and presented at 60FPS.

ON and OFF stimuli were presented as full contrast increments and decrements of light on a 50% luminance gray background. Initial mapping was performed using a stimulus consisting of full contrast ON (100% luminance) and OFF (0% luminance) rectangular spots (24x18deg) on a 6x4 grid spanning the projection screen, presented in a random order for a one second duration, for a total recording time of 5min. This stimulus was also repeated at the end of the experimental session to confirm stability and viability of the preparation. Full RF mapping was performed using a sparse noise stimulus, consisting of white and black spots (radius = 3, 6, 12 deg; density = 10%) on a gray (50% luminance) background, along with full-field white or black on 2% of frames. Each stimulus frame was presented for 1sec in a randomized order for a total duration of 10min. Preparations were kept in the dark for 10min between each stimulus set presentation. The results of presenting each stimulus set once to each of six animals are shown here. In some preparations additional stimuli were presented at the same or other recording locations but are not included in this study. Recordings reported here were taken 2-5.5 hours after injection.

Quantification and Statistical Analysis

Data Analysis

Data analysis was performed using custom software in MATLAB. We applied a rigid alignment of imaging data using the *sbxalign* function in Scanbox (Neurolabware, Inc.). In order to detect large movements that were not corrected by the alignment algorithm, for each frame we calculated the pixel-wise correlation coefficient to the mean image. Frames with less that 90% correlation were discarded from further analyses.

We calculated the fluorescence activity (dF/F0) at each pixel as the standard (F(t) - F0) / F0, where F(t) is the fluorescence intensity of the pixel on each frame and F0 is the median

fluorescence intensity of the pixel across the recording. To analyze local responses, we defined "units" as a 20μmx20μm wide square window, centered on local peaks within the mean fluorescence that were above the background fluorescence, to ensure that only areas with sufficient dye loading were analyzed. dF/F0 for each unit was calculated as the mean dF/F0 across pixels within the unit. Units were manually assigned to anatomical layers (OGL, IGL, Plex, and Med) based on location within the mean fluorescence image from the recording session.

To analyze receptive fields (RFs), based on the sparse noise stimulus, we first calculated the evoked response, $r(t)$, for each frame as the mean dF/F0 across the one second duration of stimulus presentation, minus the mean dF/F0 in the preceding 300msec. RFs were calculated by reverse correlation between the each stimulus frame, $s(x, y, t)$, and the evoked response to that frame.

$$RF(x, y) = \sum_{t} s(x, y, t) * r(t) \; / \; \sum_{t} r(t)$$

We computed the z-score for each RF based on the maximum absolute value of the RF, divided by the standard deviation across pixels. We used a z-score of 5.5 as the threshold for significant responses.

In order to analyze RF size and location, we fit each RF to a Gaussian function, defined as

$$RF_{fit}(x, y) = A * exp((x - x_0)^2 \; / \; 2\sigma_x^2 \; + \; (y - y_0)^2 \; / \; 2\sigma_y^2) \; + \; B$$

We used x_0, y_0 as the receptive field center, and computed RF radius as $(\sigma_x + \sigma_y)/2$. To quantify topographic maps, we performed a linear regression for each recording for responses to both azimuth and elevation, as a function of each unit's location within the optic lobe from the Gaussian fit, and used the coefficient of determination and standard deviation of residuals (scatter) as metrics of retinotopy.

Statistical Analysis

Statistical tests for comparison of responses across populations within the optic lobe were performed using a t-test. To account for the nested design (many units per recording) of this analysis, all statistical tests were performed at the level of recordings, rather than total number of units recorded. Summary statistics in text and figures are presented as mean +/- standard error, unless otherwise noted.

References

1. Packard, A. (1972). Cephalopods and Fish: The Limits of Convergence. Biol. Revs. *47*, 241–307.

2. Hanlon, R.T., and Messenger, J.B. (2018). Cephalopod Behaviour 2nd ed. (Cambridge University Press).

3. Schnell, A.K., Hanlon, R.T., Benkada, A., and Jozet-Alves, C. (2016). Lateralization of Eye Use in Cuttlefish: Opposite Direction for Anti-Predatory and Predatory Behaviors. Front. Physiol. *7*, 620.

4. Bidel, F., Bennett, N.C., and Wardill, T.J. (2022). Octopus bimaculoides' arm recruitment and use during visually evoked prey capture. Curr. Biol. *32*, 4780–4781.

5. Shashar, N., Rutledge, P., and Cronin, T. (1996). Polarization vision in cuttlefish in a concealed communication channel? J. Exp. Biol. *199*, 2077–2084.

6. Hanlon, R.T., Naud, M.-J., Shaw, P.W., and Havenhand, J.N. (2005). Behavioural ecology: transient sexual mimicry leads to fertilization. Nature *433*, 212.

7. Karson, M.A., Jean, G.B., and Hanlon, R.T. (2003). Experimental evidence for spatial learning in cuttlefish (Sepia officinalis). J. Comp. Psychol. *117*, 149–155.

8. Alves, C., Boal, J.G., and Dickel, L. (2008). Short-distance navigation in cephalopods: a review and synthesis. Cogn. Process. *9*, 239–247.

9. Chiao, C.-C., Ulmer, K.M., Siemann, L.A., Buresch, K.C., Chubb, C., and Hanlon, R.T. (2013). How visual edge features influence cuttlefish camouflage patterning. Vision Res. *83*, 40–47.

10. Nagar, A.E., El Nagar, A., Osorio, D., Zylinski, S., and Sait, S.M. (2021). Visual perception and camouflage response to 3D backgrounds and cast shadows in the European cuttlefish, *Sepia officinalis*. J. Exp. Biol. *224*, jeb238717.

11. Reiter, S., and Laurent, G. (2020). Visual perception and cuttlefish camouflage. Curr. Op. Neurobio. *60*, 47–54.

12. Wells, M.J. (1962). The Brain and Behavior of Cephalopods (Stanford University Press).

13. Ramón y Cajal, S. (1930). Contribución al conocimiento de la retina y centros ópticos de los cefalópodos (Unión Internacional de Ciencias Biológicas, Comité Español).

14. Young, J.Z. (1960). The Visual System of Octopus:(1) Regularities in the Retina and Optic Lobes of Octopus in Relation to Form Discrimination. Nature *186*, 836–839.

15. Young, J.Z. (1962). The optic lobes of Octopus vulgaris. Philos. Trans. R. Soc. Lond. *245*, 19–58.

16. Young, J.Z. (1971). The Anatomy of the Nervous System of Octopus Vulgaris (Oxford University Press).

17. Young, J.Z. (1974). The central nervous system of Loligo. I. The optic lobe. Philos. Trans. R. Soc. Lond. B Biol. Sci. *267*, 263–302.

18. Saidel, W.M. (1982). Connections of the octopus optic lobe: an HRP study. J. Comp. Neurol. *206*, 346–358.

19. Chung, W.-S., Kurniawan, N.D., and Marshall, N.J. (2020). Toward an MRI-Based Mesoscale Connectome of the Squid Brain. iScience *23*, 100816.

20. Williamson, R., and Chrachri, A. (2004). Cephalopod neural networks. Neurosignals *13*, 87–98.

21. Liu, Y.-C., Liu, T.-H., Su, C.-H., and Chiao, C.-C. (2017). Neural Organization of the Optic Lobe Changes Steadily from Late Embryonic Stage to Adulthood in Cuttlefish. Front. Physiol. *8*, 538.

22. Styfhals, R., Zolotarov, G., Hulselmans, G., Spanier, K.I., Poovathingal, S., Elagoz, A.M., De Winter, S., Deryckere, A., Rajewsky, N., Ponte, G., et al. (2022). Cell type diversity in a developing octopus brain. Nat. Commun. *13*, 7392.

23. Duruz, J., Sprecher, M., Kaldun, J.C., Al-Soudy, A.-S., Lischer, H.E.L., van Geest, G., Nicholson, P., Bruggmann, R., and Sprecher, S.G. (2023). Molecular characterization of cell types in the squid. Elife *12*. 10.7554/eLife.80670.

24. Songco-Casey, J.O., Coffing, G.C., Piscopo, D.M., Pungor, J.R., Kern, A.D., Miller, A.C., and Niell, C.M. (2022). Cell types and molecular architecture of the Octopus bimaculoides visual system. Curr. Biol. *32*, 5031–5044.e4.

25. Gavriouchkina, D., Tan, Y., Ziadi-Künzli, F., Hasegawa, Y., Piovani, L., Zhang, L., Sugimoto, C., Luscombe, N., Marlétaz, F., and Rokhsar, D.S. A single-cell atlas of bobtail squid visual and nervous system highlights molecular principles of convergent evolution. 10.1101/2022.05.26.490366.

26. Hamasaki, D.I. (1968). The ERG-Determined Spectral Sensitivity of the Octopus. Vision Res. *8*, 1013–1021.

27. Lange, G.D., and Hartline, P.H. (1974). Retinal responses in squid and octopus. J.Comp. Physiol. A *93*, 19–36.

28. Land, M.F., and Fernald, R.D. (1992). The evolution of eyes. Annu. Rev. Neurosci. *15*, 1–29.

29. Moccia, F., Cristo, C.D., and Di Cosmo, A. (2009). Lost in phototransduction: a few facts and hypotheses on cephalopod photoresponse. Front. Biosci. *1*, 319–328.

30. Brown, P.K., and Brown, P.S. (1958). Visual pigments of the octopus and cuttlefish. Nature *182*, 1288–1290.

31. Messenger, J.B., Wilson, a. P., and Hedge, A. (1973). Some evidence for colour-blindness in Octopus. J. Exp. Biol. *59*, 77–94.

32. Marshall, N.J., and Messenger, J.B. (1996). Colour-blind camouflage. Nature *382*, 408–409.

33. Tasaki, K., Oikawa, T., and Norton, A.C. (1963). The Dual Nature of the Octopus Electroretinogram. Vision Res. *3*, 61–73.

34. Norton, A.C., Fukada, Y., Motokawa, K., and Tasaki, K. (1965). An Investigation of the Lateral Spread of Potentials in the Octopus Retina. Vision Res. *5*, 253–267.

35. Hartline, P.H., and Lange, G.D. (1974). Optic nerve responses to visual stimuli in squid. J. Comp. Physiol. A *93*, 37–54.

36. Saidel, W.M., Shashar, N., Schmolesky, M.T., and Hanlon, R.T. (2005). Discriminative responses of squid (Loligo pealeii) photoreceptors to polarized light. Comp. Biochem. Physiol. A Mol. Integr. Physiol. *142*, 340–346.

37. Patterson, J.A., and Silver, S.C. (1983). Afferent and Efferent Components of Octopus Retina. J. Comp. Physiol. A *151*, 381–387.

38. Boycott, B.B., Lettvin, J.Y., Maturana, H.R., and Wall, P.D. (1965). Octopus Optic Nerve Responses. Exp. Neurol. *12*, 247–256.

39. Westheimer, G. (2007). The ON–OFF dichotomy in visual processing: From receptors to perception. Prog. Retin. Eye Res. *26*, 636–648.

40. Ichinose, T., and Habib, S. (2022). ON and OFF Signaling Pathways in the Retina and the Visual System. Front Ophthalmol (Lausanne) *2*. 10.3389/fopht.2022.989002.

41. Ryu, L., Kim, S.Y., and Kim, A.J. (2022). From Photons to Behaviors: Neural Implementations of Visual Behaviors in Drosophila. Front. Neurosci. *16*, 883640.

42. Fournier, J., Müller, C.M., Schneider, I., and Laurent, G. (2018). Spatial Information in a Non-retinotopic Visual Cortex. Neuron *97*, 164–180.e7.

43. Pickford, G.E., and McConnaughey, B.H. (1949). The Octopus Bimaculatus Problem: A Study in Sibling Species. Bulletin of the Bingham Oceanographic Collection *12*, 1–66.

44. Albertin, C.B., and Simakov, O. (2020). Cephalopod Biology: At the Intersection Between Genomic and Organismal Novelties. Annu Rev Anim Biosci *8*, 71–90.

45. Niell, C.M., and Smith, S.J. (2005). Functional imaging reveals rapid development of visual response properties in the zebrafish tectum. Neuron *45*, 941–951.

46. Garaschuk, O., Milos, R.-I., Grienberger, C., Marandi, N., Adelsberger, H., and Konnerth, A. (2006). Optical monitoring of brain function in vivo: From neurons to networks. Pflugers Arch. *453*, 385–396.

47. Piscopo, D.M., El-Danaf, R.N., Huberman, A.D., and Niell, C.M. (2013). Diverse Visual Features Encoded in Mouse Lateral Geniculate Nucleus. J. Neurosci. *33*, 4642–4656.

48. Chung, W.-S., and Justin Marshall, N. (2017). Complex Visual Adaptations in Squid for Specific Tasks in Different Environments. Frontiers Physiol. *8*, 105.

49. Grasso, F.W., and Basil, J.A. (2009). The evolution of flexible behavioral repertoires in cephalopod molluscs. Brain, Beh. and Evo. *74*, 231–245.

50. Saidel, W.M. (1979). Relationship Between Photoreceptor Terminations and Centrifugal Neurons in the Optic Lobe of Octopus. Cell Tissue Res. *204*, 463–472.

51. Chung, W.-S., Kurniawan, N.D., and Marshall, N.J. (2022). Comparative brain structure and visual processing in octopus from different habitats. Curr. Biol. *32*, 97–110.e4.

52. Zullo, L., Sumbre, G., Agnisola, C., Flash, T., and Hochner, B. (2009). Nonsomatotopic organization of the higher motor centers in octopus. Curr. Biol. *19*, 1632–1636.

53. Sanes, J.R., and Zipursky, S.L. (2010). Design principles of insect and vertebrate visual systems. Neuron *66*, 15–36.

54. Dowling, J.E. (2012). The Retina: An Approachable Part of the Brain, Revised Edition (Harvard University Press).

55. Behnia, R., Clark, D.A., Carter, A.G., Clandinin, T.R., and Desplan, C. (2014). Processing properties of ON and OFF pathways for Drosophila motion detection. Nature *512*, 427–430.

56. Leonhardt, A., Ammer, G., Meier, M., Serbe, E., Bahl, A., and Borst, A. (2016). Asymmetry of Drosophila ON and OFF motion detectors enhances real-world velocity estimation. Nat. Neurosci. *19*, 706–715.

57. Clark, D.A., Fitzgerald, J.E., Ales, J.M., Gohl, D.M., Silies, M.A., Norcia, A.M., and Clandinin, T.R. (2014). Flies and humans share a motion estimation strategy that exploits natural scene statistics. Nat. Neurosci. *17*, 296–303.

58. Emran, F., Rihel, J., Adolph, A.R., Wong, K.Y., Kraves, S., and Dowling, J.E. (2007). OFF ganglion cells cannot drive the optokinetic reflex in zebrafish. Proc. Natl. Acad. Sci. U. S. A. *104*, 19126–19131.

59. Zhou, M., Bear, J., Roberts, P., Janiak, F., Semmelhack, J., Yoshimatsu, T., and Baden, T. (2020). Zebrafish Retinal Ganglion Cells Asymmetrically Encode Spectral and Temporal Information across Visual Space. Curr. Biol. *30*, 2927–2942.e7.

60. Mazade, R., Jin, J., Pons, C., and Alonso, J.-M. (2019). Functional Specialization of ON and

OFF Cortical Pathways for Global-Slow and Local-Fast Vision. Cell Rep. *27*, 2881–2894.e5.

61. Cronin, T.W., Johnsen, S., Justin Marshall, N., and Warrant, E.J. (2014). Visual Ecology (Princeton University Press).

62. Chung, W.-S., and Marshall, N.J. (2016). Comparative visual ecology of cephalopods from different habitats. Proc. Roy. Soc. B *283*, 20161346.

63. Young, J.Z. (1962). The optic lobes of Octopus vulgaris. Philos. Trans. R. Soc. Lond. B Biol. Sci. *245*, 19–58.

64. Strother, J.A., Nern, A., and Reiser, M.B. (2014). Direct Observation of ON and OFF Pathways in the Drosophila Visual System. Curr Biol. *24*, 976–983.

65. Byrne, R.A., Kuba, M.J., and Meisel, D.V. (2004). Lateralized eye use in Octopus vulgaris shows antisymmetrical distribution. Animal Beh. *68*, 1107–1114.

66. Frasnelli, E., Ponte, G., Vallortigara, G., and Fiorito, G. (2019). Visual Lateralization in the Cephalopod Mollusk Octopus vulgaris. Symmetry *11*, 1121.

67. Shashar, N. (2014). Polarization Vision in Cephalopods. Polarized Light and Polarization Vision in Animal Sciences, 217–224. 10.1007/978-3-642-54718-8_8.

68. Fiorito, G., Affuso, A., Basil, J., Cole, A., de Girolamo, P., D'Angelo, L., Dickel, L., Gestal, C., Grasso, F., Kuba, M., et al. (2015). Guidelines for the Care and Welfare of Cephalopods in Research -A consensus based on an initiative by CephRes, FELASA and the Boyd Group. Lab. Anim. *49*, 1–90.

69. Fiorito, G., Affuso, A., Anderson, D.B., Basil, J., Bonnaud, L., Botta, G., Cole, A., D'Angelo, L., De Girolamo, P., Dennison, N., et al. (2014). Cephalopods in neuroscience: regulations, research and the 3Rs. Invert. Neurosci. *14*, 13–36.

70. Koizumi, M., Shigeno, S., Mizunami, M., and Tanaka, N.K. (2018). Calcium imaging method to visualize the spatial patterns of neural responses in the pygmy squid, Idiosepius paradoxus, central nervous system. J. Neurosci. Methods *294*, 67–71.

71. McCormick, L.R., Levin, L.A., and Oesch, N.W. (2019). Vision is highly sensitive to oxygen availability in marine invertebrate larvae. J. Exp. Biol. *222*. 10.1242/jeb.200899.

72. Brainard, D.H. (1997). The Psychophysics Toolbox. Spatial Vis. *10*, 433–436.

CELL TYPES AND MOLECULAR ARCHITECTURE OF THE *OCTOPUS BIMACULOIDES* VISUAL SYSTEM

* This chapter contains previously published co-authored material.

JO Songco-Casey, GC Coffing, DM Piscopo, JR Pungor, AD Kern, AC Miller, and CM Niell. Current Biology, Volume 32, Issue 23, 05 December 2022.

Author contributions: C.M.N. and A.C.M. conceived and oversaw the project. J.O.SC., D.M.P., and J.R.P. collected sequencing data. G.C.C. and A.D.K. performed genome assembly and annotation, J.R.P. performed cross-species gene identification, J.O.SC., A.C.M., and C.M.N. performed scRNA-seq analysis. J.O.SC. and D.M.P. performed FISH experiments. All authors contributed to writing and editing of the manuscript.

Introduction

Cephalopods represent a unique branch of the animal kingdom for studying vision. Coleoid cephalopods (octopuses, squids, and cuttlefish) have the largest brain among invertebrates[1–3], much of which is comprised of areas dedicated to visual processing: the optic lobes[4,5]. Their visual system facilitates a range of behaviors such as navigation, prey capture, and complex camouflage[1,6–8]. However, the neural basis of central visual processing in cephalopods is largely unknown.

Despite diverging over 500 million years ago, octopuses independently evolved camera-type eyes similar to those of vertebrates[9]. However, the neural organization of structures that process visual information is dramatically different in the two lineages. In contrast to the vertebrate retina, which is an intricate neural circuit with a diversity of cell types, the octopus retina consists only of photoreceptors and supporting cells[10,11]. The photoreceptors send axons into the central brain, targeting the optic lobes that lie directly behind the eyes[10] (Figure 1A). The optic lobes, which make up approximately two-thirds of the octopus' central brain[12,13], are where the

bulk of visual processing is hypothesized to occur[12–14]. Optic lobe outputs project to deeper brain regions, including those involved in learning/memory and motor behavior[12,15–19].

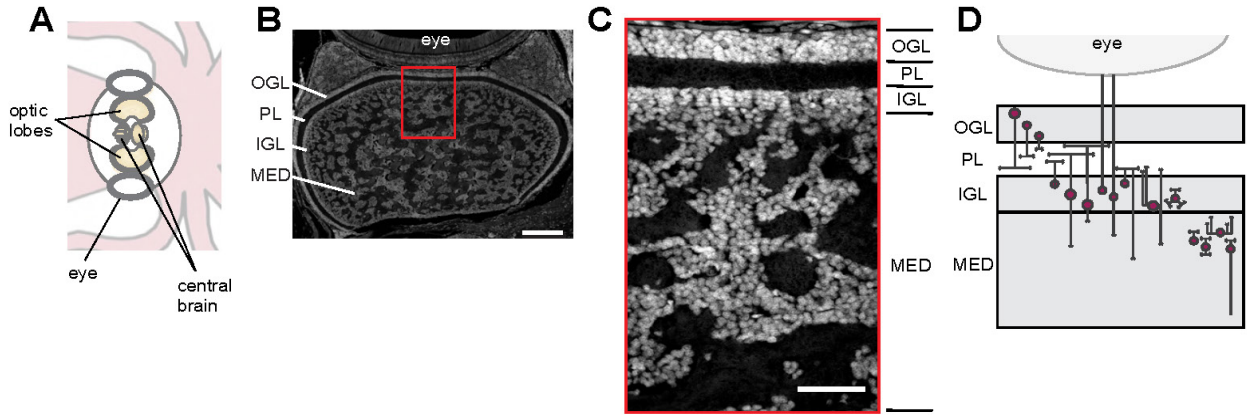

Figure 1. Laminar organization of *O.bimaculoides* optic lobes
(A) Schematic showing the octopus central nervous system, which includes optic lobes behind each eye and the central brain in between.
(B) Overview of one optic lobe and eye. Nuclei are stained with DAPI. Scale bar indicates 200 um. Red box denotes the region shown in C. OGL, outer granular layer; PL, plexiform layer; IGL, inner granular layer; MED, medulla.
(C) Laminar organization of the optic lobe demonstrated by nuclear staining of a cross-section. Scale bar indicates 50 um.
(D) Schematic of the anatomical organization of the visual system, in terms of neuronal morphologies, adapted from [5].

Histological studies by Young[5] have provided a description of the optic lobe's anatomical organization and neuronal morphologies (Figure 1B-D), which we briefly summarize here. The outermost region of the optic lobe is a cell body layer, termed the outer granular layer (OGL). The OGL contains cells traditionally referred to as amacrine cells based on their morphology[18,20], which have multipolar processes that ramify within the plexiform layer (PL) below the OGL. The PL is a dense neuropil and is the primary termination site of photoreceptor axons, optic lobe neuronal processes, and projections from deeper brain regions[12,20]. Below the PL is another cell body layer, the inner granular layer (IGL), which has a varied population including (1) neurons with bipolar morphology, (2) neurons that send centrifugal axons back to the retina, and (3) neurons of amacrine morphology with processes in the plexiform layer[12,18]. Finally, a deeper structure termed the medulla comprises the bulk of the optic lobe. The cells within the medulla are organized in a branching tree-like fashion which, in cross-section, appear as islands of cell bodies surrounded by neuropil[21]. The superficial region of the medulla is organized into columns

and is referred to as the outer radial columnar zone, whereas the deeper region of the medulla includes processes that extend tangentially and is termed the central tangential zone[5]. Given the anatomical organization, it has been hypothesized that the outer layers of the optic lobe (OGL, PL, IGL) may perform similar functions to the vertebrate retina, leading it to be termed the "deep retina"[22], while the medulla may engage in higher order processing analogous to central visual areas in other species[12].

While the anatomy of these cell classes suggest an organizational foundation, fully understanding the neural circuitry necessitates knowledge of the molecular identities of these cell types, including both functional determinants (e.g. neurotransmitter and receptor repertoires) and developmental determinants (e.g. transcription factors and adhesion molecules). Recent molecular taxonomies in other species have provided new insight into the circuit organization of a number of brain regions including the fly visual system[23], the mouse and primate retina[24,25] and the mouse visual cortex[26]. We therefore sought to create a systematic molecular characterization of the octopus visual system by combining single-cell RNA sequencing (scRNA-seq), to determine transcriptional cell types, with multiplexed RNA fluorescence in situ hybridization (FISH), to determine the location of these cell types within the optic lobe.

Results

ScRNA-Seq of the Octopus Optic Lobe

We performed scRNA-seq in juvenile (1.5 months of age) *Octopus bimaculoides*. Despite their continued growth throughout their lifetime (1-2 years), the overall body organization, behavior, and visual system of *O. bimaculoides* are mature by this age[27,28], allowing us to identify neural circuitry involved in a fully functioning, yet still growing, visual system. We performed Chromium 10x sequencing of cells from the optic lobes of two animals, processed separately as biological replicates, and aligned reads to an updated genome assembly and gene annotation using CellRanger (see Methods, Figure S1 and Table S1).

A robust scRNA-seq analysis requires a contiguous genome with accurate, full-length gene annotations. The first genome assembly of *O. bimaculoides* (Octopus_bimaculoides_v2_0) is

broken into over 150,000 scaffolds, with many split or truncated gene annotations. Alignment of our single cell reads to this genome therefore resulted in low mapping. To resolve this, we used single molecule high fidelity (HiFi) sequencing to create a new contig level genome assembly and combined new Iso-seq reads with existing bulk RNA-seq data to generate an improved genome annotation (see Methods, Figure S1 and Table S1) containing 5,437 contigs and 18,896 gene annotations. The new assembly is more contiguous and helped lengthen the 3' ends of many annotated genes, capturing more reads (Figure S1) and thus achieving higher resolution.

Using standard filtering, normalization, integration and clustering in Seurat[29,30], we identified a total of 28,855 cells across two biological replicates. Our analysis resulted in a total of 41 clusters, where each sample contributed cells to all of the identified clusters in similar proportions, supporting the reproducibility of this approach (Figure S2).

We first sought to broadly characterize the identified clusters in terms of neuronal and non-neuronal populations (Figure S3). We used a homologous sequence identifier, OrthoFinder[31], to assign gene-family and orthology relationships using genes from *Drosophila*, vertebrates, and other cephalopod species (see Methods, Figure S3A for example gene trees). Genes that were not assigned to orthology groups by OrthoFinder were manually annotated using NCBI BLAST[32] if possible. Throughout, we name the octopus genes according to their assigned identity: e.g. synaptotagmin (*syt*), as summarized in Table S2, although we note that these assignments may be improved as our understanding of gene homology in cephalopods advances.

We expected a large proportion of the cells to have high expression of genes related to mature neurons, as well as potentially developing neurons, as the octopus brain continues to grow and add neurons throughout its lifetime[33]. To identify neurons within our scRNA-seq data, we first looked at the expression of genes related to synaptic vesicle release. We found that most clusters (33/41) expressed the *O. bimaculoides* SNARE genes, while only seven were likely to be non-neuronal, based on the absence of expression of these markers (Figure S3). The non-neuronal clusters represented ~8% of the cells and had relatively high expression of genes falling within gene families with functions consistent with proliferation, blood, endothelium, and glia (Figure

S3). We used FISH to localize expression of non-neuronal genes and found several to be primarily expressed outside of the optic lobe (see Figure S3 for further characterization). We therefore removed these clusters from subsequent analyses that aimed to delineate neuronal cell types, which included a total of 26,092 cells across 33 clusters.

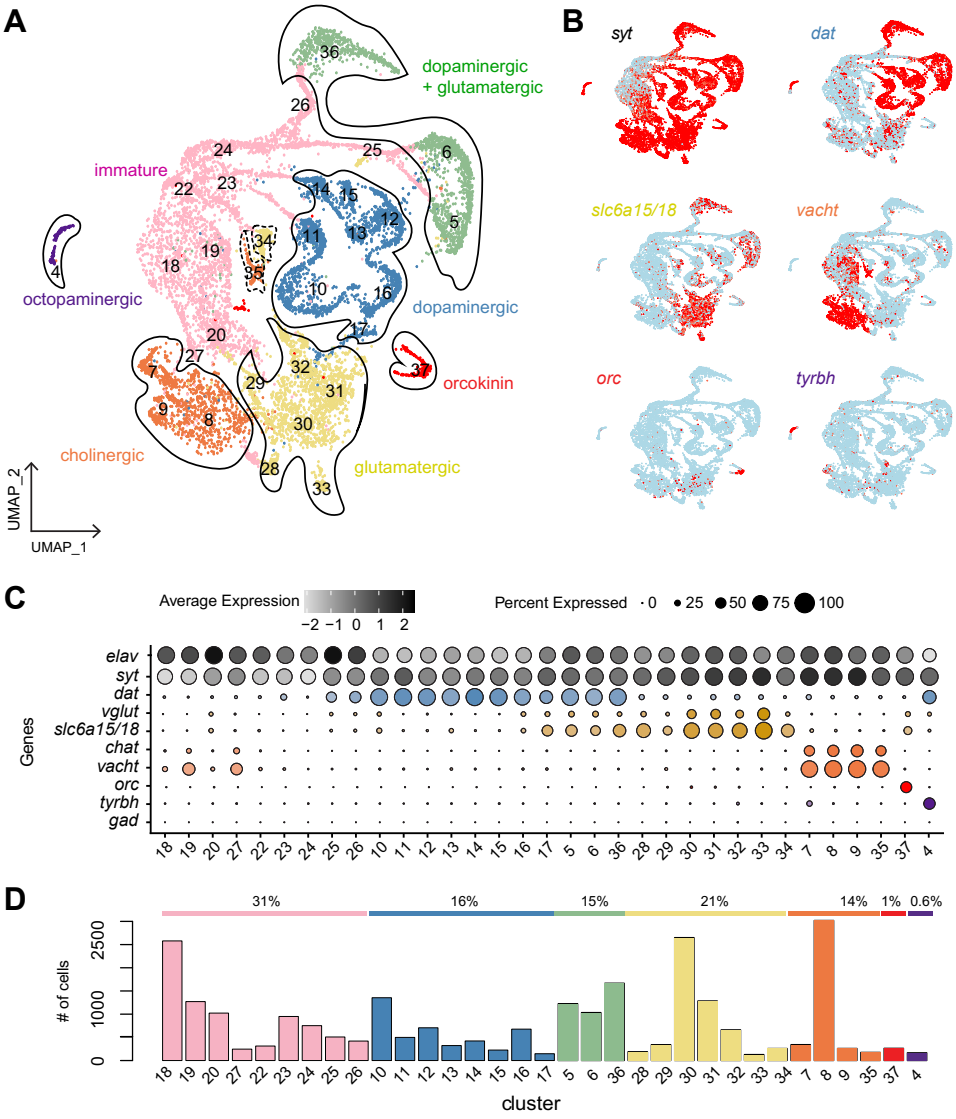

Figure 2. scRNA-seq reveals six major neuronal classes
(A) UMAP of putative neuronal clusters. A total of 33 clusters are color-coded based on major cell classes.
(B) Feature plots showing expression patterns of marker genes for neurons (*syt*) and neurotransmitter phenotypes (dopaminergic cells (*dat*), glutamatergic cells (*slc6a15/18*), cholinergic cells (*vacht*), orcokinin cells (*orc*), and octopaminergic cells (*tyrbh*).
(C) Dot plot of markers delineating molecular cell classes.

(D) Bar graph indicating total number of cells in each cluster as colored in (A) as well as the relative proportion of each cell class across the entire population of neurons in the optic lobe. See also Figures S1-S4, Tables S1-S2

To further explore the potential neural cell type classes within the scRNA-seq clusters, we first examined the expression patterns of markers for neurotransmitter usage (Figure 2). Previous work identified dopamine, glutamate, and acetylcholine as the primary neurotransmitters used in the cephalopod optic lobe[34], so we looked for standard markers of these neurotransmitter types based on their biosynthetic and vesicular packaging pathways (dopamine transporter (*dat*), vesicular glutamate transporter (*slc17a7*, or *vglut*), vesicular acetylcholine transporter (*slc18a3,* or *vacht*), and choline acetyltransferase (*chat*)) (Figures 2B-C, S4). In addition, we identified a gene in the solute carrier gene superfamily (*slc6a15/18*), which acts to support glutamate synthesis via transport of glutamate precursors[35] and was closely co-expressed with *vglut* in both scRNA-seq data (Figure 2C) and FISH (Figure S4). We used *slc6a15/18* as an additional marker of glutamatergic neurons along with *vglut*, since, despite strong FISH signal, we found a relatively low number of scRNA-seq reads aligned to *vglut*, which may be due to an incomplete gene model for this gene.

Together, scRNA-seq expression of neurotransmitter markers delineated the majority of putative neurons (22/33 clusters) into four broad classes defined by either unique or combinatorial expression of these genes (Figure 2B-C). Each of these broad categories consisted of a number of unique clusters (Figure 2A, C), suggesting further cell type heterogeneity within. In addition, two smaller neuronal clusters were identified, one of which did not express markers for any neurotransmitters, but did express the neuropeptide orcokinin (*orc*) (Figure 2B) and another that expressed a combination of *dat* and a marker for octopamine synthesis, tyramine beta-hydroxylase (*tyrbh*), previously identified in octopus optic lobe neurons[36]. We did not find a significant population of GABAergic neurons (based on expression of glutamate decarboxylase (*gad*), Figure 2C), consistent with previous findings of the minimal role of GABA in the optic lobe[37].

Finally, we found a large population of cells (9 clusters) that appear to be immature neurons, based on higher expression levels of early neural specification genes (i.e. embryonic lethal

abnormal vision (*elav*) and CUG triplet repeat RNA binding protein (*celf*)), lower levels of genes involved in synaptic transmission, and no expression of any neurotransmitter markers (Figures 2C, S3). As described below, this class of cells expressed a diversity of evolutionarily conserved developmental genes and distinct subgroups had expression profiles suggestive of a relationship to distinct mature cell clusters.

Taken together, these findings support the idea that the scRNA-seq data captured expression profiles of unique classes of mature and immature neurons in the optic lobe. We used these data to delineate molecular cell types and assign them to an anatomical organization within the octopus optic lobe.

A Molecular and Spatial Taxonomy of Mature Neural Cell Types

Our scRNA-seq data show that neurotransmitter usage divides the majority of octopus optic lobe neurons into four large classes – dopaminergic, dopaminergic+glutamatergic, glutamatergic, and cholinergic neurons – along with two smaller classes that utilize orcokinin or octopamine. To examine the localization of the four major neurotransmitter cell clases within the optic lobe, we performed FISH for *dat*, *slc6a15/18*, and *vacht* (Figure 3). Each of these neurotransmitter markers showed a distinct pattern of expression within the cell body layers of the OGL, IGL, and medulla (Figure 3B). Dopaminergic (*dat*+) cells were found predominantly in the OGL, with sparser expression in the IGL and medulla. Glutamatergic cells (*slc6a15/18+,* and see *vglut* in Figure S4) were found across the optic lobe, including in some *dat*+ cells in the OGL and IGL. Cholinergic cells (*vacht*+, and see *chat* in Figure S4) were restricted to the IGL and the medulla. As suggested by the scRNA-seq data (Figure 3A), glutamatergic and cholinergic neurons are segregated in their spatial expression patterns – both are expressed in non-overlapping cells in the IGL and medulla, with *slc6a15/18*+ expressed more strongly in the tangential region of the medulla and *vacht*+ expressed more strongly in the radial columnar region (Figure 3B). These mappings confirm that the scRNA-seq data identified distinct populations of neurons that correlate with distinct anatomical spatial expression patterns.

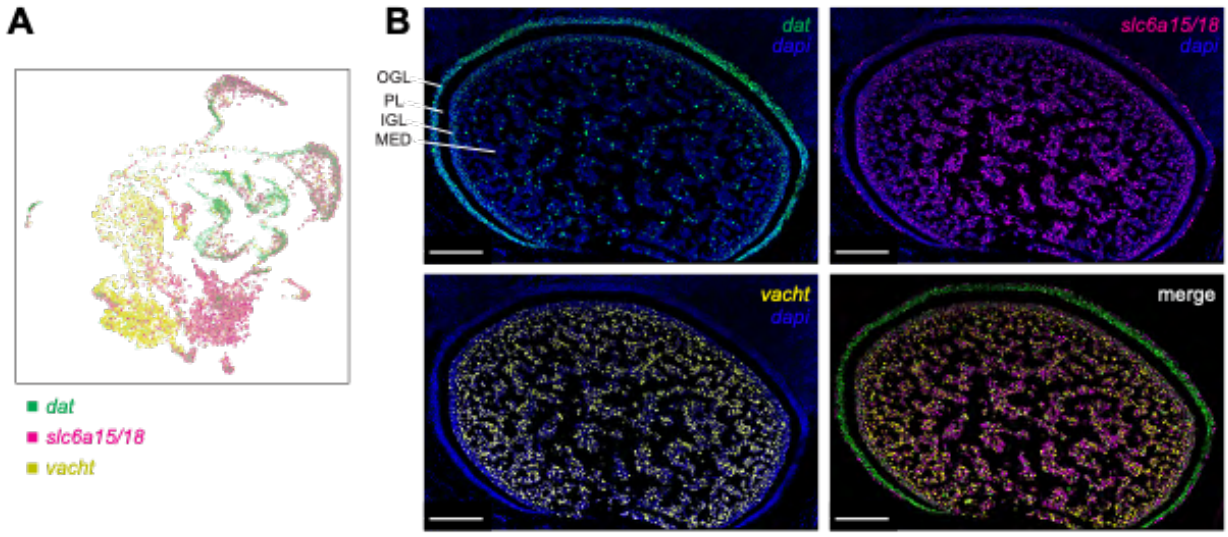

Figure 3. Neurotransmitter usage divides the majority of cells into four large populations
(A) UMAP of overlay of *dat*, *slc6a15/18*, and *vacht* expression.
(B) FISH of *dat*, *slc6a15/18*, *vacht*, with nuclei stained in DAPI, and merged FISH of the three neurotransmitter-related genes. Scale bars represent 100um. Here and below, merged images are shown without DAPI to emphasize relative expression patterns.
See also Figure S4, Table S2

Within each of the large neurotransmitter-defined populations, further transcriptional heterogeneity was present, suggesting that the clusters within these populations may correspond to neuronal subtypes (Figure 2). We sought to determine if such cell types, as identified by their unique gene expression profiles, would occupy distinct anatomical locations within the optic lobe.

Dopaminergic Neurons

In the scRNA-seq data, dopaminergic neurons spanned seven clusters (Figure 2), and *dat*+-only neurons were predominantly localized to the OGL (Figure 3B). We examined gene expression across *dat*+ clusters and found two subgroups defined by the complementary expression of either the homeobox transcription factor *six4/5* (clusters 12-17) or the neuropeptide *fmrf* (clusters 10-11) (Figure 4A). Across model species, the *six* family of genes are key regulators in head development[38], eye specification, and retinal determination[39–41]. *fmrf* neuropeptides are known to regulate a variety of functions in mollusks[42], including reproduction[43] and chromatophore

control[44,45]. FISH revealed that within the *dat*+ cells in the OGL, the *six4/5*+ population represented a broad sub-layer of neurons in the middle of the OGL, while *fmrf* expression corresponded to a sub-layer of neurons deeper in the OGL, along the border of the plexiform layer. Thus, the *dat*+-only cells contain two subtypes that are differentiated by expression of a homeobox transcription factor and a neuropeptide respectively. Notably, these are mainly localized within the OGL and hence likely represent a subset of the amacrine neurons of Young's anatomical classifications[5].

Expression heterogeneity of additional genes suggested these two dopaminergic cell groups can be further subdivided. The clusters within the *six4/5*+ group differentially express several genes encoding neuropeptides (*pxfv*, *lxgkr*, and *flri*) which are largely non-overlapping, though FISH reveals a low level of co-expression (Figure 4A, see Figure 7D). This set of neuropeptides is particularly interesting as they were manually assigned identities based on repetitive protein sequences, but there is little information regarding their function in other organisms, let alone cephalopods. Further, a subset of cells within the *fmrf*+ group expresses the adhesion molecular *dscam*, which has been shown to mediate cell-type specific self-avoidance among dopaminergic amacrine cells[46] and sublayer-specific connectivity in amacrine and bipolar cells[47] in the vertebrate retina. *dscam*+ cells form a discrete narrow band along the deep border of the OGL and the plexiform layer (Figure 4A), suggesting *dscam* could play a role in assigning their sublayer specificity. Together, these data demonstrate further heterogeneity within dopaminergic cell types in the OGL, identifying laminar organization from the superficial to deep layers.

Dopaminergic + Glutamatergic Neurons

Based on the co-expression of *dat* and *slc6a15/18* in both the scRNA-seq and FISH data, we sought to further delineate this cell class. The scRNA-seq clusters with overlapping *dat* and *slc6a15/18* expression suggested that two prominent groups, clusters 5/6 and 37, might correspond to subtypes. Furthermore, the expression of *dat* and *slc6a15/18* significantly overlapped in both the OGL and IGL, suggesting that these two locations might correspond to the two groups (Figure 3A-B).

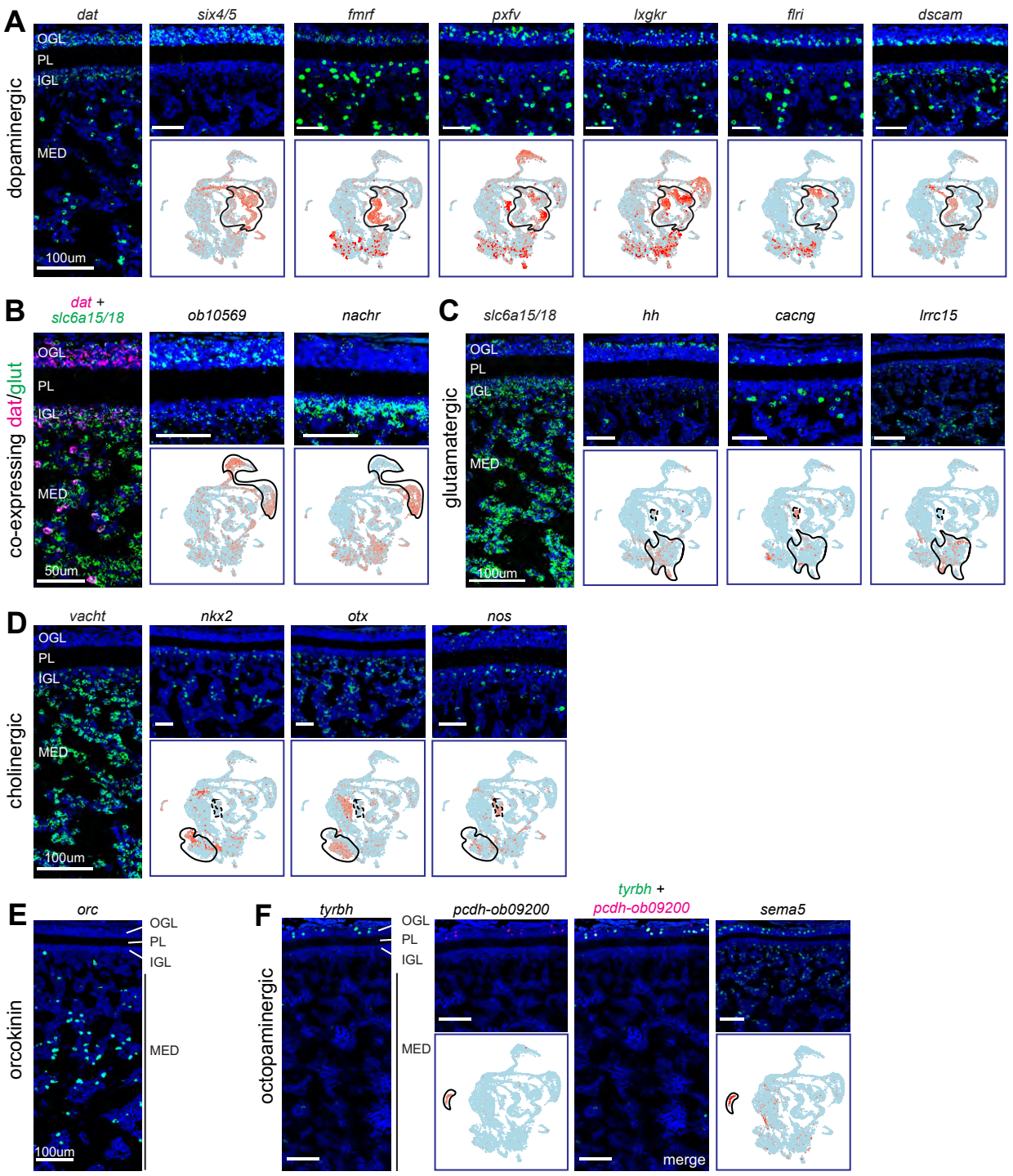

Figure 4. Anatomical organization of major cell classes and subtypes based on scRNA-seq and FISH
(A) Dopaminergic neuron organization. *dat*+ cells are divided into two major subtypes based on the additional differential expression of either *six4/5*+ or *fmrf*+, depicted through FISH and scRNA-seq feature plots.

Corresponding cell classes are outlined in black on the feature plots, nuclei are stained with DAPI (blue), and scale bars represent 50um.
(B) Neuron organization for scRNA-seq clusters that co-express *dat* and *slc6a15/18*.
(C) Glutamatergic subtype neuron organization.
(D) Cholinergic subtype neuron organization.
(E) Orcokinin neuron organization.
(F) Octopaminergic neuron organization. From left to right: *tyrbh*, *pcdh-obimac0009200*, double FISH of *tyrbh* and *pcdh-obimac0009200*, and a single FISH of *sema5*.
See also Table S2, Methods S1

The currently uncharacterized gene *obimac0010569* (see Methods S1 for further information) was uniquely expressed in cluster 37, and FISH revealed that these cells were located in the OGL (Figure 4B). This represents an additional population of OGL neurons, beyond the dopaminergic neurons discussed above. On the other hand, a nicotinic acetylcholine receptor (*nachr*) was expressed in clusters 5/6, and these were localized to a broad band in the IGL (Figure 4B). Together, these data demonstrate that the scRNA-seq dopamine+glutamatergic clusters consist of two distinct subtypes, one in the OGL (*obimac0010569+)* and one in the IGL (*nachr+)*.

Glutamatergic Neurons

We next focused on the subtypes of putative glutamatergic neurons, which include several smaller clusters (33-34, 28) in addition to a set of larger clusters (29-32) (Figure 2A). Examining genes in the smaller clusters revealed that these contain further subtypes. The first cluster (33) was defined by hedgehog (*hh*), a signaling molecule involved in axon guidance and patterning in the nervous system across many species[48]. FISH showed that *hh+ cells* are mainly restricted to a narrow band of neurons in the most superficial OGL, identifying yet another subtype within the OGL (Figure 4C). A second cluster (34) is marked by the voltage gated calcium channel gamma subunit 5/7 (*cacng*), which FISH demonstrated corresponds to a narrow band of neurons at the border of the IGL and medulla (Figure 4C). Finally, a third cluster (28) specifically expressed a member of the leucine-rich repeat family of cell adhesion molecules (*lrrc15*), which is involved in cell-type specific synaptic connectivity in fly and mammalian nervous systems[49]. This group was localized to the deeper region of the medulla (Figure 4C). Within the larger set of glutamatergic clusters (29-32), we found that a subset of neurons express vesicular amine transporter 1 (*slc18a1*, or *vat1*), which FISH demonstrated to also be localized to cell bodies in

the deeper region of the medulla (Figure 7F). Thus, the glutamatergic neurons primarily constitute a large population of cells within the medulla, along with two subtypes with highly specific sublayer localization within the outer OGL and inner IGL.

Cholinergic Neurons

The last neurotransmitter class of cells in the octopus optic lobe is the putative cholinergic neurons. scRNA-seq data revealed a large population of cells (clusters 7-9) and a much smaller population (cluster 35) that both express *vacht*, a marker for cholinergic transmission. FISH for *vacht* showed that cholinergic neurons are located throughout the medulla, with more restricted expression in IGL (Figures 3B, 4D). Moreover, the scRNA-seq data revealed that clusters that comprise this larger population can be delineated based on the expression of family members of two homeobox transcription factors, *nkx2* and *otx*. FISH for these two markers demonstrated that the *nkx2*+ population is located in the IGL and superficial region of the medulla, while the *otx*+ population is not expressed in the IGL and, instead, is found throughout the medulla (Figure 4D). In exploring the scRNA-seq data, we found that the *nkx2*+ cluster also expresses a protocadherin (*obimac0026462*), and FISH confirms that *obimac0026462*+ cells are expressed both in the IGL and medulla (Figure 7E).

We observed that neurons in the smaller cholinergic cluster (35) selectively express nitric oxide synthase (*nos*), suggesting that they represent a distinct cell type that uses this neuropeptide as a signaling molecule in addition to acetylcholine. FISH for *nos* revealed these neurons form a narrow sub-layer within the superficial to central IGL (Figure 4D). scRNA-seq data show that *nos*+ cells and the glutamatergic *cacng*+ cells, both in the IGL, also express an unidentified gene *obimac0022194* (see Methods S1), suggesting that these clusters may have some shared function based on expression of this unidentified gene.

Thus, the cholinergic neurons constitute a large population of the IGL and medullar cells, with distinct anatomical positions defined by a small sub-layer of *nkx2*+ cells in the IGL and superficial medulla, *otx*+ cells throughout the medulla, and *nos*+ cells mainly in the superficial IGL.

Orcokinin and Octopaminergic Neurons

We sought to determine the identity of the two remaining mature neuronal clusters (37 and 4), which were defined by highly specific expression of *orc* and *tyrbh*, respectively (Figure 2A-C). Cluster 37 did not express any of the neurotransmitter markers we assessed, but was demarcated by the expression of the neuropeptide *orc,* and FISH revealed that *orc*+ cells are a sparse, scattered population throughout the deeper region of the medulla (Figure 4E). The final cluster of mature neurons, cluster 4, selectively expressed a number of genes, including *tyrbh*, the synthetic enzyme for octopamine, generally considered to be the invertebrate analog of norepinephrine[50], which plays a role in arousal and other aspects of behavioral state across species. FISH showed a discrete population of octopaminergic *tyrbh*+ neurons in the OGL (Figure 4F). Among the other genes that were unique to this cluster is a protocadherin family member (*obimac0009200*), which co-expresses with *tyrbh* exclusively in the OGL (Figure 4F), and semaphorin-5 (*sema5*), which is highly expressed in the same region of the OGL, along with some expression throughout the medulla (Figure 4F). Thus, this cluster also expresses genes that serve as adhesion molecules (protocadherin *obimac0009200*) and axon guidance cues (*sema5*) in the visual system of other species[51,52].

Immature Neurons

Finally, we examined the putative immature neuronal clusters, representing 31% of all neurons, which were identified in the scRNA-seq data based on lower expression of *syt* and the absence of mature neurotransmitter markers. We observed that in the U-MAP these clusters were organized into several ‘arms’, suggesting that they may represent discrete populations of developing neurons associated with mature cell types (Figure 2A). One unidentified gene (*obimac0011980*) appears to encompass all nine immature clusters (Figure 5A-B, see Methods S1 for further characterization). The immature clusters can then be segregated into three subgroups that are demarcated by complementary expression of genes: a previously unidentified gene *obimac0032150* which contains a tumor necrosis factor receptor domain (*tnfr;* clusters 18-20, 27), myoneurin (*mynn;* clusters 22-24), and big brain (*bib;* clusters 25-26) (Figure 5A-B), all of which are known to play a role in neural development in other species. Since these three genes

segregate the population of immature neurons, we used FISH to identify the expression and examine their relationships to the location of the mature cell types described above (Figure 5C).

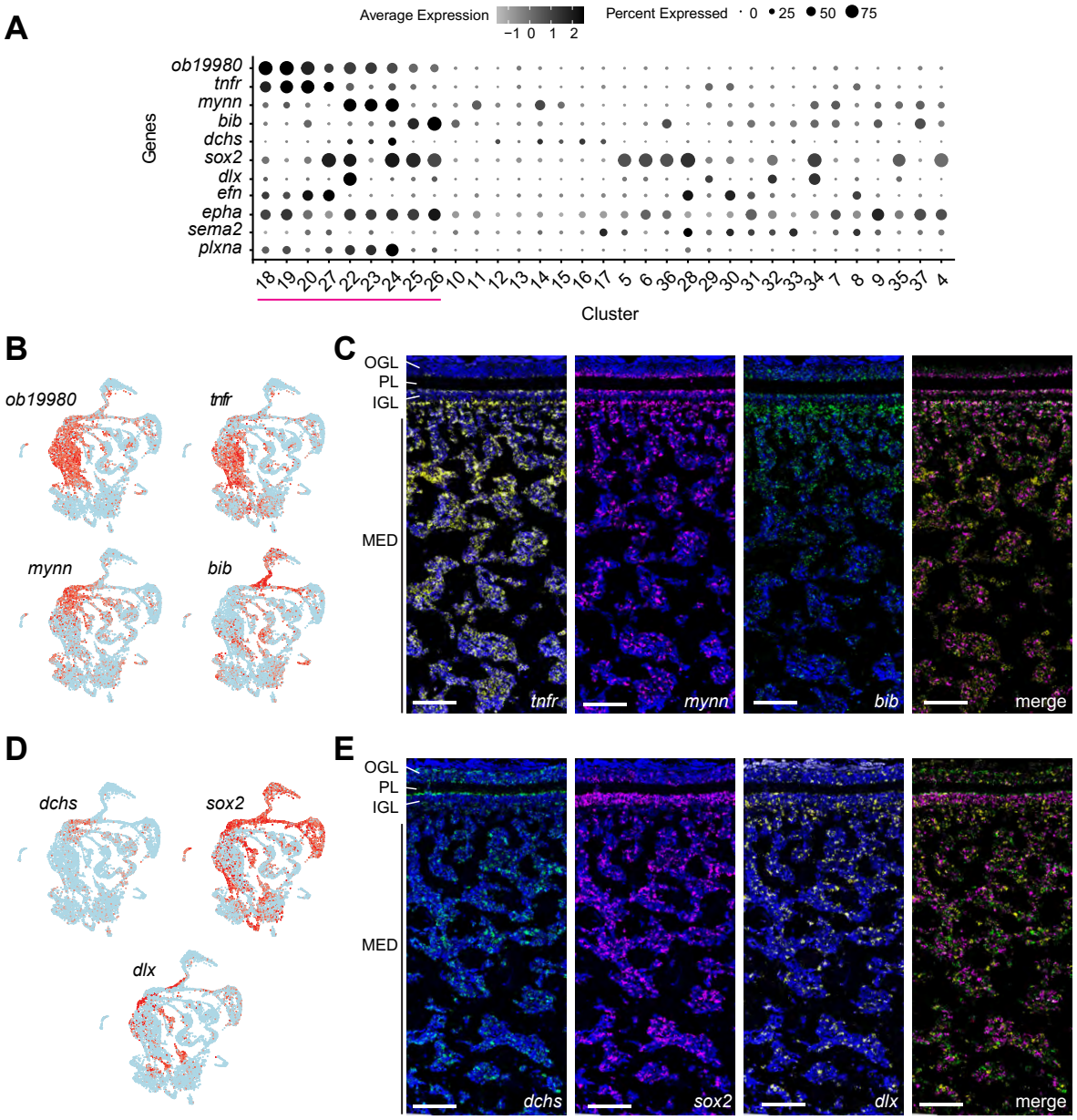

Figure 5. Gene expression and spatial organization of putative immature neurons
(A) Dot plot of genes expressed in immature neurons, with magenta line highlighting immature clusters.
(B) Feature plot of uncharacterized cephalopod-specific gene *obimac0019980*, which demarcates the putative immature neuronal clusters, as well as three genes that define distinct subgroups within the immature neurons: *tnfr*, *mynn*, and *bib*.
(C) FISH of the genes delineating the three subgroups shown in B, including a merged FISH. Throughout this figure, DAPI is shown in blue on individual FISHs, and scale bars indicate 100um.

(D) Feature plots of additional markers from development-related gene family trees demonstrating further cell type diversity.
(E) FISH showing anatomical organization of the genes shown in D, including a merged FISH.
See also Table S2, Methods S1

In the first sub-group, *tnfr* expression appeared in scRNA-seq clusters that are transcriptionally related to mature clusters of cholinergic and glutamatergic neurons (Figures 2A, 5B), which are largely found in the medulla. FISH data for *tnfr* revealed more extensive expression in the medulla, compared to the other putative immature subtypes (Figure 5C). In the second sub-group, scRNA-seq data showed that *mynn*, a zinc finger protein family member associated with neuromuscular synapse formation in mice[53], is expressed in a number of clusters in the "arms" leading to mature cell types for dopaminergic neurons of the OGL (Figures 2A, 5B). Correspondingly, FISH data shows that the *mynn*+ cell types border the plexiform layer along both the OGL and IGL, together with some cells in the medulla (Figure 5C). In the third subgroup, *bib,* a known neurogenic molecule in *Drosophila*[54], was expressed in "arms" leading to the clusters that correspond to the two prominent clusters of dopaminergic+glutamatergic neurons (Figures 2A, 5B). We found *bib* was expressed most strongly, though not exclusively, in cells along the bottom borders of the IGL and OGL (Figure 5C). As mentioned above, all of these subgroup markers are also expressed throughout the medulla, suggesting they may represent the ongoing migration of immature neurons into the optic lobe. They also have increased expression in stratifications along the borders of the OGL and IGL, raising the possibility that the laminar borders may be an important locus for the incorporation of immature neurons.

Other known developmental genes (Figure 5A, D) were expressed in the immature clusters in the scRNA-seq data, and we investigated the expression patterns of three of these genes using FISH: *dschs, sox2, and dlx* (Figure 5E). We also identified two receptor-ligand pairs that have well established roles in patterning the nervous system in vertebrates and other invertebrates[51,55] - ephrin (*efn*)/Eph receptor (*epha)* and semaphorin-2 (*sema2*)/plexin (*plxna*) - all of which had complementary expression patterns to each other across the scRNA-seq data (Figure 6A-B). Graded expression of ephrins and semaphorins, and their respective receptors, play important

roles in establishing large-scale organization during development in other species, including topographic map formation[51,55]. Notably, the ligand-receptor pair *efn* and *epha* were expressed in opposing gradients from superficial to deep in the optic lobe (Figure 6A). Likewise, *sema2* was expressed in a gradient with strongest expression in the deep medulla, while its potential receptor *plxna* had stronger expression along the borders of the OGL and IGL (Figure 6B).

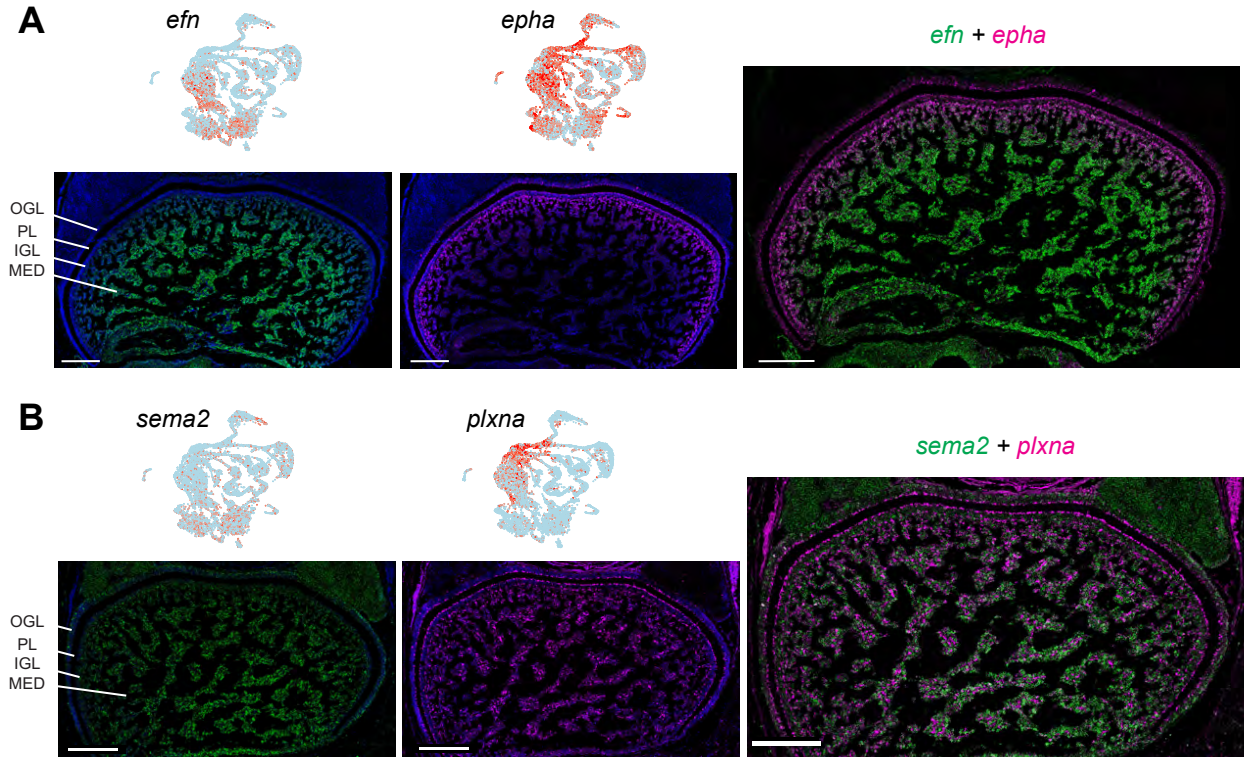

Figure 6. Expression of conserved patterning molecules
(A) Feature plots showing complementary scRNA-seq expression of an ephrin/Eph-receptor pair. FISH for these genes shows corresponding gradients of expression.
(B) Feature plots showing scRNA-seq complementary expression of a semaphorin/plexin pair. FISH for these genes shows corresponding spatial patterns of expression. In A,B, nuclei are stained with DAPI in blue, and scale bars indicate 200 um.
See also Table S2

Together, these data demonstrate that these putative immature neurons are found in distinct anatomical locations with discrete subtypes that can be molecularly defined. Moreover, conserved families of developmental genes, as well as novel cephalopod- or octopus-specific

genes, define these subtypes, suggesting the possibility of both evolutionarily conserved and lineage-specific molecular mechanisms for development and function.

Cell-Type and Sub-Layer Organization of Mature Neurons in the Optic Lobe

A driving goal of this project was to identify the "parts list" of the octopus optic lobe and create an integrated model of cell type organization within their visual system. We therefore incorporated the findings for the mature neurons into a schematic spatial map of the optic lobe (Figure 7A-B). Here, we summarize this organization, and present multiplexed FISH data for markers within each layer to explicitly demonstrate the sub-layer organization.

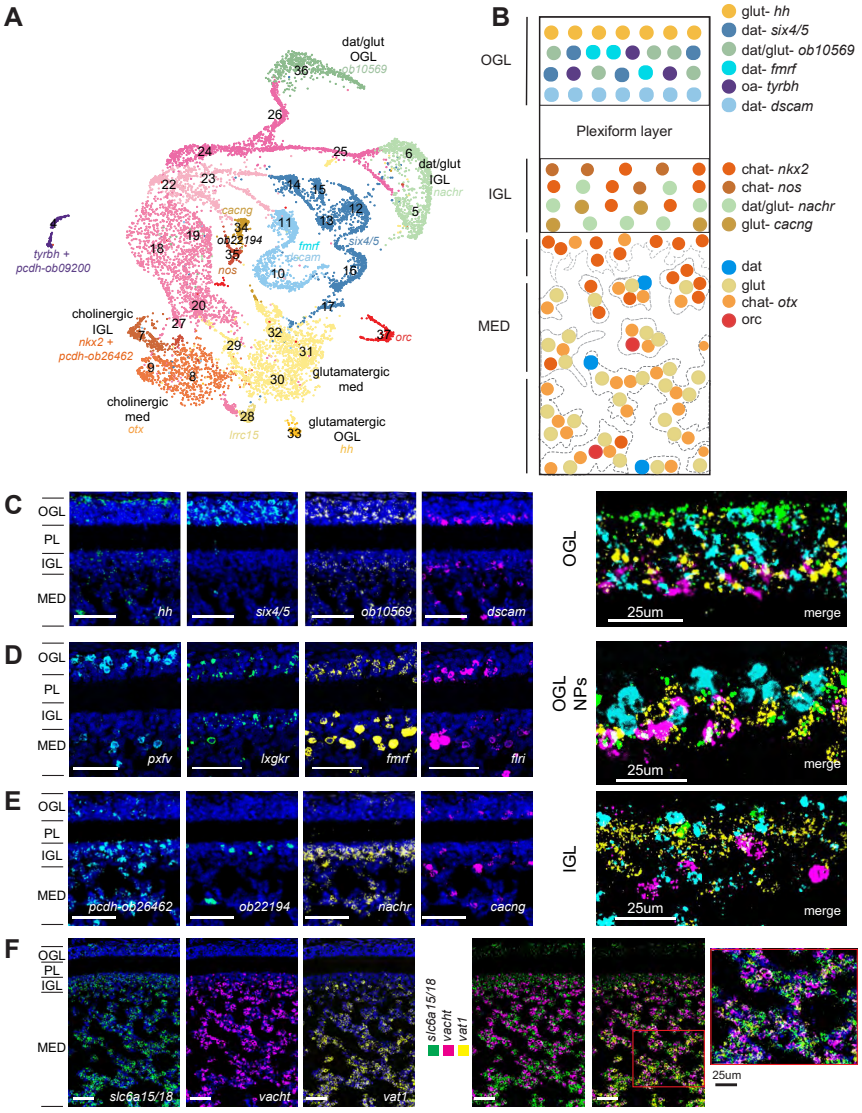

Figure 7. Summary of mature neuronal architecture

(A) UMAP showing cell subtypes in each neuronal class, along with annotation of spatial localization within the optic lobe.
(B) Schematic of cell type organization of the optic lobe. Genes defining subtypes are color-coordinated to match their clusters in (A).
(C) FISH showing sublayers of the OGL. Sublayers of OGL are demarcated from most superficial to deepest in order by expression of *hh*, *six4/5*, unidentified gene *obimac0010569*, and *dscam*. Throughout this figure, nuclei are stained with DAPI in blue, and, unless otherwise noted, scale bars represent 50um.
(D) FISH of neuropeptides that subdivide dopaminergic neurons in the OGL. In order from most superficial to the deepest: *pxvf*, *lxgkr*, *fmrf*, and *flri*.
(E) FISH showing sublayers of IGL based on expression of *pcdh-obimac0026462* , unidentified gene *obimac0022194*, *nachr*, and *cacng*.
(F) FISH showing organization of the medulla. The medulla has cell body islands with non-overlapping expression of populations of glutamatergic (*slc6a15/18+*) and cholinergic (*vacht+*) neurons, while *vat1* is expressed in a subset of medulla cell bodies.
See also Table S2, Methods S1.

Outer Granular Layer

We found four broad groups of cell types within the OGL (Figure 7C). First, a cluster of glutamatergic cells lines the most superficial aspect of the OGL, which also expresses *hh*. Second, one group of neurons from the dopaminergic+glutamatergic clusters is located in the central OGL, marked by an uncharacterized gene *obimac0010569*. Third, we identified a specific subset of octopaminergic neurons that co-expresses *tyrbh* and *pcdh-ob09200*. Finally, a diverse group of dopaminergic-only neurons spans sublayers of the OGL. This group falls into two major divisions: *six4/5+* in the central OGL and *dscam+* in the deep OGL. Notably, the expression of neuropeptides within the *dat+* group also shows a progression across the depth of the OGL (Figure 7D).

Inner Granular Layer

We found significant cell type diversity within the IGL (Figure 7E), consisting of at least four neuronal cell types with distinct sub-layer expression patterns. The largest population of cells therein consists of neurons from one of the dopaminergic+glutamatergic clusters, which forms a distinct band as identified by expression of an *nachr*. A small population of cholinergic neurons expressing *nos* lines the superficial IGL (*obimac0022194+* is shown in Figure 7E as proxy for *nos+* cells), while a sub-group of glutamatergic neurons (*cacng*) lines the deep IGL. In addition, the *nkx2+* cholinergic group spans from the IGL into the medulla (Figure 7E includes *obimac0026462* in place of *nkx2*).

Medulla

The medulla comprises a majority of the octopus optic lobe, and largely consists of two distinct populations of glutamatergic and cholinergic neurons (Figure 7F), with glutamatergic neurons more prevalent in the central tangential region. Notably, these are intermingled within the cell body "islands" of the medulla, suggesting that, at least at the level of these two large populations, there is no functional segregation across the islands. However, there are apparent distinctions in gene expression across the depth of the medulla. Within the cholinergic group, *nkx2*+ neurons are more superficial, while *otx*+ neurons are located throughout the medulla (Figure 7B). In addition, there is a superficial-to-deep gradient of *vat1* expression that is shared across the cholinergic and glutamatergic neurons (Figure 7F). Finally, there are sparse populations of neurons that express extremely high levels of neuropeptides (Figure 4A, E). It is possible that these represent neurons projecting to downstream brain regions where these neuropeptides could play a role in regulating behavioral outputs[12,16,18,19,56].

Discussion

This study provides a comprehensive molecular description of neural subtype organization of the optic lobe cell types, to complement the anatomical descriptions provided by Young[5]. In addition to identifying non-neuronal and developing cells in our dataset, we reveal six major cell classes of mature neurons and a number of subtypes within these that correlate with discrete locations of the optic lobe, uncovering previously unknown cell type diversity and sub-layer organization of the octopus visual system. This study thereby contributes to a recently growing literature on transcriptomics of the cephalopod nervous system[57–59] and lays the basis for both the investigation of the role of distinct cell types in visual processing as well as the development of tools for targeting specific cell classes based on their molecular signatures. In addition to revealing the overall molecular architecture of the optic lobe, a number of the specific findings shown here have implications for elucidating the functional and development of the octopus visual system.

We found a wide array of cell types within the OGL, which was previously shown to consist of amacrine cells. Among the three broad classes of amacrine cells in the OGL that Young described[5], we found at least eight clusters of specific cell types that all have distinct spatial localizations within sublayers of the OGL (Figure 7C-D). These cell types are defined by neurotransmitters (largely dopaminergic but also some glutamatergic), neuropeptides, a transcription factor (*six4/5*), an adhesion molecule (*dscam*), and a developmental signaling molecule (*hh*). This array of cell types bears a strong resemblance to the diversity of amacrine cells in the vertebrate retina, where over 60 amacrine cell types have been identified in mice[60]. However, in contrast to vertebrates, where amacrine cells primarily express the inhibitory neurotransmitters GABA or glycine[61], in the octopus we find that OGL neurons are predominantly dopaminergic. Notably, there is a specific population of dopaminergic amacrine cells in the vertebrate retina[62], and it has been shown that dendritic tiling in these amacrine cells is dependent on *dscam*[46], which strikingly is also expressed in a subset of dopaminergic OGL cells here. Moreover, in the vertebrate retina, distinct amacrine cell classes have been linked to a range of specific visual computations[63]. It will be intriguing to see whether similar functions can be assigned to the diversity of cells within the OGL based on the markers we have identified.

We identified a sparse but highly distinct population of neurons in the OGL that express *tyrbh*, the synthetic enzyme for octopamine. In both flies and mice, locomotion and arousal have profound effects on visual processing[64–66], which, in flies, are mediated by octopamine[67], and in mice are mediated in part by norepinephrine[6850]. Strikingly similar impacts of arousal on visual responses in octopuses were observed in an early study in the octopus EEG[69], suggesting a potential similar role for this octopaminergic system.

Another notable finding is the delineation of a large population of putative immature neurons within the octopus visual system. *O. bimaculoides* are born capable of feeding and living independently from hatching, relying on a variety of visually guided behaviors[27,28]. Despite this, octopuses continue to grow exponentially in size throughout their lifetime[70], increasing their mass by approximately 10x every two months, including growth of the optic lobes and other brain regions[71,72]. Hence, the finding of such a large population of immature neurons is not

surprising given the octopus's need for neurogenesis in order to support such massive brain growth. It has recently been shown in octopus embryos that neurogenesis occurs outside of the optic lobe, followed by long-distance migration into the optic lobe[73]. Therefore the immature population we observe likely represents post-mitotic, developing neurons that have recently completed migration, rather than a neurogenic population within the optic lobe itself.

In fish and birds, the visual system continues to grow throughout the animal's lifetime by expanding along the periphery in a proliferative marginal zone[74]. By contrast, we find that the immature neuronal population in the octopus is broadly distributed tangentially across the optic lobe, though with potential radial stratification along the borders of the OGL and IGL. Future work examining the ongoing developmental expansion of the optic lobe will be needed to reveal how new neurons coordinate their integration into the fully functioning visual system of the growing octopus.

We found genes associated with both the immature and mature cell types that may contribute to developmental establishment of identity, connectivity, and function, including both conserved (e.g. *hh, dscam, nkx, bib, pcdhs*) and novel (*obimac0011980, obimac0010569*) genes. We also identified subtypes within immature cell populations that are associated with mature neuronal cell types, suggesting different developmental trajectories and progenitor populations. Another striking developmental finding is the presence of complementary expression of ephrin/Eph-receptor and semaphorin/plexin pairs in the optic lobe, suggesting that these receptor-ligand pairs may play a similar role in setting up the spatial organization of the visual system as they do in flies and vertebrates.

Implications for Future Studies

We note that although we have delineated a number of subtypes within the major populations of cells in the octopus optic lobe, there is almost certainly additional diversity to be explored in future studies. Indeed, studies of the vertebrate retina have progressed from the early delineation of five major neuronal cell types to our current understanding of the tremendous diversity within each of these, including 30+ cell types within the retinal ganglion cells alone[75]. This initial

description of cell types for the octopus visual system that we provide here can serve as a basis for delving further into such diversity.

In the current study, we defined cell types in the octopus visual system based on gene expression and related these cell types to their anatomical location. Future studies that relate these cell types to other aspects of neural identity, including anatomical morphology via single-cell labeling, downstream projection targets based on retrograde tracing, and visual response properties identified through calcium imaging, will be crucial in decoding cephalopod visual function. The molecular mapping we present here provides a roadmap for such studies and more generally provides a path forward towards cracking the functional, developmental, and evolutionary logic of the cephalopod visual system.

Methods

Experimental Model and Subject Details

Octopus bimaculoides were obtained from the Cephalopod Resource Center at the Marine Biology Laboratory (Woods Hole, MA) and from Aquatic Research Consultants (San Pedro, CA). They were kept at the University of Oregon in a closed circulating 250 gallon aquarium system in artificial seawater, and fed daily on a rotating diet of frozen shrimp, crabs, and fish. All husbandry and experimental protocols were in accordance with the EU 2010/63/EU[76] and AAALAC guidelines for the use and care of cephalopods for research.

Method Details

Genome Sample Collection and Sequencing

Optic lobe tissue was dissected from an adult female *O. bimaculoides* for whole genome sequencing. Tissue was sent to the University of Oregon Genomics & Cell Characterization Core Facility (GC3F) for DNA extraction and sequencing. High molecular weight genomic DNA was extracted using a Nanobind Tissue Big DNA kit (Circulomics). A Pacific Biosciences standard HiFi library was prepped with a SMRTbell Express Template Prep Kit 2.0. Genomic DNA was sheared at 20kb target size with a Megaruptor 2 instrument (Diagenode). BluePippin size selection (Sage Science) was used to omit the smallest fragments (<10-14kb) to enrich for longer

fragments. Two HiFi genomic circular consensus sequencing (CCS) SMRTbell libraries were prepared as input for five HiFi SMRT cells. Single molecule sequencing of both libraries was conducted with a PacBio Sequel II system. After sequencing, data was imported into SMRT Link to generate 5.8 million HiFi reads with the CCS algorithm and create fastq files.

Four tissues were dissected from 6 week old juvenile octopuses to be used in Iso-Seq sequencing: optic lobe, central brain, retina, and arm. RNA extractions were performed using a RNeasy Plus Mini Kit (QIAGEN). A single bulk non-barcoded SMRTbell Iso-Seq library was prepared according to the manufacturer's protocol (PacBio) by GC3F. A multiplexed Iso-Seq library was sequenced across a single PacBio Sequel II SMRT cell. IsoSeq3 in SMRT Link was used to generate fastq files containing 1.08 million full-length transcripts.

Genome Re-assembly and Annotation

We used HiFiASM v0.15.5-r352[77] to assemble a contig-level genome with HiFi reads as input and default parameters. After initial assembly, duplications were removed using Purge_dups[78]. Protein-coding genes were annotated using existing bulk RNA sequences and our newly generated Iso-Seq data. Bulk RNA data was aligned to the genome assembly using Hisat v2.2.1[79] and gene predictions were assembled with StringTie v2.1.6[80] using parameters -c 4 -m 200 -j 3. All other parameters were set to default. To generate gene predictions with Iso-Seq data, we mapped the full length, non-chimeric reads (FLNC) to the genome using minimap2[81] using parameters -ax splice -uf --secondary=no -C5 -O6,24 -B4. After alignment, cDNA_cupcake (https://github.com/Magdoll/cDNA_Cupcake) was used to collapse alignments into transcript models. Unique transcripts with degraded 5' ends were filtered out of the final annotation file with filter_away_subset.py. StringTie and cDNA_cupcake annotations were combined using TAMA merge[82] with parameters -e longest_ends -d merge_dup.

The transcripts of the resulting gtf were used to run blastp against a Uniprot database and to run hmmer against the pfam database. The resulting hits were used as input for Transdecoder v5.5.0 (https://github.com/TransDecoder/TransDecoder) to predict single best coding regions. The

existing mitochondrial genome and annotation were concatenated to the assembled genome and annotation files, respectively. This resulted in a final number of 18,896 gene annotations.

Orthologous relationships between our predicted genes and those of distant species were identified using OrthoFinder v2.5.2[31]. We used default parameters to cluster sequences into orthologue groups using sequences from eight species including *Homo sapiens* (hg38)*, Mus musculus* (GCA_000001635.9)*, Drosophila melanogaster* (GCA_000001215.4)*, Aplysia californica* (GCA_000002075.2)*, Crassostrea gigas* (GCA_902806645.1)*, Octopus sinensis* (GCA_006345805.1), and *Sepia pharaonis* (GCA_903632075.3). For orthologue groups that contained fewer than four genes, a tree was not generated. These genes were manually annotated using NCBI BLAST[32,83] to assign putative identity based on homology to deposited sequences in other species. Identities for putative neuropeptides (*flri*, *fmrf, lxgkr,* and *pxfv*) were assigned based on repeats within their predicted protein sequences.

Cell Dissociation for scRNA-Seq

Animals used for scRNA-seq were 6 week old juveniles with mantle lengths of 6.5mm-9.0mm. *O. bimaculoides* optic lobes were dissected on ice in Leibovitz-15 medium (Gibco) supplemented with 400mM NaCl, 10mM KCl, 15mM Hepes, 200 U/mL penicillin, and 0.2 mg/mL streptomycin. Single cell dissociation was performed by incubating tissue in papain (1 mg/ml; Worthington Biochemical Co) plus 1% DNase (10mg/ml in HBSS) in supplemented L-15 medium for 10 min at RT. The cells/tissue were gently pipetted up and down several times to dissociate large chunks. The cells/tissue were incubated for another 10 min at RT, pipetted up and down several times, and quenched in wash solution containing 2.5M glucose, 5mM Hepes, and 5% FBS in CMFSS (12mM Hepes, 435mM NaCl, 10.7mM KCl, 21mM Na2HPO4, 16.6mM glucose). Dissociated cells were passed through a 40 μM cell strainer (Fisherbrand), washed again, and resuspended in L-15 medium. A final sample cell concentration of 2000 cells per microliter, as determined on a BioRad TC20 cell counter, was used for cDNA library preparation. Dissociated samples were prepared in tandem, on the same day.

Single-Cell cDNA Library Preparation

Sample preparation for two biological replicates was performed by the University of Oregon Genomics and Cell Characterization core facility (https://gc3f.uoregon.edu/). Dissociated cells were run on a 10X Chromium platform using 10x v.3 chemistry targeting 10,000 cells. The resulting cDNA libraries were amplified with 11 cycles of PCR and sequenced on either an Illumina Hi-seq or an Illumina Next-seq.

RNA Fluorescence In Situ Hybridization

Tissue collection for RNA fluorescence in situ hybridization consisted of juvenile octopuses (~4-6 weeks in age, 7mm in mantle length), which were first anesthetized in 4% EtOH in Artificial Seawater prior to fixation. Anesthetic replaced the seawater in the octopus' home chamber, and the chamber was placed on ice until the octopus was no longer ventilating or responsive. The mantle and arms were removed, leaving the central brain complex which was immediately placed into 10% Neutral Buffered Formalin. The brains were fixed for 24 hours at room temperature before being processed and embedded in paraffin and sectioned into 7um slices.

Custom probes were designed and ordered through Advanced Cell Diagnostics (ACDBio) (Hayward, CA). We followed the protocol available for ACDBio RNAscope[84], with minor changes to optimize it for use in paraffin-embedded octopus tissue. Briefly, we first removed the paraffin through baking, xylenes, and ethanol washes. We then fixed the tissue for 30 minutes in formalin at room temperature before dehydrating the tissue with an ethanol series. We proceeded with hybridization and target retrieval: 10min pre-treatment of H_2O_2, 12min target retrieval in a pressure cooker, and protease plus for 25min at 40C. Slides incubated with probes for 2 hours before going into washes and 5X SSC overnight. On Day 2, we proceeded with amplification and used the appropriate HRPs and opal dyes before adding the HRP block. For multiple probes, additional HRP conjugates were added in a series-wise manner (HRP, opal dyes, block) before slides were mounted with DAPI and ProLong Gold Antifade.

Microscopy

Slides were imaged on the Leica SP8 confocal at 40x. Confocal images were scanned in a z-stack at 1um steps (2um steps for Figure S3) and were tiled. The resulting tiling merged image

was then processed in FIJI[85]. The maximum intensity projection was generally taken across 8 planes (13 for Figure 1, 9 for Figure 6, 5 for Figure S3). When applicable, background subtraction was applied with a rolling ball radius of 100 pixels.

Quantification and Statistical Analysis

Cluster Analysis

The sequencing data were analyzed using the 10X Cell Ranger pipeline, version 3.1.0 (Zheng et al., 2017) and the Seurat (version 3.1.4; Satija et al., 2015) software package for R, version 4.1.2, using standard quality control, normalization, and analysis steps.
Briefly, raw data from each biological replicate were read into R, with a minimum threshold of 3 cells and 500 genes. After visualizing the raw reads, genes, and mitochondrial percentage, we set thresholds of counts between 1000 and 20000, features above 600 genes, and less than 6 percent of mitochondrial content for downstream processing.

To correct for batch effects between our replicates, we followed guidelines for normalization and integration provided by [86] and [29] respectively. We selected integration features within each dataset and applied SCTransform normalization before integrating the datasets based on Canonical Correlation Analysis[29]. For generating cell type clusters, we ran all of the following analyses on the "integrated" assay, but performed differential expression analysis on the "SCT" assay. Following standard downstream processing steps, we ran principal component analysis and UMAP on 25 dimensions. We ran FindNeighbors (dims 1:25) and FindClusters (resolution 0.85). We then generated a dendrogram and renumbered clusters based on this output. We identified the top differentially expressed markers and used these data to identify and subset the putative neurons. We also excluded one cluster from the rest of the analyses due to low number of transcripts and genes, suggesting this cluster did not represent real cellular expression. We re-ran UMAP on the subset of neurons and used this output for visualization and further cell type identification based on top differentially expressed markers. All UMAPs, including feature plots, are shown with datasets that are downsampled to 500 cells for visualization purposes. However, all dot plots show gene expression for full datasets. Feature plots for Figure 2B are shown with a min.cutoff of 0 and a max.cutoff of 1, except for *syt* which has a min.cutoff of 1 and a max.cutoff

of 2. Feature plots for Figures 3-4 are shown with a min.cutoff of 0 and a max.cutoff of 4. Feature plots for Figures 5-6 are shown with a min.cutoff of 0 and a max.cutoff of 2.

Methods S1. Elucidating Unidentified Genes. Related to Figures 4, 5, and 7.

In a number of cases, genes of interest were not well annotated using orthogroup assignment or simple BLAST searches to the non-redundant database. Here we describe additional steps we took to try to assign likely functions to our candidates. In most of these cases orthologous protein predictions could be retrieved from other cephalopod genomes, but not beyond, suggesting that these uncharacterized genes are novel and potentially specific to cephalopods or octopuses. With these in hand, we sought to predict function via deep homology searching as well as structure and function prediction. Homology search and function prediction included the use of the hidden Markov model based tools HHblits and HHpreds[S1,S2], and PSI-BLAST[S3]. In each case we predicted protein structures using ColabFold[S4], which itself is based on AlphaFold2.0[S5]. With these predicted structures in hand, we then searched for distant structural homologues using foldseek[S6].

obimac0010569

Obimac0010569 aligns well to an uncharacterized protein found in *O. vulgaris* and *O. sinensis* called LOC115219258. This hit however combines two separate predicted genes from the previous *O. bimaculoides* genome: obimac0010569 and obimac0010570. While we have Iso-Seq reads that cover obimac0010570, we have none that link obimac0010569 and obimac0010570. Assuming our gene model has split this locus in error, we created multiple species alignments of the candidate and used the resulting multiple species alignment (MSA) for homology search. HHblits revealed a strong signal of a conserved m13 domain on c-terminal side of the predicted protein, with aligns to proteins like putative m13 family peptidases (e-vals ~ 1e-100) and endothelin converting enzymes (e-vals ~ 1e-90). HHPred showed similar signals, with peptidases and in particular metallopeptidases showing homology on the c-terminal end. Interestingly there is some weak homology to Protocadherin-15, but e-values were all >> 0.01

obimac0022194

We were able to find obimac0022194 orthologs from *O. sinensis*, *O. vulgaris*, and *O. minor*. Using a multiple sequence alignment from these orthologs as input to HHblits revealed hits to uncharacterized proteins from the cuttlefish, *S. pharaonis* (e-val ~ 2.2e-15), the limpet *Lottia gigantea* (e-val ~ 3.9e-8), and slightly weaker hits to a protein annotated as luquin1 in the land slug *Deroceras reticulatum* (e-val 9.9e-8) and a protein annotated as luquin neuropeptide fragment in the annelid polychaete *Platynereis dumerilii* (e-val 2.6e-5). HHpred gave no further insight. We then used AlphaFold2.0 to computationally predict a structure using our MSA. The resulting structures were generally low confidence and largely disordered. A representative view of the rank1 model is shown below in Figure ST1. We further searched for structural homologs using foldseek, but zero hits were returned.

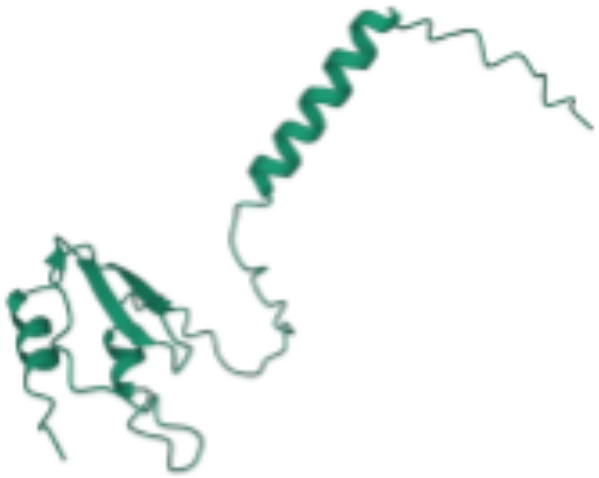

Figure ST1. AlphaFold prediction for obimac0022194 showing the structure of the rank1 model.

obimac0019980

Using protein BLAST searches against individual cephalopod genomes we were able to find an *O. sinensis* ortholog to obimac0019980 with strong homology (e-val ~ 3e-88) and only a very weak hit to the cuttlefish *Sepia officinalis* (e-val = 0.003). We used pairwise alignments of the *O. bimaculoides* and *O. sinensis* proteins as input to HHblits and HHpred. HHblits recovered no

significant homology. HHpred similarly did not recover orthologs in distant genomes but did predict a transmembrane domain and a signal peptide sequence within obimac0019980. We used DeepTMHMM[S7] to confirm the presence of the signal peptide and transmembrane domain. A clear signal peptide is present and DeepTMHMM classifies this protein as globular + signal peptide (Figure ST2). We further used AlphaFold2.0 to provide a predicted structure. This structure was largely disordered but two clear helical regions are revealed. Topology searching using foldseek revealed no similar structures.

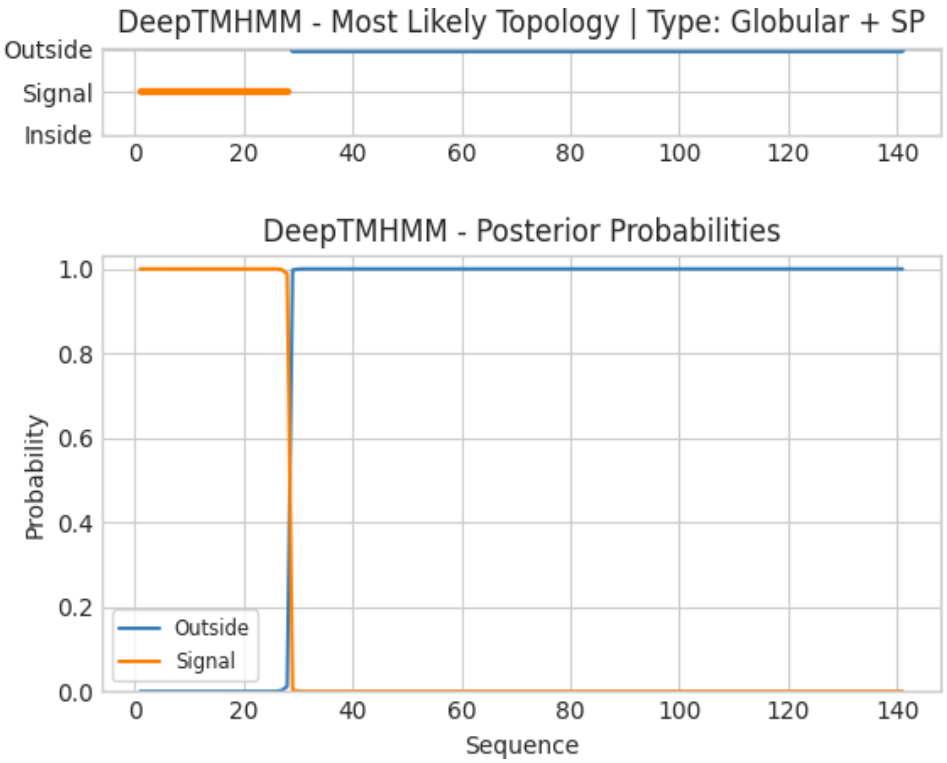

Figure ST2. Evidence of a globular protein plus signal peptide structure for obimac0019980 as predicted by DeepTMHMM[S7].

Supplementary Figures

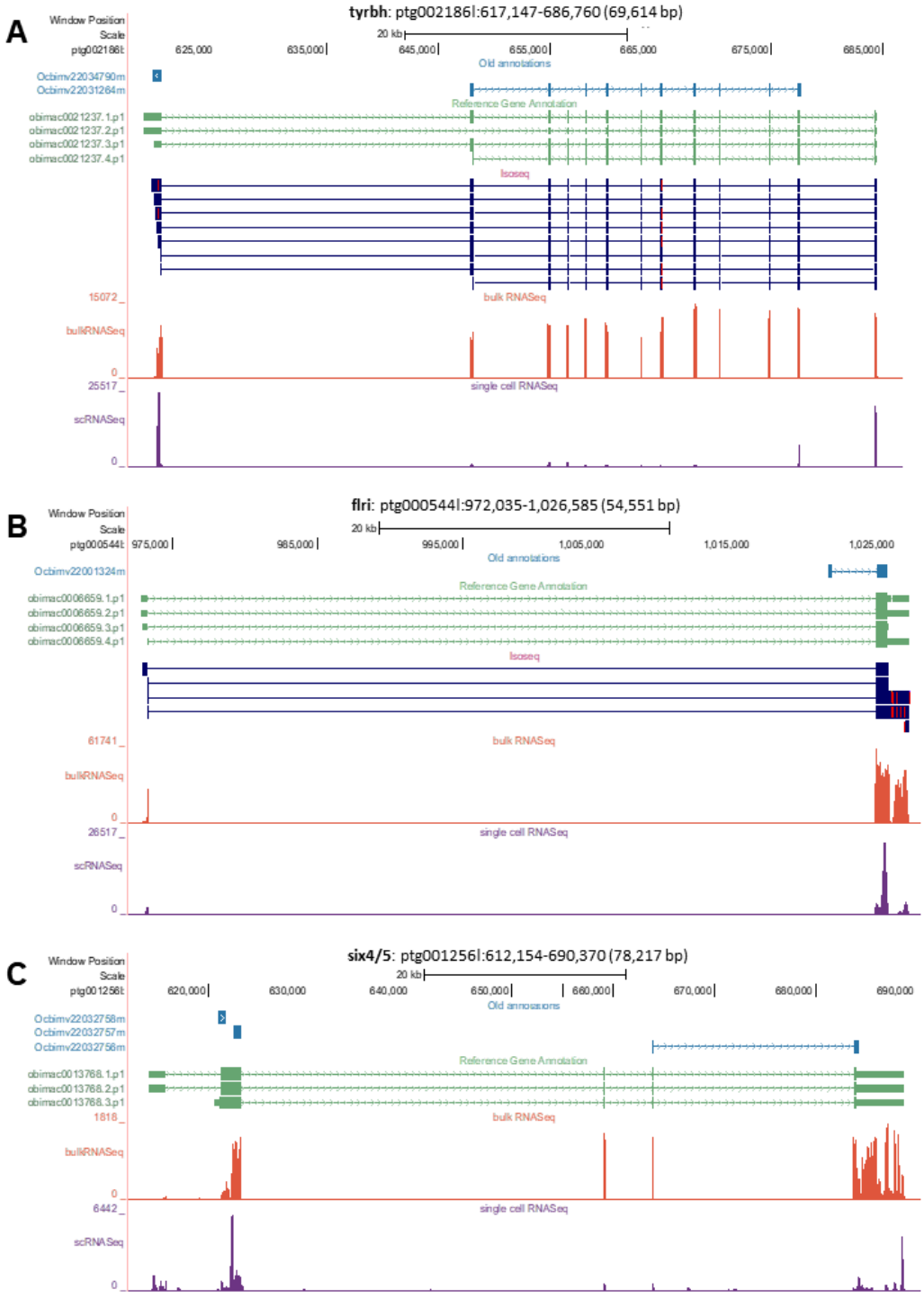

Figure S1. Genome browser output showing improved gene models. Related to Figure 2. Three genes are shown to demonstrate examples of the substantial improvement our gene models achieved with an updated annotation. Each panel contains the following tracks: old gene annotations (blue) from the original *O. bimaculoides* genome annotation all isoforms of new annotations (green), Iso-seq alignment data (dark blue, if present), bulk RNA

sequencing alignment data (orange), and single-cell RNA sequencing alignment data (purple). Our single-cell data is poly-A captured, meaning most reads align to the 3’ ends of genes or areas of the genome.
(A) ***tyrbh*.** New gene models (labeled in green, with each potential isoform represented by the obimac gene identifier followed by a period and numeric) include two additional exons compared to the original annotation, one on each end of the gene. These new exons are supported by both Iso-Seq data and bulk RNA-seq data. By including both of these exons, we have captured two piles of scRNA-seq read alignments on each end of the gene.
(B) ***flri*.** New models lengthened the 3’ ends and included an additional exon on the 5’ end compared to the original model. Both of these changes to this gene are supported by Iso-Seq bulk RNA-seq read alignments and improved the amount of scRNA-seq data we are able to capture.
(C) ***six4/5***. This gene was not present in our Iso-Seq data, but shows an example of where the new gene model substantially improved annotation of this region. The new models lengthened the 3’ end and added two exons in the 5’ direction, allowing us to capture more of the scRNA-seq data. We were able to stitch together three genes from the old model (Ocbimv22032756m, Ocbimv22032757m, and Ocbimv22032758m) into a single gene model (obimac0013768). If we had used the old gene model for our single cell analysis, then it would appear that three separate genes have similar expression patterns.

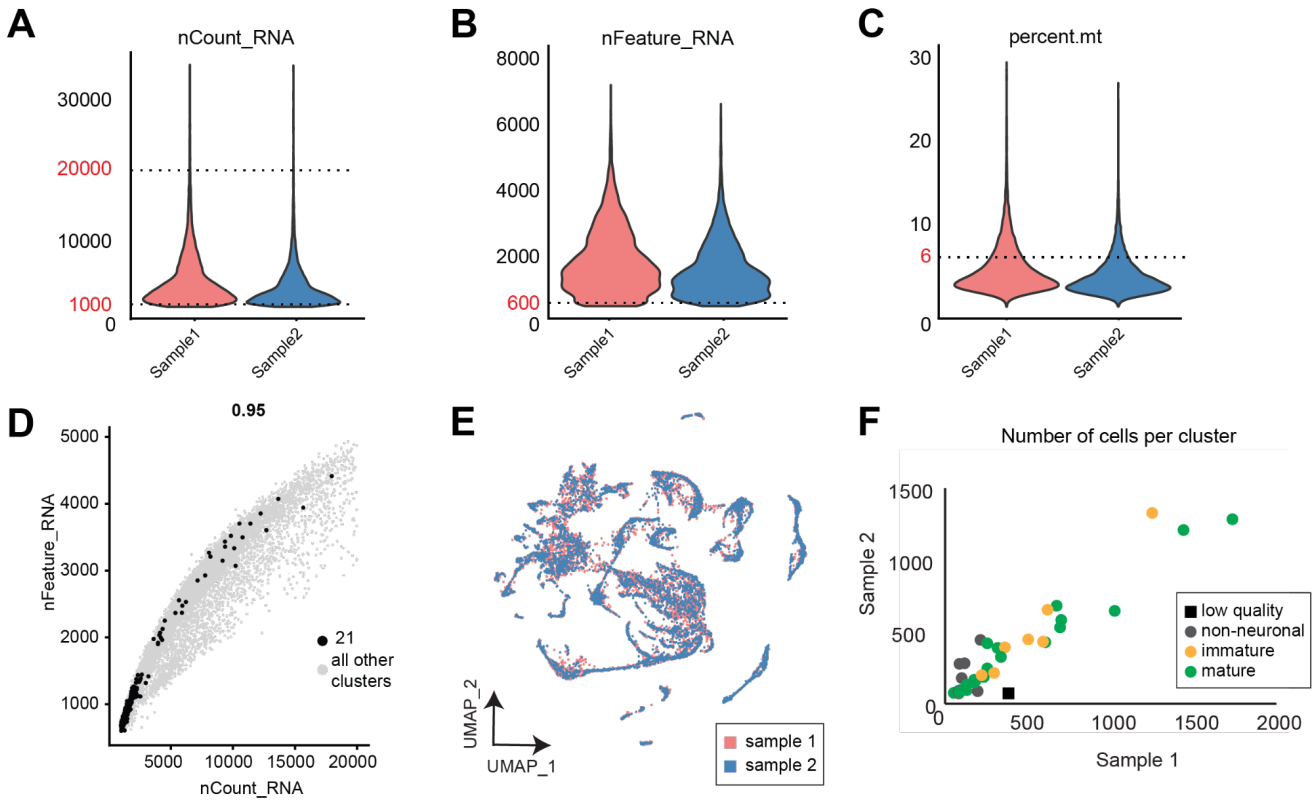

Figure S2. Single-cell RNA sequencing quality control metrics. Related to Figure 2.
(A-C) Violin plot showing raw reads (nCount_RNA), genes (nFeature_RNA), and mitochondrial percentage (percent.mt) across the two biological replicates used in this study. Dashed lines and red text indicate thresholds set for downstream processing.
(D) Scatter plot showing the correlation between the number of reads and the number of genes for all cells. One cluster (21) had low reads and gene counts and did not have a specific gene expression profile (data not shown). Cluster 21 was therefore excluded from further analysis.
(E) UMAP showing representation of each sample across clusters after applying sctransform normalization and integration via Canonical Correlation Analysis.
(F) Scatter plot of number of cells per cluster, with each biological replicate plotted on each axis. Points are color-coded based on whether they represent clusters from non-neuronal, immature, or mature neuronal populations. Neuronal cell types were represented similarly in the two replicates. On the other hand non-neuronal clusters were more variable, perhaps due to their presence in neighboring tissue. The "low quality" cluster (21), which was discarded from analysis, is represented by a black square and was only present in one replicate.

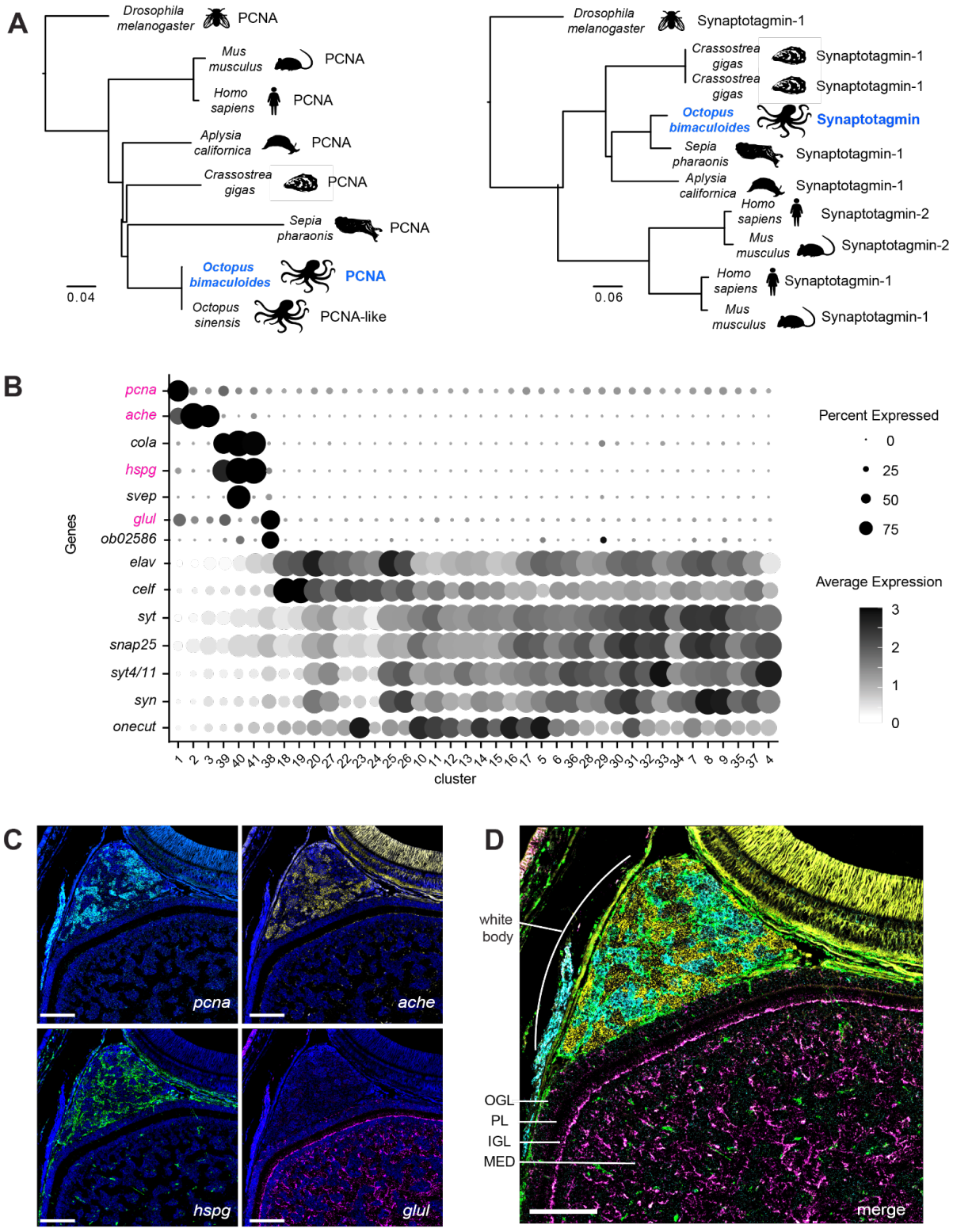

Figure S3. Characterization of non-neuronal clusters. Related to Figure 2.

(A) Phylogenetic trees from OrthoFinder, demonstrating the method for assignment of gene identities in our updated gene model.
(B) Dot plot of conserved markers, showing demarcation of neuronal vs. non-neuronal cells, as well as subtypes within non-neuronal cells. One subset (clusters 1-3) of non-neuronal cells has relatively high expression of markers relating to proliferation and blood (proliferating cell nuclear antigen (*pcna*)[S1] and acetylcholinesterase (*ache*)[S2]), whereas a second subset (clusters 39-41) are marked by relatively high expression of genes relating to endothelium (collagen type 1 alpha 1 (*cola*)[S3], heparan sulfate proteoglycan 2 (*hspg)*, and sushi von willebrand factor type a (*svep*)). Finally, a third cluster (38) has high expression of glutamine synthase (*glul*)[S4], which is expressed in glia. Interestingly, this cluster also has an uncharacterized gene obimac0002586. Markers for these clusters are contrasted with neuronal markers/clusters below.
(C) FISH of genes to demonstrate anatomical locations of non-neuronal cell types. In mapping putative non-neuronal cell clusters to their anatomical locations via FISH, we found several markers to be primarily expressed outside of the optic lobe, mostly in the white body, which is involved in hematopoiesis[S5]. *pcna* (top left) marks dividing cells and is localized to the white body, along with *ache* (top right), which is a marker of blood cells. Together, *pcna* and *ache* expression is consistent with the suggested role of the white body in hematopoiesis. *hspg* (bottom left) demarcates endothelial cells and is prominent in the white body as well as the optic lobe, where their morphology resembles vasculature. One prominent marker gene from these clusters that is expressed in the optic lobe is *glul* (bottom right), a glial marker, which identified a population of cell bodies at the boundary of the plexiform layer and IGL, with expression extending into the neuropils of the medulla, consistent with glial organization in other invertebrate nervous systems[S6]. *glul* can be seen within the optic lobe, prominently labeling nuclei on the superficial border of IGL but also extending throughout the neuropil of the medulla. Scale bars indicate 100 um. Nuclei are stained in DAPI.
(D) A quadruple FISH of the genes shown in C without nuclei staining. OGL, outer granular layer; PL, plexiform layer; IGL, inner granular layer; MED, medulla. Scale bar indicates 100 um.

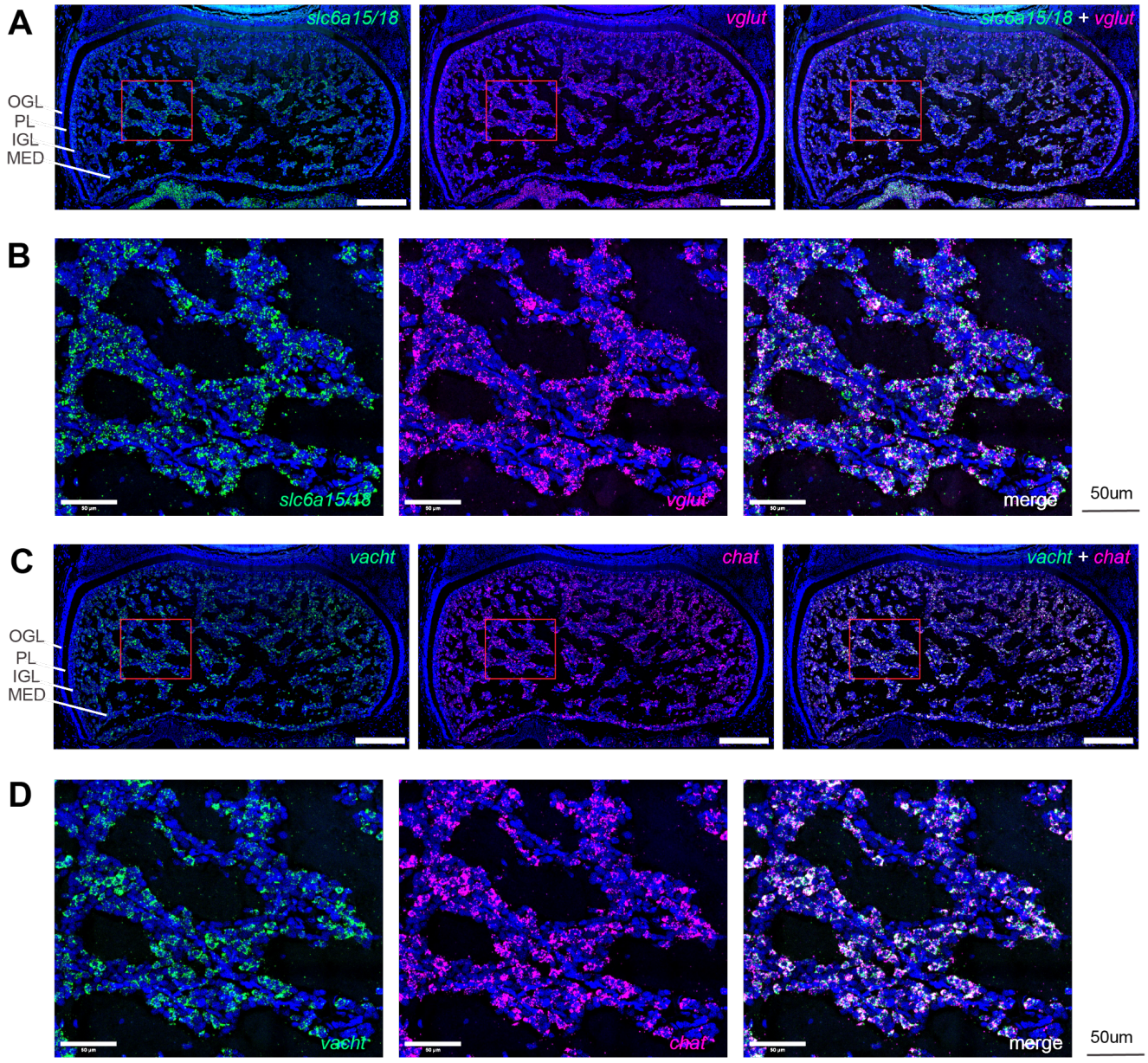

Figure S4. Validation of glutamatergic and cholinergic markers. Related to Figures 2-3.
(A-B) 2-color FISH of two glutamatergic markers, *slc6a15/18* and *vglut,* demonstrating co-expression in the optic lobe. Red box in (A) denotes a zoomed-in portion of the medulla in (B). Here and below, nuclei are stained with DAPI and the scale bar represents 200um unless otherwise noted.
(C-D) 2-color FISH of two cholinergic markers, *vacht* and *chat,* demonstrating co-expression. Red box in (C) denotes the region depicted in (D).

Assembly statistic	Octopus_bimaculoides_v2_0 (2015 assembly)	o_bimaculoides_hifi_v1.0.0 (2022 assembly)
Size	2.34 Gb	2.34 Gb
Number of contigs	151,674	5,437
Average contig length	15.42 Kb	430.95 Kb
Longest contig	4.06 Mb	7.63 Mb
Contig N50	475 Kb (n = 1333)	880.44 Kb (n = 755)
Number of gaps	548,450	5 (115 Ns)
Coverage	~60x	34x
BUSCO (Eukaryota)	C:91.8%[S:90.6%,D:1.2%]F:6.7%,M:1.5%,n:255	C:92.2%[S:90.6%,D:1.6%],F:6.7%,M:1.1%,n:255
Number of annotated genes	33,638	18,896

Table S1. Genome assembly statistics for o_bimaculoides_hifi_v1.0.0 and Octopus_bimaculoides_v2_0. Related to Figure 2. The computational pipeline that led to these results is described in Methods. Benchmarking Universal Single-Copy Orthologs (BUSCO v. 3)[S7] was run against the eukaryota_odb9 database to show an overall completeness of 92.2% (C: complete, S: complete and single-copy, D: complete and duplicated, F: fragmented, M: missing). We used the Eukaryote database rather than Mollusc or Metazoa because those databases contain the original *O. bimaculoides* proteome, thus biasing results. The older gene model contains many fragmented gene annotations, which led to an inflated number of total genes in the original gene annotation file. The new genome annotation contains fewer genes because many of the fragmented annotations have been connected.

Gene	Obimac ID	Gene	Obimac ID
ache	obimac0020279	*ob19980*	obimac0019980
bib	obimac0026684	*ob22194*	obimac0022194
cacng	obimac0027453	*octr*	obimac0000086
celf	obimac0028033	*onecut*	obimac0002891
chat	obimac0030402	*orc*	obimac0002637
cola	obimac0002036	*otx*	obimac0030353
dat	obimac0021555	*pcdh-ob09200*	obimac0009200
dchs	obimac0020142	*pcdh-ob26462*	obimac0026462
dlx	obimac0024037	*pcna*	obimac0019754
dscam	obimac0017416	*plxna*	obimac0017384
efn	obimac0011807	*pxfv*	obimac0025590
elav	obimac0020958	*sema2*	obimac0002144
epha	obimac0017206	*sema5*	obimac0023141
flri	obimac0006659	*six4/5*	obimac0013768
fmrf1	obimac0015407	*slc6a15/18*	obimac0030399
gad	obimac0007601	*snap25*	obimac0010589
glul	obimac0032988	*sox2*	obimac0011874
hh	obimac0025144	*svep*	obimac0000862
hspg	obimac0022794	*syn*	obimac0011778
lrrc15	obimac0011126	*syt*	obimac0014441
lxgkr	obimac0011766	*syt4/11*	obimac0020553
mynn	obimac0021831	*tnfr*	obimac0032150
nachr	obimac0008351	*tyrbh*	obimac0021237
nkx2	obimac0032473	*vacht*	obimac0013580
nos	obimac0011102	*vat1*	obimac0023625
ob02586	obimac0002586	*vglut*	obimac0012076
ob10569	obimac0010569		

Table S2. Reference gene table. Related to Figures 2-7. Obimac gene identifiers and corresponding gene assignment for all genes described in this study. See Methods for more information about gene assignments.

References

1. Williamson, R., and Chrachri, A. (2004). Cephalopod neural networks. Neurosignals *13*, 87–98.

2. Budelmann, B.U. (1995). The cephalopod nervous system: What evolution has made of the molluscan design. Experientia Supplementum, 115–138. 10.1007/978-3-0348-9219-3_7.

3. Nixon, M., and Young, J.Z. (2003). The Brains and Lives of Cephalopods (Oxford University Press).

4. Young, J.Z. (1961). Learning and discrimination in the octopus. Biol. Rev. Camb. Philos. Soc. *36*, 32–96.

5. Young, J.Z. (1962). The optic lobes of Octopus vulgaris. Philos. Trans. R. Soc. Lond. B Biol. Sci. *245*, 19–58.

6. Wells, M.J. (1962). Brain and Behaviour in Cephalopods (Stanford University Press).

7. Chiao, C.C., and Hanlon, R.T. (2001). Cuttlefish camouflage: visual perception of size, contrast and number of white squares on artificial checkerboard substrata initiates disruptive coloration. J. Exp. Biol. *204*, 2119–2125.

8. Hanlon, R.T., and Messenger, J.B. (2018). Cephalopod Behaviour (Cambridge University Press).

9. Ogura, A., Ikeo, K., and Gojobori, T. (2004). Comparative analysis of gene expression for convergent evolution of camera eye between octopus and human. Genome Res. *14*, 1555–1561.

10. Young, J.Z. (1962). The Retina of Cephalopods and Its Degeneration After Optic Nerve Section. Philosophical Transactions of the Royal Society of London B *245*, 1–18.

11. Yamamoto, T., Tasaki, K., Sugawara, Y., and Tonosaki, A. (1965). Fine structure of the octopus retina. J. Cell Biol. *25*, 345–359.

12. Young, J.Z. (1971). The Anatomy of the Nervous System of Octopus Vulgaris (Oxford University Press, USA).

13. Messenger, J.B. (1981). Comparative Physiology of Vision in Molluscs. Comparative Physiology and Evolution of Vision in Invertebrates, 93–200. 10.1007/978-3-642-67868-4_2.

14. Bullock, T.H., and Budelmann, B.U. (1991). Sensory evoked potentials in unanesthetized unrestrained cuttlefish: a new preparation for brain physiology in cephalopods. J. Comp. Physiol. A *168*, 141–150.

15. Young, J.Z. (1979). The Nervous System of Loligo: V. The vertical lobe complex.

Philosophical Transactions of the Royal Society of London B. Biological Sciences *285*, 311–354.

16. Chichery, R., and Chanelet, J. (1976). Motor and behavioral responses obtained by stimulation with chronic electrodes of the optic lobe of Sepia officinalis. Brain Res. *105*, 525–532.

17. Shigeno, S., Andrews, P.L.R., Ponte, G., and Fiorito, G. (2018). Cephalopod Brains: An Overview of Current Knowledge to Facilitate Comparison With Vertebrates. Frontiers in Physiology *9*. 10.3389/fphys.2018.00952.

18. Young, J.Z. (1974). The central nervous system of Loligo. I. The optic lobe. Philos. Trans. R. Soc. Lond. B Biol. Sci. *267*, 263–302.

19. Boycott, B.B., and Young, J.Z. (1961). The functional organization of the brain of the cuttlefish Sepia officinalis. Proceedings of the Royal Society of London. Series B. Biological Sciences *153*, 503–534.

20. Saidel, W.M. (1982). Connections of the octopus optic lobe: an HRP study. J. Comp. Neurol. *206*, 346–358.

21. Liu, Y.-C., Liu, T.-H., Su, C.-H., and Chiao, C.-C. (2017). Neural Organization of the Optic Lobe Changes Steadily from Late Embryonic Stage to Adulthood in Cuttlefish Sepia pharaonis. Front. Physiol. *8*. 10.3389/fphys.2017.00538.

22. y Cajal, S.R. (1930). Contribución al conocimiento de la retina y centros ópticos de los cefalópodos (Unión Internacional de Ciencias Biológicas, Comité Español).

23. Konstantinides, N., Kapuralin, K., Fadil, C., Barboza, L., Satija, R., and Desplan, C. (2018). Phenotypic Convergence: Distinct Transcription Factors Regulate Common Terminal Features. Cell *174*, 622–635.e13.

24. Peng, Y.-R., Shekhar, K., Yan, W., Herrmann, D., Sappington, A., Bryman, G.S., van Zyl, T., Do, M.T.H., Regev, A., and Sanes, J.R. (2019). Molecular Classification and Comparative Taxonomics of Foveal and Peripheral Cells in Primate Retina. Cell *176*, 1222–1237.e22.

25. Macosko, E.Z., Basu, A., Satija, R., Nemesh, J., Shekhar, K., Goldman, M., Tirosh, I., Bialas, A.R., Kamitaki, N., Martersteck, E.M., et al. (2015). Highly Parallel Genome-wide Expression Profiling of Individual Cells Using Nanoliter Droplets. Cell *161*, 1202–1214.

26. Tasic, B., Menon, V., Nguyen, T.N., Kim, T.K., Jarsky, T., Yao, Z., Levi, B., Gray, L.T., Sorensen, S.A., Dolbeare, T., et al. (2016). Adult mouse cortical cell taxonomy revealed by single cell transcriptomics. Nat. Neurosci. *19*, 335–346.

27. Solorzano, Y., Viana, M.T., López, L.M., Correa, J.G., True, C.C., and Rosas, C. (2009). Response of newly hatched Octopus bimaculoides fed enriched Artemia salina: Growth

performance, ontogeny of the digestive enzyme and tissue amino acid content. Aquaculture *289*, 84–90.

28. Hanlon, R.T., and Forsythe, J.W. (1985). Advances in the laboratory culture of octopuses for biomedical research. Lab. Anim. Sci. *35*, 33–40.

29. Stuart, T., Butler, A., Hoffman, P., Hafemeister, C., Papalexi, E., Mauck, W.M., 3rd, Hao, Y., Stoeckius, M., Smibert, P., and Satija, R. (2019). Comprehensive Integration of Single-Cell Data. Cell *177*, 1888–1902.e21.

30. Zheng, G.X.Y., Terry, J.M., Belgrader, P., Ryvkin, P., Bent, Z.W., Wilson, R., Ziraldo, S.B., Wheeler, T.D., McDermott, G.P., Zhu, J., et al. (2017). Massively parallel digital transcriptional profiling of single cells. Nat. Commun. *8*, 14049.

31. Emms, D.M., and Kelly, S. (2019). OrthoFinder: phylogenetic orthology inference for comparative genomics. Genome Biol. *20*, 238.

32. Altschul, S.F., Gish, W., Miller, W., Myers, E.W., and Lipman, D.J. (1990). Basic local alignment search tool. J. Mol. Biol. *215*, 403–410.

33. Deryckere, A., and Seuntjens, E. (2018). The Cephalopod Large Brain Enigma: Are Conserved Mechanisms of Stem Cell Expansion the Key? Front. Physiol. *9*, 1160.

34. Messenger, J.B. (1996). Neurotransmitters of cephalopods. Invertebrate Neuroscience *2*, 95–114. 10.1007/bf02214113.

35. Bröer, A., Tietze, N., Kowalczuk, S., Chubb, S., Munzinger, M., Bak, L.K., and Bröer, S. (2006). The orphan transporter v7-3 (slc6a15) is a Na -dependent neutral amino acid transporter (B0AT2). Biochemical Journal *393*, 421–430. 10.1042/bj20051273.

36. Juorio, A.V., and Molinoff, P.B. (1971). Distribution of octopamine in nervous tissues of Octopus vulgaris. Br. J. Pharmacol. *43*, 438P–439P.

37. Cornwell, C.J., Messenger, J.B., and Williamson, R. (1993). Distribution of GABA-like immunoreactivity in the octopus brain. Brain Res. *621*, 353–357.

38. Seo, H.C., Curtiss, J., Mlodzik, M., and Fjose, A. (1999). Six class homeobox genes in drosophila belong to three distinct families and are involved in head development. Mech. Dev. *83*, 127–139.

39. Kumar, J.P. (2009). The sine oculis homeobox (SIX) family of transcription factors as regulators of development and disease. Cell. Mol. Life Sci. *66*, 565–583.

40. Weasner, B.P., Anderson, J., and Kumar, J.P. (2004). The Eye Specification Network in Drosophila. Proc. Indian Natl. Sci. Acad. *B70*, 517–530.

41. Kawakami, K., Sato, S., Ozaki, H., and Ikeda, K. (2000). Six family genes--structure and function as transcription factors and their roles in development. Bioessays *22*, 616–626.

42. Krajniak, K.G. (2013). Invertebrate FMRFamide related peptides. Protein Pept. Lett. *20*, 647–670.

43. Zatylny-Gaudin, C., and Favrel, P. (2014). Diversity of the RFamide Peptide Family in Mollusks. Front. Endocrinol. *5*, 178.

44. Loi, P., Saunders, R., Young, D., and Tublitz, N. (1996). Peptidergic regulation of chromatophore function in the European cuttlefish Sepia officinalis. J. Exp. Biol. *199*, 1177–1187.

45. Loi, P.K., and Tublitz, N.J. (2000). Roles of glutamate and FMRFamide-related peptides at the chromatophore neuromuscular junction in the cuttlefish, Sepia officinalis. J. Comp. Neurol. *420*, 499–511.

46. Fuerst, P.G., Koizumi, A., Masland, R.H., and Burgess, R.W. (2008). Neurite arborization and mosaic spacing in the mouse retina require DSCAM. Nature *451*, 470–474.

47. Yamagata, M., and Sanes, J.R. (2008). Dscam and Sidekick proteins direct lamina-specific synaptic connections in vertebrate retina. Nature *451*, 465–469.

48. Yang, C., Qi, Y., and Sun, Z. (2021). The Role of Sonic Hedgehog Pathway in the Development of the Central Nervous System and Aging-Related Neurodegenerative Diseases. Front Mol Biosci *8*, 711710.

49. de Wit, J., Hong, W., Luo, L., and Ghosh, A. (2011). Role of leucine-rich repeat proteins in the development and function of neural circuits. Annu. Rev. Cell Dev. Biol. *27*, 697–729.

50. Roeder, T. (1999). Octopamine in invertebrates. Prog. Neurobiol. *59*, 533–561.

51. Pasterkamp, R.J. (2012). Getting neural circuits into shape with semaphorins. Nat. Rev. Neurosci. *13*, 605–618.

52. Peek, S.L., Mah, K.M., and Weiner, J.A. (2017). Regulation of neural circuit formation by protocadherins. Cell. Mol. Life Sci. *74*, 4133–4157.

53. Cifuentes-Diaz, C., Bitoun, M., Goudou, D., Seddiqi, N., Romero, N., Rieger, F., Perin, J.-P., and Alliel, P.M. (2004). Neuromuscular expression of the BTB/POZ and zinc finger protein myoneurin. Muscle Nerve *29*, 59–65.

54. Rao, Y., Bodmer, R., Jan, L.Y., and Jan, Y.N. (1992). The big brain gene of Drosophila functions to control the number of neuronal precursors in the peripheral nervous system. Development *116*, 31–40.

55. Wilkinson, D.G. (2001). Multiple roles of EPH receptors and ephrins in neural development. Nat. Rev. Neurosci. *2*, 155–164.

56. Liu, T.-H., and Chiao, C.-C. (2017). Mosaic Organization of Body Pattern Control in the Optic Lobe of Squids. J. Neurosci. *37*, 768–780.

57. Styfhals, R., Zolotarov, G., Hulselmans, G., Spanier, K.I., Poovathingal, S., Elagoz, A.M., Deryckere, A., Rajewsky, N., Ponte, G., Fiorito, G., et al. (2022). Cell type diversity in a developing octopus brain. bioRxiv, 2022.01.24.477459. 10.1101/2022.01.24.477459.

58. Duruz, J., Sprecher, M., Kaldun, J.C., Alsoudy, A., Tschanz-Lischer, H., van Geest, G., Nicholson, P., Bruggmann, R., and Sprecher, S.G. (2022). Molecular characterization of cell types in the squid Loligo vulgaris. bioRxiv, 2022.03.28.485983. 10.1101/2022.03.28.485983.

59. Gavriouchkina, D., Tan, Y., Ziadi-Künzli, F., Hasegawa, Y., Piovani, L., Zhang, L., Sugimoto, C., Luscombe, N., Marlétaz, F., and Rokhsar, D.S. (2022). A single-cell atlas of bobtail squid visual and nervous system highlights molecular principles of convergent evolution. bioRxiv, 2022.05.26.490366. 10.1101/2022.05.26.490366.

60. Yan, W., Laboulaye, M.A., Tran, N.M., Whitney, I.E., Benhar, I., and Sanes, J.R. (2020). Mouse Retinal Cell Atlas: Molecular Identification of over Sixty Amacrine Cell Types. J. Neurosci. *40*, 5177–5195.

61. Diamond, J.S. (2017). Inhibitory Interneurons in the Retina: Types, Circuitry, and Function. Annu Rev Vis Sci *3*, 1–24.

62. Witkovsky, P. (2004). Dopamine and retinal function. Doc. Ophthalmol. *108*, 17–40.

63. Masland, R.H. (2012). The tasks of amacrine cells. Vis. Neurosci. *29*, 3–9.

64. Niell, C.M., and Stryker, M.P. (2010). Modulation of visual responses by behavioral state in mouse visual cortex. Neuron *65*, 472–479.

65. Chiappe, M.E., Seelig, J.D., Reiser, M.B., and Jayaraman, V. (2010). Walking modulates speed sensitivity in Drosophila motion vision. Curr. Biol. *20*, 1470–1475.

66. Vinck, M., Batista-Brito, R., Knoblich, U., and Cardin, J.A. (2015). Arousal and locomotion make distinct contributions to cortical activity patterns and visual encoding. Neuron *86*, 740–754.

67. Suver, M.P., Mamiya, A., and Dickinson, M.H. (2012). Octopamine neurons mediate flight-induced modulation of visual processing in Drosophila. Curr. Biol. *22*, 2294–2302.

68. Polack, P.-O., Friedman, J., and Golshani, P. (2013). Cellular mechanisms of brain state-dependent gain modulation in visual cortex. Nat. Neurosci. *16*, 1331–1339.

69. Boycott, B.B., Lettvin, J.Y., Maturana, H.R., and Wall, P.D. (1965). Octopus optic responses. Exp. Neurol. *12*, 247–256.

70. Forsythe, J.W., and Hanlon, R.T. (1988). Effect of temperature on laboratory growth, reproduction and life span of Octopus bimaculoides. Marine Biology *98*, 369–379. 10.1007/bf00391113.

71. Yamazaki, A., Yoshida, M., and Uematsu, K. (2002). Post-hatching development of the brain in Octopus ocellatus. Zoolog. Sci. *19*, 763–771.

72. Kerbl, A., Handschuh, S., Nödl, M.-T., Metscher, B., Walzl, M., and Wanninger, A. (2013). Micro-CT in cephalopod research: Investigating the internal anatomy of a sepiolid squid using a non-destructive technique with special focus on the ganglionic system. J. Exp. Mar. Bio. Ecol. *447*, 140–148.

73. Deryckere, A., Styfhals, R., Elagoz, A.M., Maes, G.E., and Seuntjens, E. (2021). Identification of neural progenitor cells and their progeny reveals long distance migration in the developing octopus brain. Elife *10*. 10.7554/eLife.69161.

74. Fernald, R.D. (1990). Teleost vision: seeing while growing. J. Exp. Zool. Suppl. *5*, 167–180.

75. Sanes, J.R., and Masland, R.H. (2015). The types of retinal ganglion cells: current status and implications for neuronal classification. Annu. Rev. Neurosci. *38*, 221–246.

76. Fiorito, G., Affuso, A., Basil, J., Cole, A., de Girolamo, P., D'Angelo, L., Dickel, L., Gestal, C., Grasso, F., Kuba, M., et al. (2015). Guidelines for the Care and Welfare of Cephalopods in Research -A consensus based on an initiative by CephRes, FELASA and the Boyd Group. Lab. Anim. *49*, 1–90.

77. Cheng, H., Concepcion, G.T., Feng, X., Zhang, H., and Li, H. (2021). Haplotype-resolved de novo assembly using phased assembly graphs with hifiasm. Nat. Methods *18*, 170–175.

78. Guan, D., McCarthy, S.A., Wood, J., Howe, K., Wang, Y., and Durbin, R. (2020). Identifying and removing haplotypic duplication in primary genome assemblies. Bioinformatics *36*, 2896–2898.

79. Kim, D., Paggi, J.M., Park, C., Bennett, C., and Salzberg, S.L. (2019). Graph-based genome alignment and genotyping with HISAT2 and HISAT-genotype. Nat. Biotechnol. *37*, 907–915.

80. Kovaka, S., Zimin, A.V., Pertea, G.M., Razaghi, R., Salzberg, S.L., and Pertea, M. (2019). Transcriptome assembly from long-read RNA-seq alignments with StringTie2. Genome Biol. *20*, 278.

81. Li, H. (2018). Minimap2: pairwise alignment for nucleotide sequences. Bioinformatics *34*, 3094–3100.

82. Kuo, R.I., Cheng, Y., Zhang, R., Brown, J.W.S., Smith, J., Archibald, A.L., and Burt, D.W. (2020). Illuminating the dark side of the human transcriptome with long read transcript sequencing. BMC Genomics *21*, 751.

83. Altschul, S.F., Madden, T.L., Schäffer, A.A., Zhang, J., Zhang, Z., Miller, W., and Lipman, D.J. (1997). Gapped BLAST and PSI-BLAST: a new generation of protein database search programs. Nucleic Acids Res. *25*, 3389–3402.

84. Wang, F., Flanagan, J., Su, N., Wang, L.-C., Bui, S., Nielson, A., Wu, X., Vo, H.-T., Ma, X.-J., and Luo, Y. (2012). RNAscope: a novel in situ RNA analysis platform for formalin-fixed, paraffin-embedded tissues. J. Mol. Diagn. *14*, 22–29.

85. Schindelin, J., Arganda-Carreras, I., Frise, E., Kaynig, V., Longair, M., Pietzsch, T., Preibisch, S., Rueden, C., Saalfeld, S., Schmid, B., et al. (2012). Fiji: an open-source platform for biological-image analysis. Nat. Methods *9*, 676–682.

86. Hafemeister, C., and Satija, R. (2019). Normalization and variance stabilization of single-cell RNA-seq data using regularized negative binomial regression. Genome Biol. *20*, 1–15.

BRAIN-WIDE GENE EXPRESSION IN THE JUVENILE *OCTOPUS BIMACULOIDES*

JO Songco-Casey, WM Langford, NM Casey, W-S Chung, and CM Niell. *Unpublished*.

Author contributions: J.O.S.-C. and C.M.N. conceived the project. J.O.S.-C. led the project and designed and performed experiments. J.O.S.-C. and W-S.C. performed brain region identification. J.O.S.-C., W.M.L., and N.M.C. performed brain region annotation and data analysis.

Introduction

Coleoid cephalopods, such as squid, cuttlefish, and octopuses, have the largest brain among invertebrates, allowing for a rich repertoire of dynamic behaviors[1–6]. Their centralized brain, which is arranged around their esophagus, is made up of large structures with specialized functions[1,7–11,11–17]. To access neural circuits underlying advanced behaviors, such as learning and memory, prey capture and predator avoidance, and rapid body-patterning known as camouflage, it is critical to understand brain organization in these animals. However, to date, few mappings, or "brain atlases", exist for these emerging model organisms, despite advancements in technological approaches to characterize and perturb neural circuitry in cephalopods.

Beyond early histology and morphological staining, several approaches have been taken to create a detailed atlas of cephalopod brain organization. 3D light microscopy was applied in developing cephalopods and demonstrated an effect of habitat and behavior on brain region volume[18] whereas confocal microscopy of hatchling and juvenile brain slices in pygmy squid *Idiosepius paradoxus* revealed over 35 lobes and found that the vertical lobe was the largest relative volume[19]. The first octopus brain atlas was published using Hematoxylin & Eoisin (H&E) staining of serial horizontal and sagittal sections in an adult *Octopus minor* and identified more than 70 subregions[20], and 3D MRI-based imaging established in squid[21–23] resulted in both the first connectome of the squid brain in *Sepioteuthis lessoniana*[24] and further evidence that brain morphology across cephalopods is influenced by habitat and behavioral demands[25].

To tie together anatomical, transcriptional, and functional studies, it will be important to understand the molecular architecture, including functional and developmental determinants, across subregions of the cephalopod brain. To provide such a resource for the growing field of cephalopod neuroscience, we combined serial coronal sections of H&E staining with multiplexed RNA fluorescence in situ hybridization (FISH) of 40 candidate markers to provide, to our understanding, the first account brain-wide gene expression in the cephalopod central nervous system.

Results

Serial Sectioning in the Juvenile Octopus bimaculoides

In addition to established methods for culturing and maintaining this species in a laboratory, the *Octopus bimaculoides* is one of the few cephalopods to have a high quality, chromosomal level assembly of its genome[26,27], therefore providing unique opportunities to investigate transcriptional and genomic novelties. *O. bimaculoides* live to be about 1-2 years old and, while they exhibit continuous growth throughout their lifespan, at ~1.5 months of age, their body organization and behaviors are established and their sensory systems are fully mature[28,29]. As such, the juvenile *O. bimaculoides* provides a unique opportunity to characterize brain-wide expression of genes related to both functionally mature as well as immature and developing neurons.

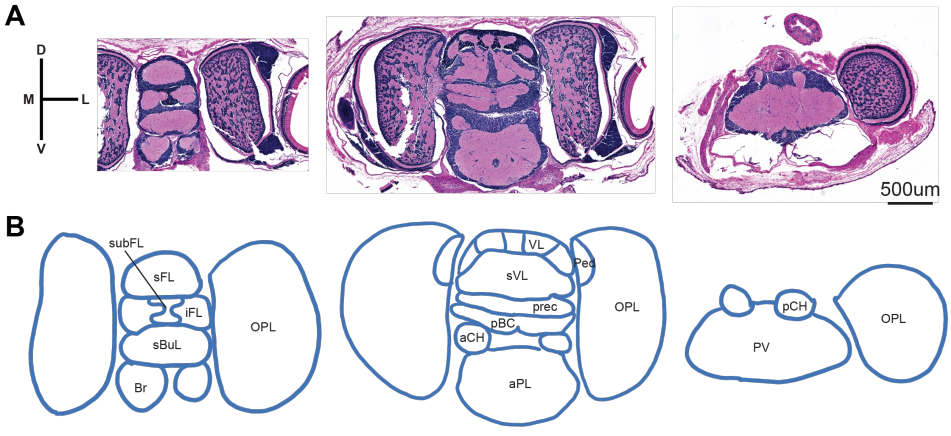

Figure 1. Examples of coronal samples.
A) 3 Representative slices stained with H&E, from anterior (left) to posterior (right).
B) Accompanying illustrations outlining a subset of identified brain regions from each slice.

We performed serial sectioning on 2 juvenile octopuses and subsequently used H&E staining to delineate nuclear layers from the neuropil/cytoplasm of the lobes (Figure 1). Brains were sectioned coronally from anterior (toward the beak) to posterior (away from the beak) at 7um. We obtained over 300 (n=305) images and carefully selected images that represented the structure of the *O. bimaculoides* brain. After delineating brain regions based on H&E, we established names for each subregion based on nomenclature used in[17]. We identified 8 lobes in the SUB and 12 in the SEM, including the optic lobes which lie on either side of the central brain complex. In total, we identified 20 lobes, some of which contain subregions and are, therefore, referred to as "complexes" (see Supplemental Table 1). Since the brain is still developing at this age, we grouped some subregions into complexes as it was not evident from nuclear staining where the boundaries between these differentiated lobes would be. Additionally, due to differences in sectioning angles, we were able to identify 1 structure, the vasomotor lobe, in only 1 sample and, therefore, we exclude this brain region from further analyses. Lastly, we did not identify 3 paired lobe structures: the optic glands, the olfactory lobes, and the subpedunculate lobes. However, these structures are all known to be involved in reproduction and, therefore, we did not expect to identify these lobes in the juvenile octopus as it has likely not yet reached sexual maturity at this age[11,30–36].

Differential Expression of Neurotransmitters and Neuropeptides

We performed multiplexed RNA FISH on serial sections across 5 additional juvenile octopuses. The brains were sectioned similarly from anterior to posterior at 10um, but representative sections were spaced ~60um apart (see Methods for more details). In addition to qualitative characterization of 40 genes (see Supplemental Table 2) across 20 lobes, which we describe below, we also provide a summary in Figure 2 of quantified gene expression using automated cell detection tools available in QuPath (see Methods for more details).

Classical Neurotransmitters

Previous work identified neurotransmitter and neuropeptide usage across different brain regions in cephalopods based on pharmacological experiments and transcriptional profiles. Therefore, we

sought to describe neurotransmitter and neuropeptide usage across 20 lobes in the juvenile *O. bimaculoides*.

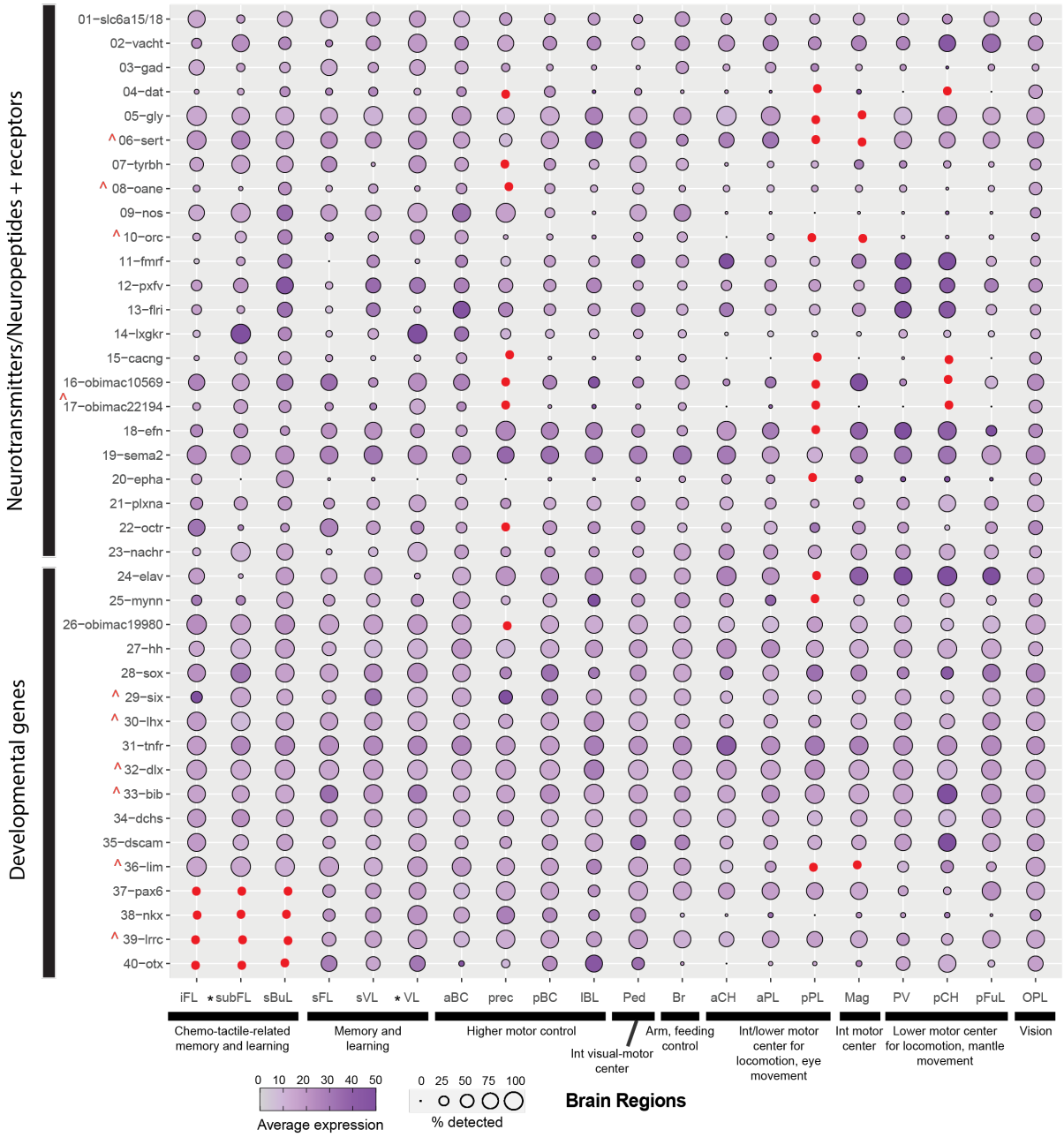

Figure 2. Preliminary DotPlot summary quantifying expression levels and cell density of 40 genes across 20 brain regions. Lobes are ordered based on functional systems outlined in Supplemental Table 1. *indicates lobes with high cell density, which are under-sampled in this preliminary quantification. ^indicates genes with either dense or dim expression in a few cells, leading to over-sampling in the quantification. iFL inferior frontal lobe; subFL subfrontal lobe; sBuL superior buccal lobe; sFL superior frontal lobe; sVL subvertical lobe; VL vertical lobe; aBC anterior basal complex; prec precommissural lobe; pBC posterior basal complex; lBL lateral basal lobe; Ped peduncle lobe; Br brachial lobe; aCH anterior chromatophore lobe; aPL anterior pedal lobe; pPL posterior pedal

lobe; Mag magnocellular lobe; PV palliovisceral lobe; pCH posterior chromatophore lobe; pFuL posterior funnel lobe; OPL optic lobe.

We stained for each of the classical neurotransmitters using the following genes: *slc6a15/18* (glutamatergic), *vacht* (cholinergic), *dat* (dopaminergic), *gad* (gabaergic), *gly1* (glycinergic), and *sert2* (serotonergic) (Figure 3). Previous work showed the presence of glutamatergic, cholinergic, and dopaminergic neurons in the optic lobe based on pharmacology and these data were supported by transcriptional profiling as well. Similar to segregated expression of glutamatergic and cholinergic neurons in the optic lobe, we also found that cells in each of the brain regions that were positive for *slc6a15/18* were not also positive for *vacht* and vice versa, suggesting these are two distinct populations throughout the brain. Moreover, we found that the vertical and subfrontal lobes showed less expression of *slc6a15/18* versus *vacht*. Similar to *dat* expression in the optic lobe, *dat* appeared more restricted in expression across central brain regions, with the most expression found in the optic and superior buccal lobes. *gad* has minimal expression in the optic lobe yet has sparse but dense expression across central brain regions, including a few *gad*+ cells lining the boundaries of vertical lobe gyri and in a subset of cells in the subvertical lobe and anterior basal complex. On the other hand, *gly1* had relatively strong expression across all central brain regions, except for sparse expression along the boundaries of vertical lobe gyri as well. Lastly, *sert2* had strong expression in a few cells across central brain regions, including the subvertical lobe, anterior basal complex, and brachial lobe. All together, these results suggest that most central brain regions have positive expression of glutamatergic and cholinergic markers, but some regions, such as the vertical and subvertical lobes, have sparse, dense expression of other neurotransmitters, which might relate to their functions downstream.

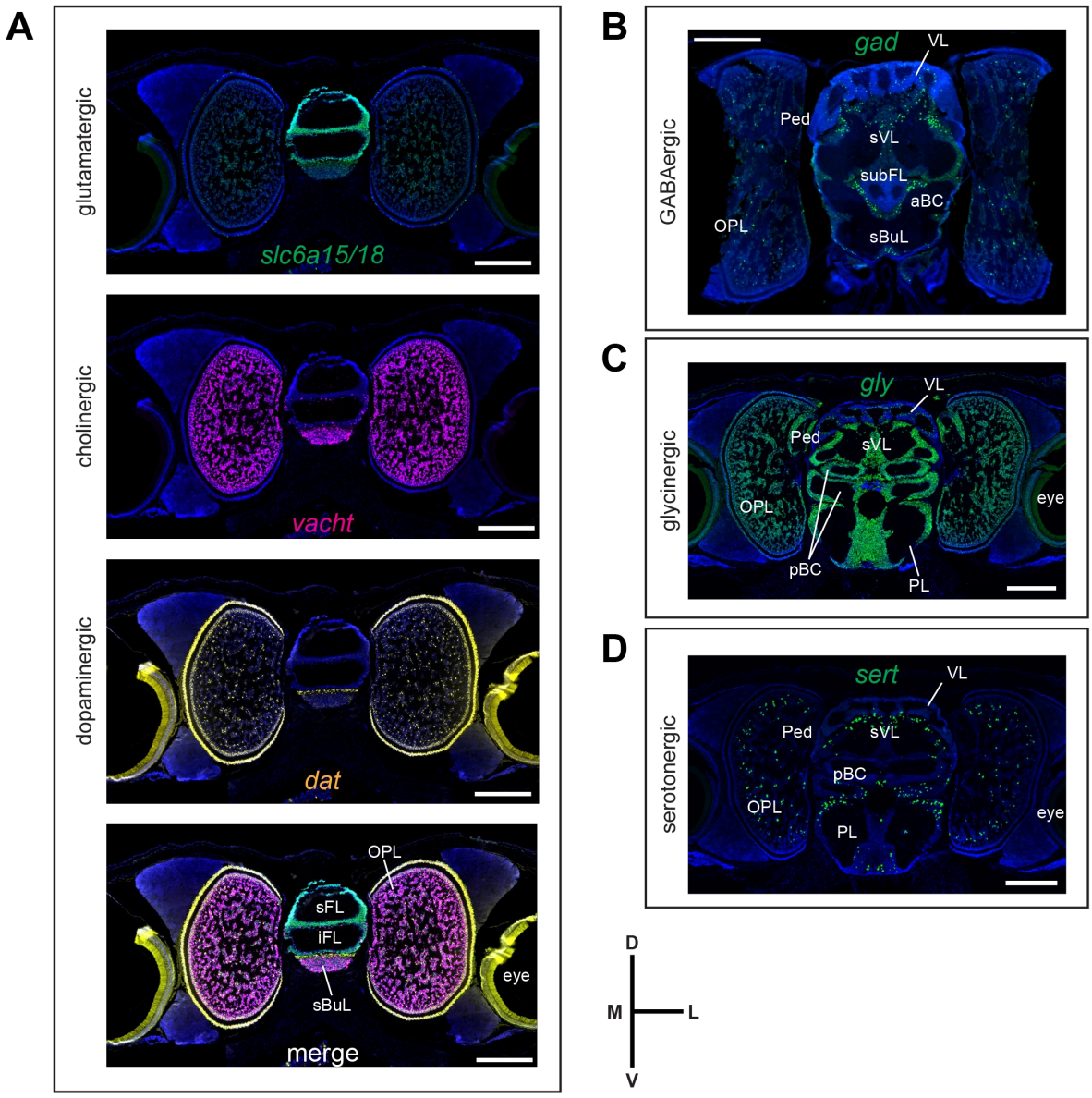

Figure 3. Neurotransmitter expression.
A) Multiplexed RNA FISH of glutamatergic (*slc6a15/18*), cholinergic (*vacht*), and dopaminergic (*dat*) neurons, with a merged image shown at the bottom.
B) Expression of GABAergic neurons (gad).
C) Expression of glycinergic neurons (gly1).
D) Expression of serotonergic neurons *(sert2).* Scale bars, 500um.

Octopaminergic Neurons

In vertebrates, norepinephrine is critical for the fight-or-flight response by increasing alertness.

In invertebrates, octopamine functions similarly as norepinephrine due to its role in helping

mobilize the body for action[37]. Octopamine is present in octopuses as well as other cephalopods[38–41] (see Reviews in[42,43]. In the optic lobe, octopaminergic neurons were identified based on expression of *tyrbh*, which is involved in the biosynthesis of tyrosine to octopamine[4044–46]. These cells were found in a restricted pattern along the outer granular layer of the optic lobe as well as in the peduncle and superior buccal lobes (Figure 4A). A candidate for an octopamine/norepinephrine transporter *oa/ne* showed strong expression in a few cells in the outer granular layer of the optic lobe, including co-localization with a subset *tyrbh*+ cells, as well as in the neuropil throughout the central brain (Figure 4A,D). FISH of a candidate for an octopamine receptor *octr* demonstrated some expression along the borders of central brain regions, but had strong expression in a spatially restricted manner as it filled cells found in the superior frontal lobe (Figure 4B). Together, FISH of these three genes suggest a signaling pathway from the optic and peduncle lobes to the superior frontal lobes, supporting a potential role of octopamine in visuo-motor control or modulation.

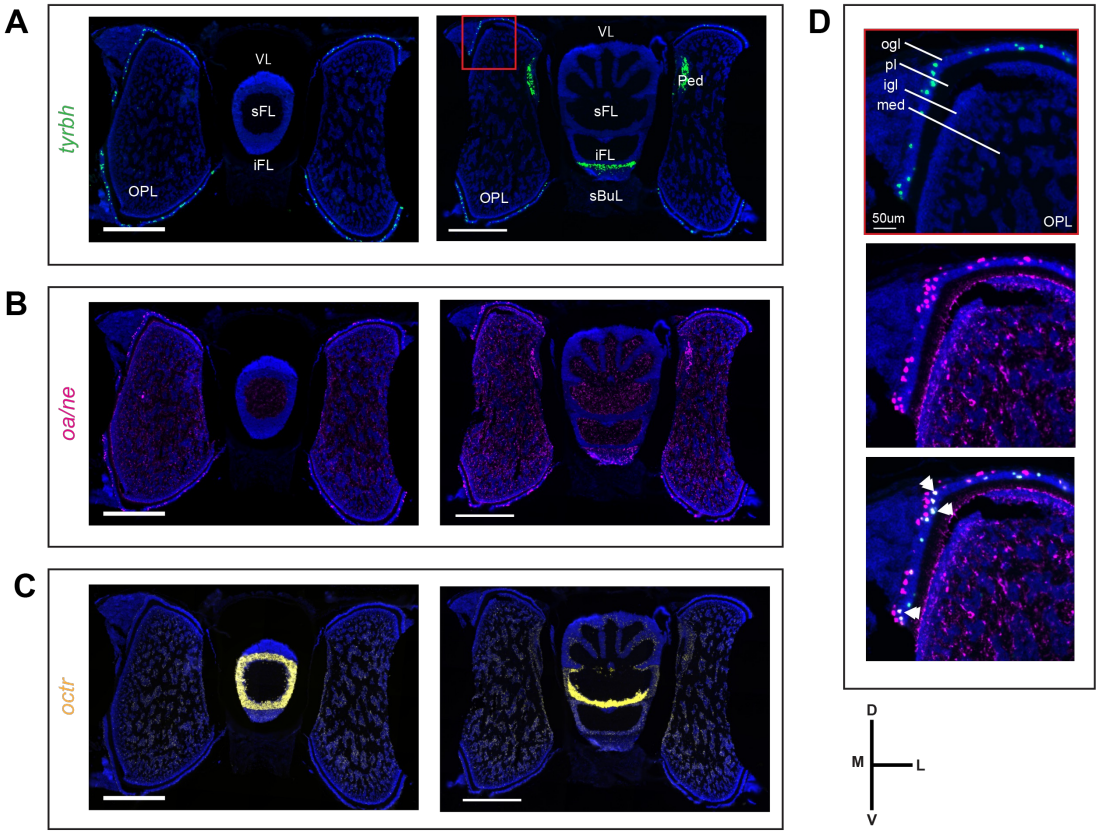

Figure 4. Expression of octopaminergic signaling, transportation, and receptor genes provide insight into potential functionally related regions.

A) *tyrbh* is localized to outer granular layer of optic lobes, superior buccal lobe, and peduncle lobes.
B) Octopamine/norepinephrine transporter candidate *oa/ne* is expressed across the whole brain but found in the neuropil, with some expression in cells in the outer granular layer of the optic lobe and in the peduncle lobe.
C) The putative octopamine receptor *octr* is localized to the superior frontal lobe.
D) Multiplexed RNA FISH of *tyrbh* and *oa/ne* showing co-localization in a subset of cells in the outer granular layer of the optic lobe. ogl outer granular layer; pl plexiform layer; igl inner granular layer; med medulla. Unless noted otherwise, scale bars, 500um.

Neuropeptide Expression

Five neuropeptides (*fmrf, flri, pxfv, lxgkr,* and *orc*) were chosen due to their known individual roles in either camouflage, feeding, or potential visual modulation based on pharmacology, biochemistry, or in situ staining. Additionally, previous studies highlight these genes as key cell type markers in the optic lobe[45,47,48], which has several inputs and outputs to other lobes in the octopus central nervous system[17,49] and therefore may be implicated in visually guided behaviors.

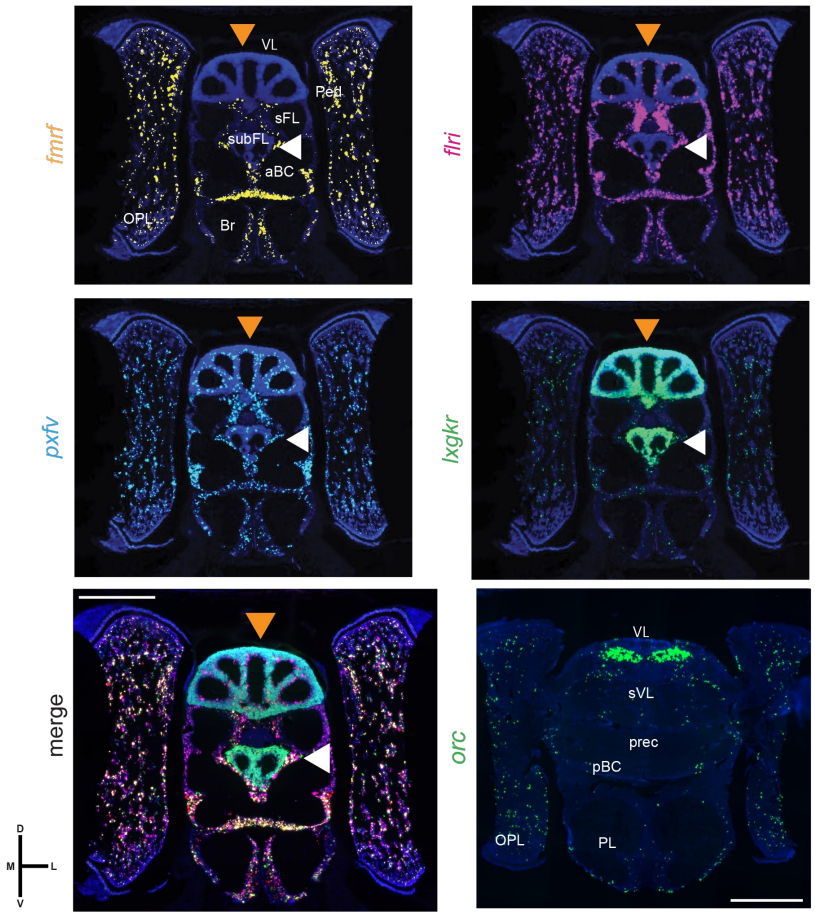

Figure 5. Differential expression of 5 neuropeptides. Neuropeptide *lxgkr* is highly expressed in vertical (orange arrows) and subfrontal lobes (white arrows), whereas *fmrf* is absent from these structures. The merged image on the

bottom left shows multiplexed RNA FISH for *fmrf, flri, pxfv,* and *lxgkr. orc* has a sparse, dense expression across brain regions, except for in a subset of cells in the subvertical lobe, where there is relatively strong expression clustered in one area. Scale bars, 500um.

Overall, we found strong but sparse, dense neuropeptide expression across several brain regions (see Figure 2). The most striking differences in gene expression were between *fmrf* and *lxgkr*, which showed inverse patterns across the subfrontal, vertical, and peduncle lobe (Figure 5). While *Fmrf* was found to be absent in the subfrontal and vertical lobes with decent expression in the peduncle lobes, *lxgkr* was expressed in 100% of cells in the subfrontal and vertical lobes and completely absent from the peduncle lobes. The subfrontal and vertical lobes are key stations in circuits involved in tactile (subfrontal) and visual (vertical) learning and memory, whereas the peduncle lobes have outputs to motor areas in the brain and respond via color changes or arm and body movements when stimulated[11]. While *lxgkr* has not been functionally characterized, *fmrf* has been investigated in several cephalopods and plays a role in physiological regulation, reproductive control, and camouflage[47,48,50–52,52–57].

Differential expression of neurotransmitters and neuropeptides reveals wide use of functional determinants across central brain regions in the octopus and supports the potential for specialized systems for 2 sets of lobes based on either complementary FISH patterns of the octopamine biosynthesis gene *tyrbh* and its putative receptor *octr* (optic, peduncle, and superior frontal lobes) or high expression of *lxgkr* (vertical and subfrontal lobes). In addition to analyzing expression of genes related to mature neuronal function, we also explored spatial patterns of developmental genes in this continuously growing brain.

Characterization of Developmental Genes

Homeobox genes are a group of transcription factors that specify cell identity and play roles in body patterning during development (Reviewed in[58,59]**).** In bilaterians, homebox genes, specifically the Hox superfamily, establishes anterior-posterior development and are thought to be involved in the generation of diverse body plans across this phylum, yet not much is known about the molecular underpinnings of body plan generation and patterning in cephalopods. For example, in *Euprymna scolopes* embryos, anterior-posterior expression was not predicted by *Hox*

collinearity[60]. However, in *Sepia officinalis*, similar genetic programs were found to be involved in arm and tentacle development as what is observed in vertebrate and arthropod limb development[61]. These results suggest the possibility that patterning may vary across the cephalopod body plan or across cephalopod species in general. Therefore, we sought to characterize a subset of homeobox, developmental, and patterningl genes across the octopus central nervous system, which we summarize below.

Homeobox and Developmental Genes

To identify developing neurons, we looked at expression for *elav,* which we found to be highly expressed across all central brain regions except for the vertical and subfrontal lobes. Next, we performed FISH for homebox genes *pax6, lhx, dlx, otx, nkx, sox, six,* and *lim*, which we found to be expressed in 1 of 3 categories (Figure 6). Like, *elav*, we found that *pax6* fell into this first category of high expression everywhere, except for the vertical and subfrontal lobes. *lhx, dlx, and otx* were expressed in lower amounts but across almost all brain regions, falling into this second category of less but homogeneous expression across the central brain. The remaining four homeobox genes fall into the last category: striking expression in a subset of regions. Notably, *nkx* was expressed in 100% of the cells in the vertical and subfrontal lobes, demonstrating a spatial expression pattern reminiscent of the neuropeptide *lxgkr* (Supplemental Figure 1). Similarly, *sox* was expressed in 100% of cells in the vertical and subfrontal lobes but also had expression across other brain regions, including a specific layer (inner granular) of the optic lobe. *six* appeared to be completely absent from the central brain, with expression only found in the outer granular layer of the optic lobe, supporting a potential conserved role for eye development as has been previously identified in drosophila and vertebrate studies (Reviewed in [62–64]). Finally, *lim* was found to be sparsely expressed across several brain regions, including the optic lobes and posterior basal complex, but had notable expression in the subvertical lobe, where it was found to be colocalized in a subset of cells expressing the neuropeptide *orc* (Supplemental Figure 1).

Previous work identified a large population of immature– but not proliferating– neurons in the optic lobes of *O. bimaculoides*, suggesting that neuronal generation may be occurring in a

different region in the brain. Therefore, we sought to characterize a subset of developmental genes (*dscam, lrrc, hh,* and *dchs*) as well as markers for immature neurons (*obimac19980, bib, mynn,* and *tnfr*) based on their potential relation to mature neuron function based on clustering data available in [45].

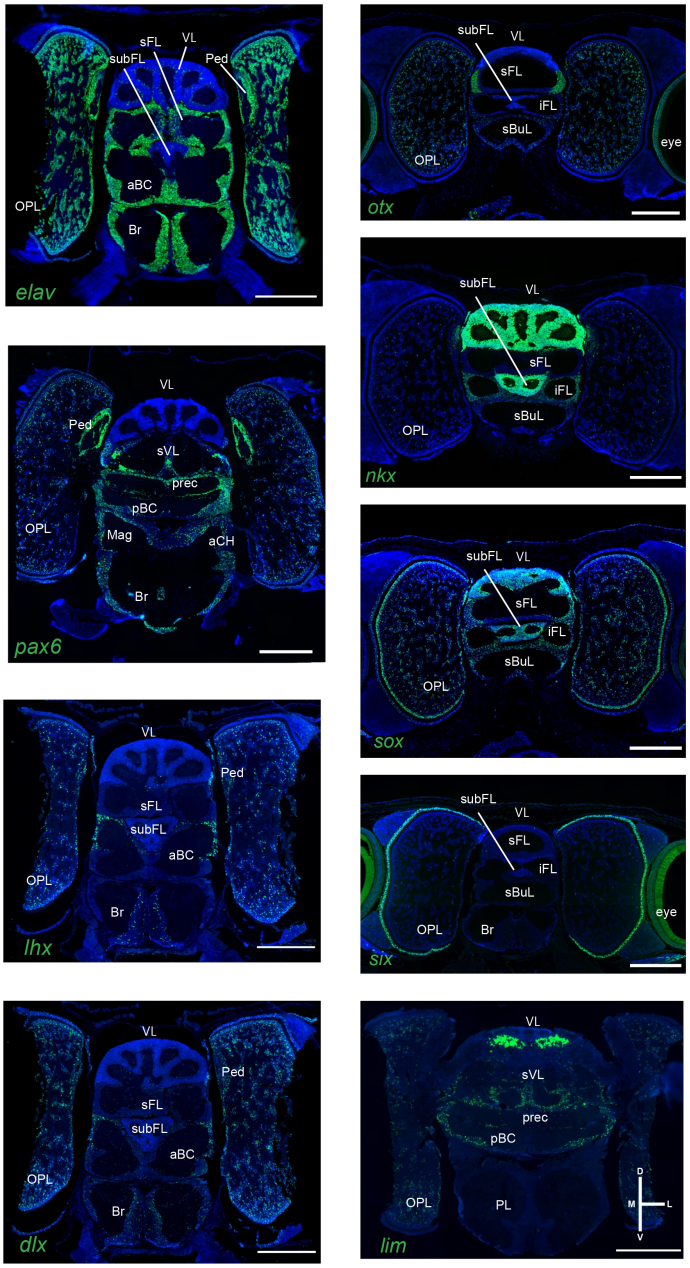

Figure 6. Differential expression of homeobox genes. Scale bars, 500um.

Single-cell data for the first three genes, *dscam*, *lrrc,* and *hh*, show that they are a small subset within clusters that belong to either dopaminergic (*dscam*) or glutamatergic (*lrrc, hh*) neurons (Supplemental Figure 2). Indeed, *dscam* is expressed in a subset of cells in anterior basal complex and in subvertical lobe. Additionally, we also find that *lrrc* is expressed in a subregion of lobes that also express *slc6a15/18* (superior buccal lobe). Unlike *slc6a15/18* expression in the optic lobe, which is expressed across all layers, *hh* is only expressed in a few cells along the edge of the outer granular layer. However, like *slc6a15/18* expression in other central brain regions, we also find that *hh* is expressed homogeneously across almost all central brain regions. Since *hh* is known to play a role in development and patterning, this spatial expression pattern may support the notion that neuronal generation and development may be occurring in different regions of the brain despite the large presence of immature neurons in the optic lobe. Lastly, *dchs* was found to be expressed in several central brain regions, with notable congregation of expression among cells at the border of superficial optic lobe layers.

Based on *O. bimaculoides* optic lobe single-cell and/or gene expression data of *obimac19980, bib, mynn,* and *tnfr*, it is possible that these genes will exhibit complementary spatial expression patterns that extend beyond the optic lobe. Previous work identified the uncharacterized gene *obimac19980* as a strong candidate that is expressed across all of the immature neuronal clusters while not being expressed in the mature neuronal clusters[45]. However, no gene expression data was provided to complement single-cell data. We performed FISH for *obimac19980* and found that it is expressed across the inner boundaries of central brain regions, except for the optic lobe where it appears that there is a potential gradient of stronger expression in the superficial layers with less expression deeper. *tnfr, mynn*, and *bib* were identified as subtypes of immature neurons in the optic lobe based on single cell data. Interestingly, each of these genes are found to be expressed across the majority of central brain regions – albeit at different levels – except for in the vertical and subfrontal lobes, where expression of these genes appears to be absent. For example, *tnfr* has strong expression across several brain regions, most notably among the brachial, peduncle, and superior frontal lobes as well as the anterior basal complex. *mynn* was expressed in these same regions but at relatively much lower levels. However, like *dchs*, we see a similar congregation of *mynn*+ cells along the borders of the superficial layers of the optic

lobe. Likewise, *bib* appears to be expressed in a similar pattern, with expression in the brachial, peduncle, and superior frontal lobes, including along the superficial layers of the optic lobe, and minimal to no expression in the subfrontal and vertical lobes.

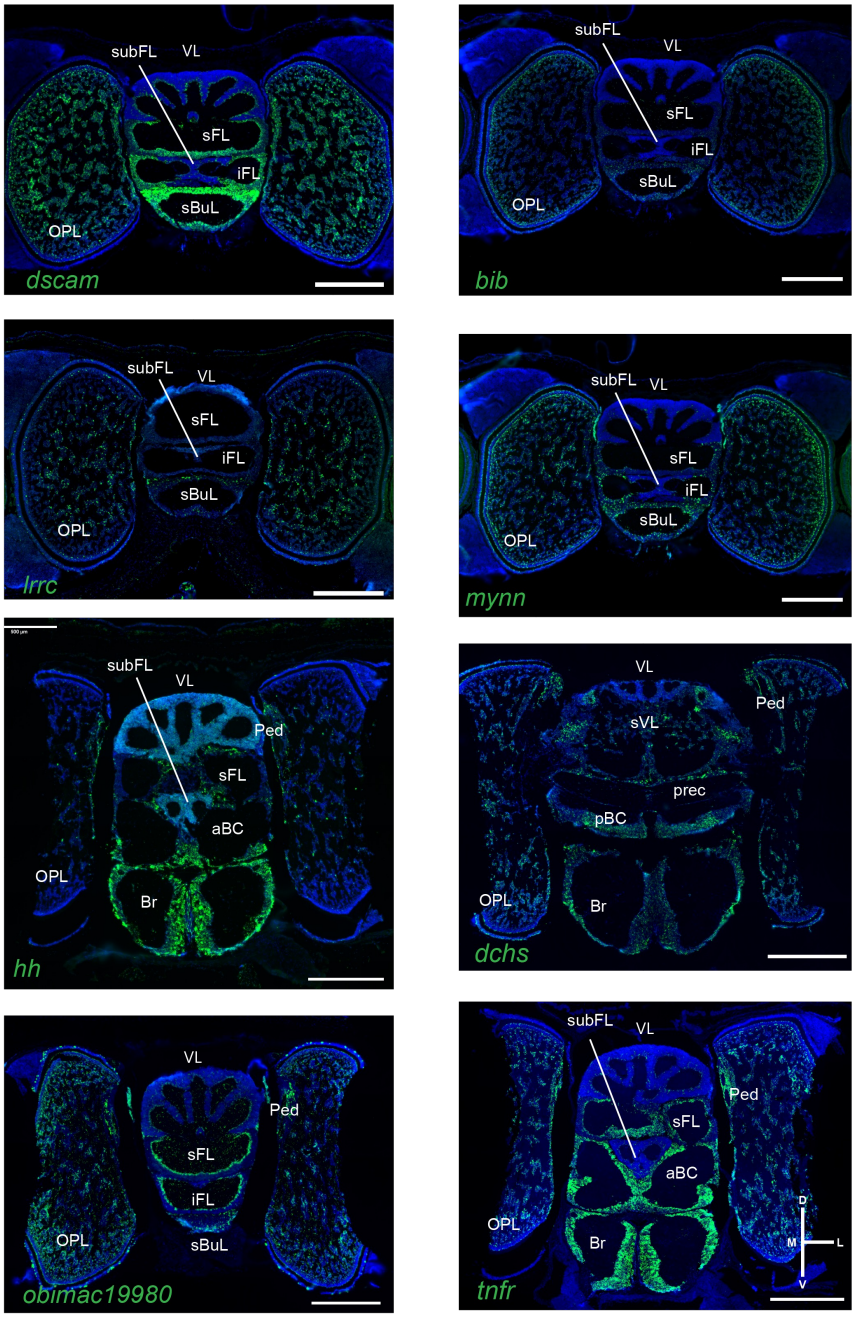

Figure 7. Differential expression of developmental genes and markers for immature neurons. Scale bars, 500um.

Collectively, these findings demonstrate the rich molecular diversity among brain regions in the continuously growing central nervous system of octopuses, which would support the dynamic behaviors that cephalopods are capable of.

Complementary Expression of Patterning Genes

Whereas homebox genes are known to be involved in patterning on a macro level (i.e., along the body axis), axon guidance molecules, such as ephrins and semaphorins, contribute to patterning in vertebrates and invertebrates on a micro level, as they regulate cell-cell adhesion and communication between cells to drive morphology and differentiation[65–68]. However, we have limited information regarding the role of ephrins and semaphorins in cephalopods. To begin to understand how complex neural circuits form (i.e. how cells find their partners) in the growing cephalopod central nervous system, we performed multiplexed FISH on two sets of patterning molecules and their receptor pairs.

We found that the signaling molecule *efn* was expressed largely in the medulla of the optic lobe as well as along other central brain regions, including the anterior basal complex, brachial lobe, and superior frontal lobe (Figure 8A). It appears that *efn* is expressed along the inner boundaries of the vertical lobe gyri and is absent from the subfrontal lobe. Its receptor pair *epha* is expressed in the other layers of the optic lobe, with some expression across central brain regions, including in the anterior basal complex, where *epha* expression appears complementary to *efn* (Figure 8B).

Similarly, the signaling molecule *sema2* is expressed largely in the medulla of the optic lobe and in other central brain regions, including the inferior frontal lobe and a subset of cells in the posterior basal complex, but appears largely absent from the vertical and subfrontal lobes (Figure 8C). Its receptor pair *plxna* is expressed in the outer layers of the optic lobe, with some expression across other central brain regions, including a separate subset of cells in the posterior basal complex and in the superior buccal lobe, with minimal expression in the vertical and subfrontal lobes (Figure 8C-E).

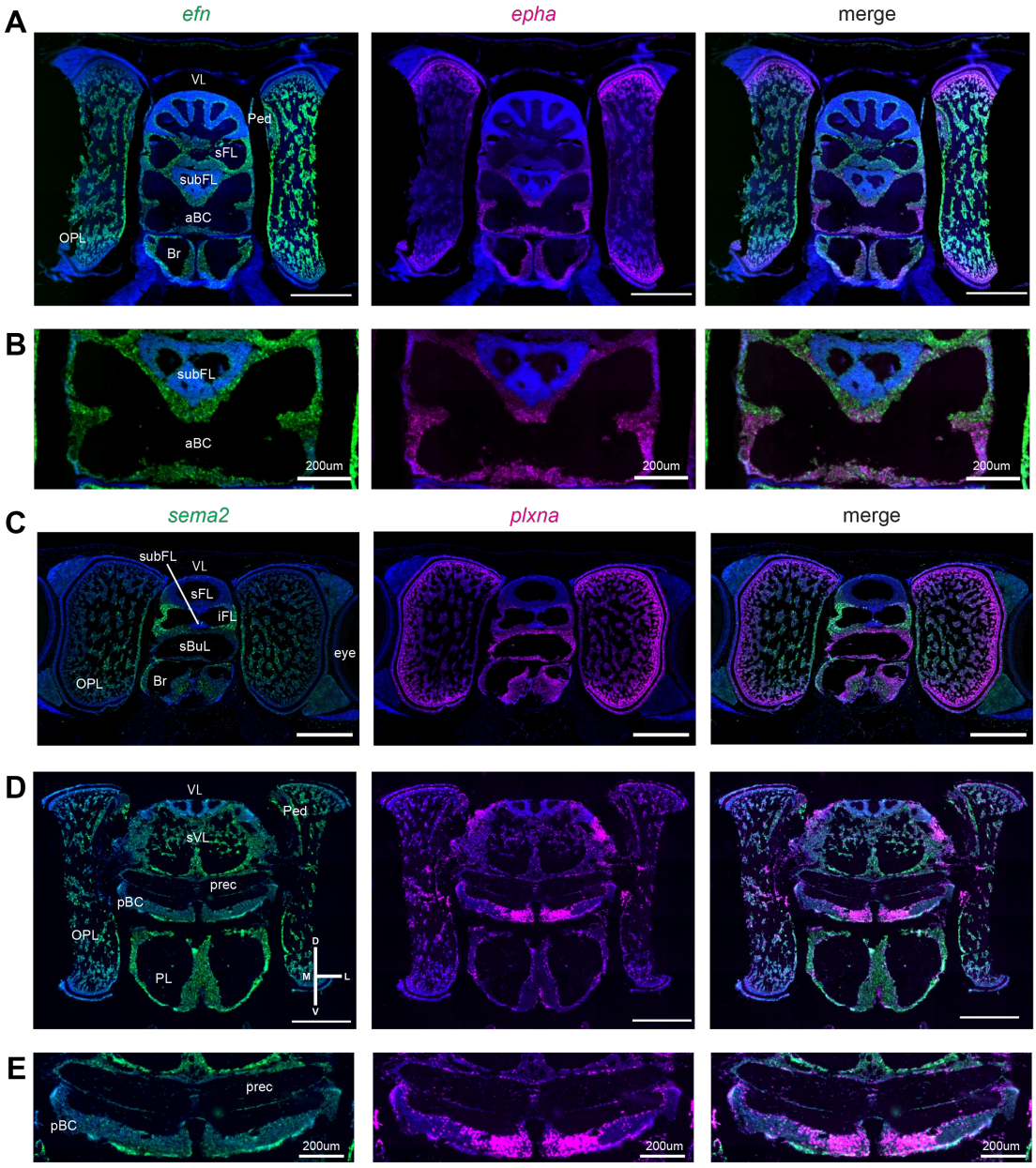

Figure 8. Complementary expression of patterning molecules.
A) FISH of signaling molecule *efn* (left) shows higher expression in the outer layers of the optic lobe and a gradient of expression from the ventral half of the anterior basal complex toward the dorsal half, whereas FISH of its receptor pair *epha* (middle) shows higher expression in deeper layers of the optic lobe and a gradient from the dorsal to ventral halves of the anterior basal complex.
B) Zoomed in expression on anterior basal complex.
C) FISH of signaling molecule *sema2* shows a similar complementary expression in the optic lobe, with higher expression in the interior frontal lobe, whereas its receptor pair *plxna* has higher expression in the outer layers of the optic lobe and in the superior buccal lobe.
D) *sema2/plxna* expression across a deeper section (i.e. more posterior), shows higher expression of *sema2* along the outer edges of the posterior basal complex, whereas its receptor pair *plxna* has higher expression on the inner portion

of the posterior basal complex.
E) Zoomed in expression on posterior basal complex. Unless otherwise noted, scale bars, 500um.

Together, we find complementary expression of signaling molecules *efn* and *sema2* with their receptor pairs *epha* and *plxna*, respectively, either within lobes (optic lobe for both pairs, anterior basal complex for *efn-epha*, posterior basal complex for *sema2-plxna*) or across nearby lobes (*sema2* in inferior frontal lobe, which is dorsal to the superior buccal lobe, where we find higher expression of *plxna*). Our observations of sub-heterogeneous gene expression within the basal complexes suggests that these structures could potentially be delineated even further due to differential gene expression. For example, even though our definition of the anterior basal complex includes the anterior anterior basal and anterior posterior basal lobes, it is possible that gene expression of *efn-epha* could further differentiate the dorsal versus ventral halves of the anterior anterior basal lobe. In sum, our data suggests that, while the organism, at this age, is still undergoing differentiation of some lobes, it is possible to already delineate some of these structures further based on gene expression.

Discussion

This study provides the first account of brain-wide gene expression in a cephalopod. In addition to identifying 20 lobes in a juvenile *O. bimaculoides*, we characterize and quantify expression for 40 genes, including functional and developmental determinants, using multiplexed RNA FISH. We demonstrate that majority of neurons across all central brain regions can be categorized into glutamatergic or cholinergic based on expression of *slc6a/15/18* or *vacht*, and we found positive *elav* expression throughout this continuously growing brain except for in the vertical and subfrontal lobes, which are both involved in tactile and visual learning and memory. Our results demonstrate molecular diversity across central brain regions, supporting the formation and function of complex neural circuits in this emerging model organism. This study therefore contributes to the expanding field of cephalopod neuroscience by providing a resource for understanding gene expression across the entire octopus brain. In addition to outlining diverse gene expression across several brain regions in the octopus, a number of specific findings here have the potential to further elucidate developmental and functional programs in the cephalopod nervous system.

Patterning Molecules in the Basal Complexes

We identified complementary expression of patterning signaling molecules and their respective pairs. In characterizing the genes *efn* and its receptor pair *epha*, we observed complementary expression patterns in both the optic lobes and in the anterior basal complex. Specifically, we found that *efn* was expressed in deeper layers in the optic lobe and in the dorsal half of the anterior basal complex (the anterior anterior basal lobe in particular), whereas *epha* was expressed in the superficial layers of the optic lobe and in the ventral half of the anterior basal complex. Similarly, we found that the signaling molecule *sema2* was expressed in the deeper layers of the optic lobe and in the inferior frontal lobe, which is found closer to the dorsal end of the central brain, whereas *plxna* was expressed in superficial layers of the optic lobe and in the superior buccal lobe, which is found just ventral of the inferior frontal lobe. Additionally, we observed non-overlapping expression of *sema2* and *plxna* within the posterior basal complex (specifically in the median basal), with *sema2* found along this structure and *plxna* expressed strongly on the inner edges of this structure.

The basal lobes are considered the main motor output centers in cephalopods[69] and receive the majority of its inputs from deeper layers of the optic lobe[49]. The anterior basal lobe, in particular, is known to control locomotion and are implicated in prey capture behavior among other behaviors[17,69–72]. The lateral basal is involved in chromatophore control and camouflage via forming skin papillae, whereas the posterior basal complex (which includes both the median and dorsal basal lobes in our dataset) is involved either in swimming and mantle movements for the former structure, with unclear and unknown functions for the latter based on electrical stimulation[17]. Our findings support the possibility that these genes, which are traditionally viewed as patterning molecules in vertebrates and other species, may be strong candidates for patterning as well in octopuses – both within structures and across multiple lobes.

Tactile and Visual Learning and Memory

We also found bimodal differences in gene expression regarding the vertical and subfrontal lobes. The vertical and subfrontal lobes are implicated in either visual or tactile learning and memory, respectively. In fact, in coordination with other brain regions, these two structures are

at the convergence of parallel circuits driving learning and memory[3,73] (Figure 9). For example, the vertical lobe, which contains 25 million amacrine cells, is a critical component of the superior frontal-vertical system, which receives input from the optic lobes to the superior frontal lobe before sending signals to the subvertical lobe. Similarly, the subfrontal lobe, which contains 5 million amacrine cells, receives tactile information from the axial nerve cord to the inferior frontal lobe before sending signals to the posterior buccal lobe. Expression of *lxgkr, nkx, and sox* in 100% of cells in both the vertical and subfrontal lobes may suggest a role for these genes in the potential integration or storage of either visual or tactile information into memory.

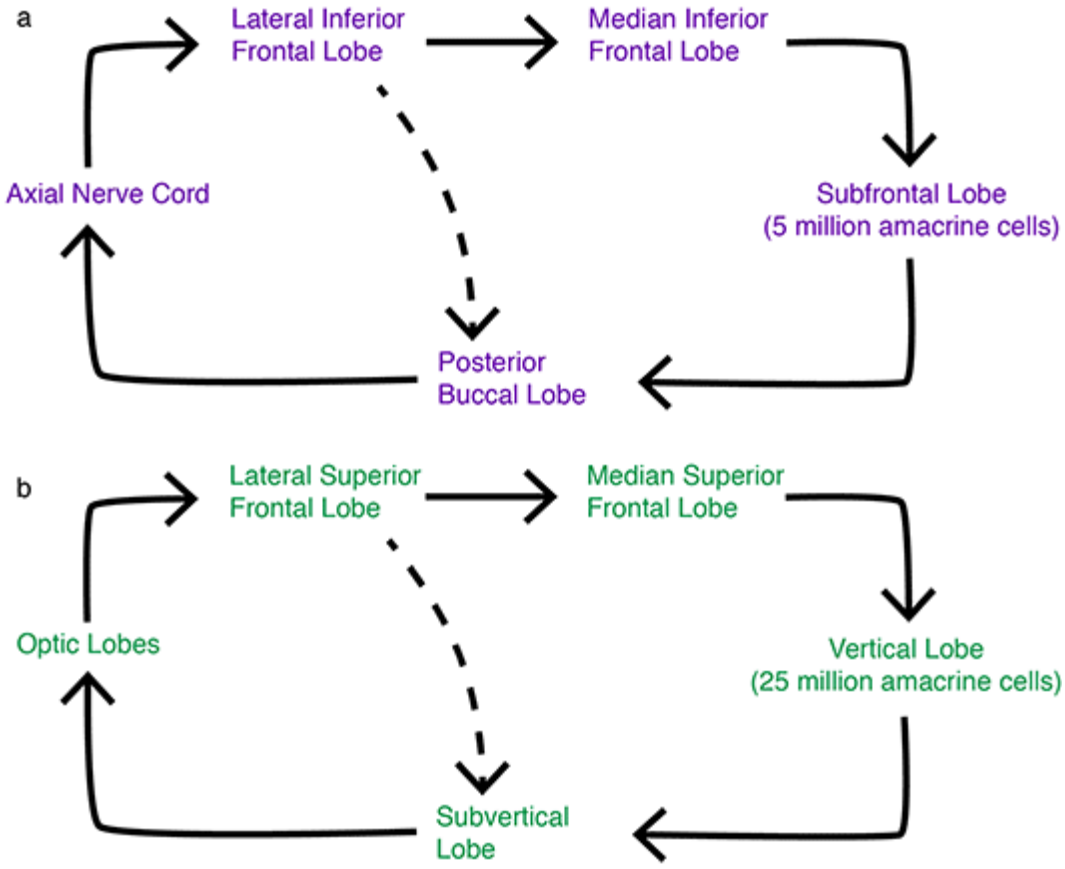

Figure 9. Circuit diagram of tactile and visual learning and memory. From [15]. Number of amacrine cells from [17].
A) Tactile learning and memory system includes convergence on subfrontal lobe and short path (dotted line) through posterior buccal lobe.
B) Visual learning and memory system includes convergence on vertical lobe and short path (dotted line) through subvertical lobe. Many of the connections for both circuits are reciprocated.

Interestingly, a number of genes were not expressed in these brain regions, and many of these have implications in development, except for 1 marker. We found that expression of *fmrf, elav,*

pax6, tnfr, mynn, dchs, and *bib* were completely absent from the vertical and subfrontal lobes. Additionally, we found that *efn* lined the gyri of the vertical lobe but was completely absent from the subfrontal lobe, whereas *sema2* was absent from both the vertical and subfrontal lobes. It is intriguing to speculate on the significance of the lack of expression of mostly developmental genes from these two critical structures involved in visual and tactile learning and memory, but further investigation into these genes are required to fully understand their function(s) in the cephalopod brain.

Co-localization of Neuropeptides and Homeobox Genes

We also note two instances where we observed colocalization of a neuropeptide and a homeobox gene for a subset of populations at the cellular level. In the vertical and subfrontal lobes, we find that *lxgkr* and *nkx* are colocalized, as both of these genes fill 100% of the cells in these regions. In addition, we find that *orc* and *lim* are colocalized in a subset of cells in the subvertical lobe. While *lxgkr* is currently uncharacterized beyond single-cell clustering and gene expression in the *O. bimaculoides*, its striking expression in these structures suggest a role for visual tactile learning and memory. *nkx*, on the other hand, has been well characterized in vertebrates and invertebrates, including a few cephalopods species, as playing a role in mediolateral patterning. Whereas *nkx* traditionally marks the medial portions of vertebrates and insects, in the developing cuttlefish embryo, it is found to be expressed at the periphery[74]. While it is not obvious in our dataset whether *nkx* is involved in patterning in these structures or along any axis in the cephalopod brain, it is possible that this gene is being utilized in an alternate manner than what it is traditionally known for in other organisms.

A second instance where there is colocalization of a neuropeptide with a homeobox gene is in a subset of cells in the subvertical lobe, which express both *orc* and *lim*. The subvertical lobe receives many inputs from different regions in the body and SUB, supporting its comparison to a vertebrate thalamus relay center[12], and it is also a component of the visual learning and memory circuit comprising the optic, superior frontal, and vertical lobes (see Figure 9). *orc* is suggested to be involved in feeding, reproduction, and movement regulation in different species[75–77], whereas *lim* is a homeobox gene traditionally known for its role in body patterning, similar to

nkx[78]. It is possible that *orc* plays a neuromodulatory role in relaying information between the frontal and vertical lobes to the rest of the SUB and body, in concert with previous literature highlighting a more homeostasis-related function. However, fully dissecting the role of *lim* in this region and whether it functions together with *orc* in some manner for regulation will warrant advancements in genetic manipulation in this or other cephalopod species.

Several advancements in technology show promise for the perturbation of neural circuits underlying dynamic cephalopod behavior that can begin to address these remaining questions. For instance, sequencing of the first cephalopod revealed several genomic novelties that might contribute to the rich repertoire of behavior we see across different cephalopod species[79]. Building upon these data, several studies utilized single-cell and single-nuclei RNA sequencing on squid and octopuses, revealing that the transcriptional landscape of the cephalopod nervous system may provide further insight into how diverse circuits may form and function in a developing, juvenile, and adult cephalopod[44,45,80]. Finally, in recent years, there have been tremendous strides in higher resolution functional studies and genetic manipulation[81–84]. By characterizing brain-wide gene expression in the octopus, our work lays a foundation for the aforementioned studies to build upon as well as for future investigations dissecting the formation and function of neural circuits in cephalopods.

Limitations of This Study

It is important to note that, while we identified 20 differentiated lobes in the juvenile octopus, there is potential to further delineate these brain regions using advanced 3D imaging. Indeed, both histological and 3D MRI studies in cephalopods were able to identify over 50-60 lobes when using data from other planes of sectioning[20,25]. Additionally, while we characterized the expression of 40 genes which include both markers for mature neuronal function as well as development, there are certainly more genes that can be included in future studies to provide information regarding brain organization in cephalopods. This initial account of brain-wide gene expression in the octopus is intended to serve as a resource for this rapidly expanding field of cephalopod neuroscience.

Here we characterized brain-wide gene expression using multiplexed RNA FISH in serial coronal sections. Future studies can relate gene expression to molecular and functional identities in cephalopod neural circuits using the growing technologies available, such as spatial transcriptomics, functional recordings, and genetic manipulation. The gene expression mapping we present here provides a resource for such studies, which will be critical for understanding how the cephalopod brain computes and executes a dynamic repertoire of advanced behaviors.

Methods

Experimental Model and Subject Details

Octopus bimaculoides were obtained from the Cephalopod Resource Center at the Marine Biology Laboratory (Woods Hole, MA) and from Aquatic Research Consultants (San Pedro, CA). They were kept at the University of Oregon in a closed circulating 250 gallon aquarium system in artificial seawater, and fed daily on a rotating diet of frozen shrimp, crabs, and fish. All husbandry and experimental protocols were in accordance with the EU 2010/63/EU[85] and AAALAC guidelines for the use and care of cephalopods for research.

Method Details

Animal Fixation

Juvenile animals (mantle lengths 7mm-9mm) were anesthetized on ice using 4% ethanol in Artificial Seawater (460mM NaCl, 10mM KCl, 10mM glucose, 10mM HEPES, 40mM MgCl2, 11mM CaCl2, and 2mM glutamine at pH 7.4). Before fixing the tissue in 10% Neutral Formalin Buffer for 24 hours at room temperature, the mantle and arms were removed, leaving only the central brain complex with the optic lobes and eyes attached.

Hematoxylin & Eoisin Staining

Samples used for Hematoxylin & Eosin (H&E) staining were approximately 4-6 weeks in age, with mantle lengths ranging from 5-7mm. The central brain complex, including optic lobes, was dissected as described above and was embedded into paraffin before being sectioned coronally at 7um. Slices were placed serially and used for the identification of major lobe complexes.

RNA Fluorescence In Situ Hybridization

Samples used for RNA fluorescence in situ hybridization were approximately 4-6 weeks in age, with mantle lengths ranging from 7-9mm. Following the fixation of the central brain complex, the lenses and part of the optic lobes were trimmed off, leaving half of the optic lobes and the entire central brain complex. The samples were embedded into paraffin and sectioned at 10um. Slices were placed in an alternating layout across 2 slides, with 5 sections per ribbon and approximately 12 ribbons per slide. Probes were ordered through Advanced Cell Diagnostics (ACDBio). Genes were stained according to a protocol previously published in [45]. Some images used for Figures 3, 6-8 were from samples sectioned at 7um and accessible/previously published [45].

Image Analysis

Slides were imaged on a Leica Aperio VERSA slide scanner at 20X magnification. Image files were then loaded into QuPath (v0.5), and brain regions were annotated within the project file. For every 5 sections on a ribbon, 1-2 sections were annotated, capturing each brain region at least once for each gene. Following annotating, mean fluorescence and percent positive were calculated per gene for each region. Positive Cell Detection was run using DAPI, with requested pixel size at 0.25um, background radius at 5um, median filter radius set to 0, sigma at 1.5, area range from 10um-500um, threshold at 0.25um, and cell expansion set to 5um. The lower threshold for DAPI ranged from 5-55 based on background autofluorescence, and exact values will be provided upon request. Cell Detection measurements were exported and read into a custom R script to generate Figure 2.

Supplementary Figures

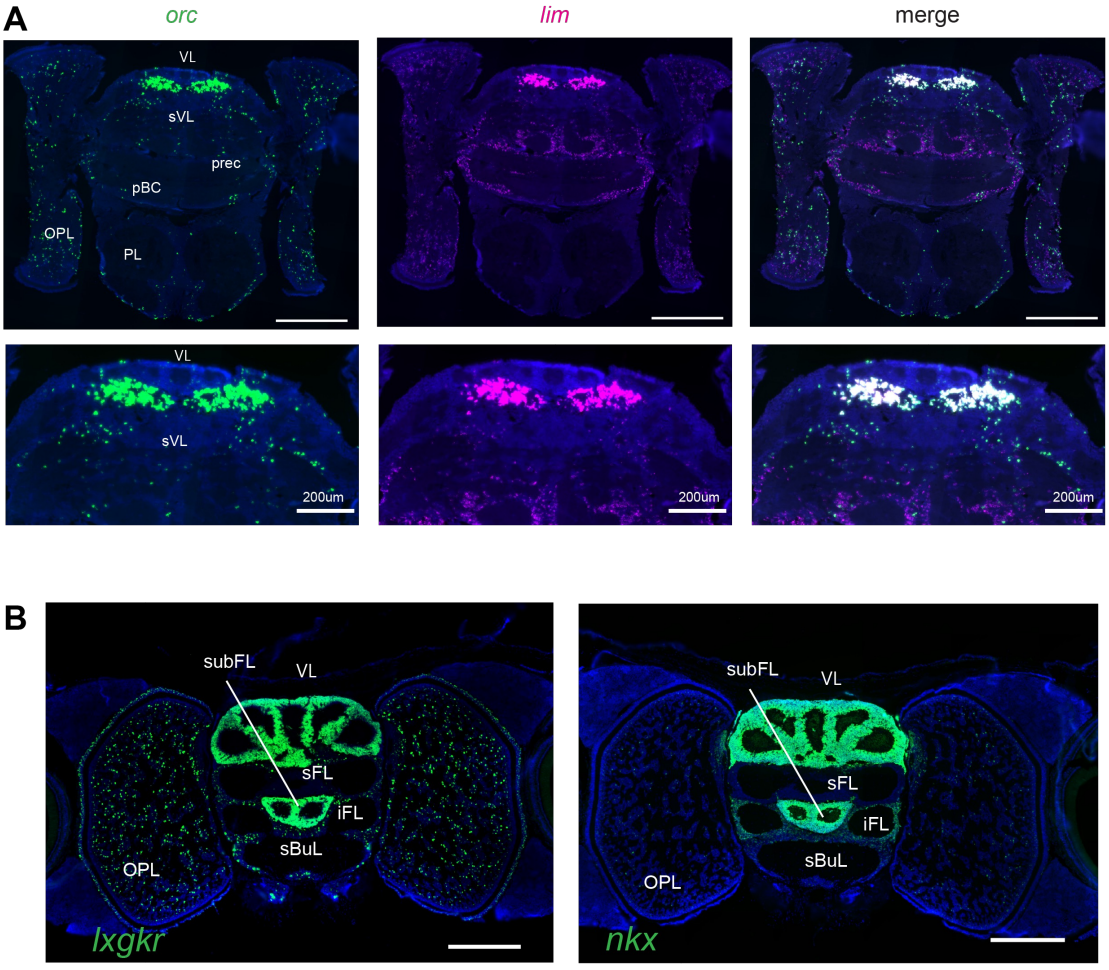

Supplemental Figure 1. Co-localization of neuropeptides with homeobox genes.
A) Co-localization of neuropeptide *orc* with homeobox gene *lim* in a subset of cells in the subvertical lobe.
B) Co-expression of neuropeptide *lxgkr* with homeobox gene *nkx* in 100% of cells in the vertical and subfrontal lobes. Unless otherwise noted, scale bars, 500um.

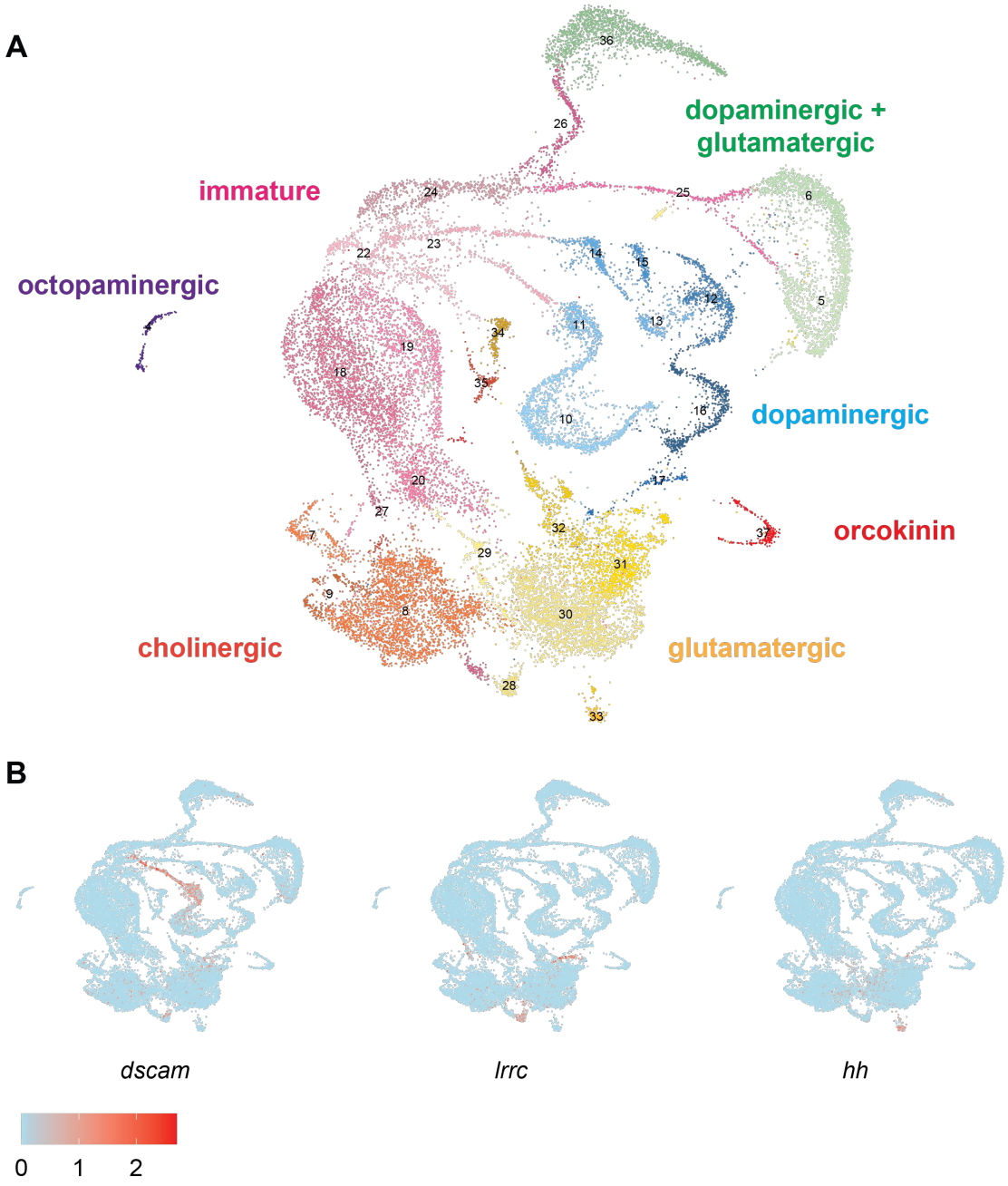

Supplemental Figure 2. Featureplots showing single-cell expression of *dscam*, *lrrc*, and *hh*.
A) UMAP from [45] showing major classes of mature neurons as well as large population of immature neurons in the octopus optic lobe.
B) Individual feature plots showing single-cell expression of developmental genes.

Functional Systems	Lobes in adult O. vulgaris	Lobes in juvenile O. bimaculoides	Abbreviations
Learning and memory	Vertical	Vertical	VL
	Subvertical	Subvertical	sVL
	Superior frontal	Superior frontal	sFL
Chemosensory and tactile learning and memory	Inferior frontal	Inferior frontal	iFL
	Subfrontal	Subfrontal	subFL
	Superior buccal	Superior buccal	sBuL
	Posterior buccal		
Visual processing	Optic	Optic	OPL
Lower visuo-motor control	Peduncle	Peduncle	Ped
	Olfactory	Not identified	-----
	Optic gland	Not identified	-----
Higher motor control for sensory processing and behavior (SEM)	Anterior basal	Anterior basal complex	aBC
	Precommissural	Precommissural	prec
	Subpedunculate	Not identified	-----
	Dorsal basal	Posterior basal complex	pBC
	Median basal		
	Lateral basal	Lateral basal	lBL
Lower motor control for funnel, arm, and mantle movement (SUB)	Brachial	Brachial	Br
	Anterior chromatophore	Anterior chromatophore	aCH
	Anterior pedal	Anterior pedal	aPL
	Posterior pedal	Posterior pedal	pPL
	Magnocellular	Magnocellular	Mag
	Palliovisceral	Palliovisceral	PV
	Posterior chromatophore	Posterior chromatophore	pCH
	Vasomotor	Identified in 1/5 samples	-----
	Funnel	Funnel	FuL

Supplemental Table 1. Comparison of identified lobes in the adult *Octopus vulgaris* central nervous system versus the juvenile *Octopus bimaculoides*, grouped based on known functions.

Neurotransmitters & Neuropeptides	Receptors	Developmental
slc6a15/18	octr	elav
vacht	cacng	pax6
dat	epha	lhx
gad	plxna	dlx
gly1	nachr	otx
sert2		nkx
tyrbh		sox
oa/ne		six
nos		lim
fmrf		dscam
pxfv		lrrc
flri		hh
lxgkr		dchs
orc		obimac19980
obimac10569		bib
obimac22194		mynn
efn		tnfr
sema2		

Supplemental Table 2. Candidate genes used for RNA FISH

References

1. Budelmann, B.U. (1995). The cephalopod nervous system: What evolution has made of the molluscan design. In The Nervous Systems of Invertebrates: An Evolutionary and Comparative Approach Experientia Supplementum., O. Breidbach and W. Kutsch, eds. (Birkhäuser Basel), pp. 115–138. https://doi.org/10.1007/978-3-0348-9219-3_7.

2. Bullock, T., and Horridge, G.A. (1965). Structure and function in the nervous systems of invertebrates. (San Francisco).

3. Nixon, M., and Young, J.Z. (2003). The brains and lives of cephalopods (Oxford University Press).

4. Packard, A. (1972). CEPHALOPODS AND FISH: THE LIMITS OF CONVERGENCE. Biol. Rev. *47*, 241–307. https://doi.org/10.1111/j.1469-185x.1972.tb00975.x.

5. Williamson, R., and Chrachri (2004). Cephalopod neural networks. Neurosignals *13*, 87–98. https://doi.org/10.1159/000076160.

6. Young, J.Z. (1963). THE NUMBER AND SIZES OF NERVE CELLS IN *OCTOPUS*. Proc. Zool. Soc. Lond. *140*, 229–254. https://doi.org/10.1111/j.1469-7998.1963.tb01862.x.

7. Boycott, B.B. (1965). LEARNING IN THE OCTOPUS. Sci. Am. *212*, 42–51.

8. Boycott, B.B., and Young, J.Z. (1955). A memory system in *Octopus vulgaris* Lamarck. Proc. R. Soc. Lond. Ser. B - Biol. Sci. *143*, 449–480. https://doi.org/10.1098/rspb.1955.0024.

9. Gray, E.G., and Young, J.Z. (1997). The fine structure of the vertical lobe of Octopus brain. Philos. Trans. R. Soc. Lond. B Biol. Sci. *258*, 379–394. https://doi.org/10.1098/rstb.1970.0040.

10. Hochner, B., Zullo, L., Shomrat, T., Levy, G., and Nesher, N. (2023). Embodied mechanisms of motor control in the octopus. Curr. Biol. *33*, R1119–R1125. https://doi.org/10.1016/j.cub.2023.09.008.

11. Messenger, J.B. (1967). The peduncle lobe: a visuo-motor centre in octopus. Proc. R. Soc. Lond. B Biol. Sci. *167*, 225–251. https://doi.org/10.1098/rspb.1967.0025.

12. Shigeno, S., Andrews, P.L.R., Ponte, G., and Fiorito, G. (2018). Cephalopod Brains: An Overview of Current Knowledge to Facilitate Comparison With Vertebrates. Front. Physiol. *9*. https://doi.org/10.3389/fphys.2018.00952.

13. Shomrat, T., Zarrella, I., Fiorito, G., and Hochner, B. (2008). The Octopus Vertical Lobe Modulates Short-Term Learning Rate and Uses LTP to Acquire Long-Term Memory. Curr. Biol. *18*, 337–342. https://doi.org/10.1016/j.cub.2008.01.056.

14. Shomrat, T., Turchetti-Maia, A.L., Stern-Mentch, N., Basil, J.A., and Hochner, B. (2015). The vertical lobe of cephalopods: an attractive brain structure for understanding the evolution of advanced learning and memory systems. J. Comp. Physiol. A *201*, 947–956. https://doi.org/10.1007/s00359-015-1023-6.

15. Wang, Z.Y., and Ragsdale, C.W. (2019). Cephalopod Nervous System Organization. In Oxford Research Encyclopedia of Neuroscience (Oxford University Press). https://doi.org/10.1093/acrefore/9780190264086.013.181.

16. Wells, M.J. (2013). Octopus: physiology and behaviour of an advanced invertebrate (Springer-Science+Business Media, B.V).

17. Young, J.Z. (1971). The anatomy of the nervous system of Octopus vulgaris (Clarendon Press).

18. Wild, E., Wollesen, T., Haszprunar, G., and Heß, M. (2015). Comparative 3D microanatomy and histology of the eyes and central nervous systems in coleoid cephalopod hatchlings. Org. Divers. Evol. *15*, 37–64. https://doi.org/10.1007/s13127-014-0184-4.

19. Koizumi, M., Shigeno, S., Mizunami, M., and Tanaka, N.K. (2016). Three-dimensional brain atlas of pygmy squid, Idiosepius paradoxus, revealing the largest relative vertical lobe system volume among the cephalopods. J. Comp. Neurol. *524*, 2142–2157. https://doi.org/10.1002/cne.23939.

20. Jung, S.-H., Song, H.Y., Hyun, Y.S., Kim, Y.-C., Whang, I., Choi, T.-Y., and Jo, S. (2018). A Brain Atlas of the Long Arm Octopus, Octopus minor. Exp. Neurobiol. *27*, 257–266. https://doi.org/10.5607/en.2018.27.4.257.

21. Chung, W.-S.M., Justin (2014). Range-finding in squid using retinal deformation and image blur. Curr. Biol. CB *24*, R64–R65. https://doi.org/10.1016/j.cub.2013.11.058.

22. Chung, W.-S., and Marshall, N.J. (2017). Complex Visual Adaptations in Squid for Specific Tasks in Different Environments. Front. Physiol. *8*. https://doi.org/10.3389/fphys.2017.00105.

23. Liu, Y.-C.C., Wen-Sung; Yu, Chun-Chieh; Hsu, Su-Ting; Chan, Fung-Lan; Liu, Tsung-Han; Su, Chia-Hao; Hwu, Yeukuang; Marshall, N. Justin; Chiao, Chuan-Chin (2017). Morphological changes of the optic lobe from late embryonic to adult stages in oval squids Sepioteuthis lessoniana. J. Morphol. *279*, 75–85. https://doi.org/10.1002/jmor.20755.

24. Chung, W.-S., Kurniawan, N.D., and Marshall, N.J. (2020). Toward an MRI-Based Mesoscale Connectome of the Squid Brain. iScience *23*, 100816. https://doi.org/10.1016/j.isci.2019.100816.

25. Chung, W.-S., Kurniawan, N.D., and Marshall, N.J. (2022). Comparative brain structure and visual processing in octopus from different habitats. Curr. Biol. *32*, 97-110.e4. https://doi.org/10.1016/j.cub.2021.10.070.

26. Schmidbaur, H., Kawaguchi, A., Clarence, T., Fu, X., Hoang, O.P., Zimmermann, B., Ritschard, E.A., Weissenbacher, A., Foster, J.S., Nyholm, S.V., et al. (2022). Emergence of novel cephalopod gene regulation and expression through large-scale genome reorganization. Nat. Commun. *13*, 2172. https://doi.org/10.1038/s41467-022-29694-7.

27. Coffing, G.C., Tittes, S., Small, S.T., Songco-Casey, J.O., Piscopo, D.M., Pungor, J.R., Miller, A.C., Niell, C.M., and Kern, A.D. (2024). Cephalopod Sex Determination and its Ancient Evolutionary Origin Revealed by Chromosome-level Assembly of the California Two-Spot Octopus. Preprint, https://doi.org/10.1101/2024.02.21.581452 https://doi.org/10.1101/2024.02.21.581452.

28. Solorzano, Y.V., María Teresa; López, Lus M.;. Correa, Juan Gabriel; True, Conal C.;. Rosas, Carlos (2009). Response of newly hatched Octopus bimaculoides fed enriched Artemia salina: Growth performance, ontogeny of the digestive enzyme and tissue amino acid content. Aquaculture *289*, 84–90. https://doi.org/10.1016/j.aquaculture.2008.12.036.

29. Hanlon, R.T.; F., John W. (1985). Advances in the laboratory culture of octopuses for biomedical research. Lab. Anim. Sci. *35*, 33–40.

30. Wells, M.J., and Wells, J. (1969). Pituitary Analogue in the Octopus. Nature *222*, 293–294. https://doi.org/10.1038/222293a0.

31. Wang, Z.Y., and Ragsdale, C.W. (2018). Multiple optic gland signaling pathways implicated in octopus maternal behaviors and death. J. Exp. Biol., jeb.185751. https://doi.org/10.1242/jeb.185751.

32. Wodinsky, J. (1977). Hormonal Inhibition of Feeding and Death in *Octopus* : Control by Optic Gland Secretion. Science *198*, 948–951. https://doi.org/10.1126/science.198.4320.948.

33. Wells, M.J., and Wells, J. (1959). Hormonal Control of Sexual Maturity in *Octopus*. J. Exp. Biol. *36*, 1–33. https://doi.org/10.1242/jeb.36.1.1.

34. Wang, Z.Y., Pergande, M.R., Ragsdale, C.W., and Cologna, S.M. (2022). Steroid hormones of the octopus self-destruct system. Curr. Biol. *32*, 2572-2579.e4. https://doi.org/10.1016/j.cub.2022.04.043.

35. Wang, Z.Y., and Ragsdale, C.W. (2023). Signaling ligand heterogeneities in the peduncle complex of the cephalopod mollusc *Octopus bimaculoides*. Preprint, https://doi.org/10.1101/2023.11.27.568875 https://doi.org/10.1101/2023.11.27.568875.

36. The nervous system of *Loligo* IV. The peduncle and olfactory lobes (1979). Philos. Trans. R. Soc. Lond. B Biol. Sci. *285*, 275–309. https://doi.org/10.1098/rstb.1979.0007.

37. Roeder, T. (1999). Octopamine in invertebrates. Prog. Neurobiol. *59*, 533–561. https://doi.org/10.1016/s0301-0082(99)00016-7.

38. Juorio, A.V.M., P.B. (1971). Distribution of octopamine in nervous tissues of Octopus vulgaris. Br. J. Pharmacol. *43*, 438P-439P.

39. Andrews, P., Messenger, J., and Tansey, T. (1983). The chromatic and motor effects of neurotransmitter injection in intact and brain-lesioned Octopus. J. Mar. Biol. Assoc. U. K. *63*, 355–370. https://doi.org/10.1017/S0025315400070739.

40. Capasso, A., Carginale, V., Madonna, L., Mancaniello, D., Scudiero, R., De Prisco, P.P., De Petrocellis, B., and Parisi, E. (1991). A dopamine- and octopamine-sensitive adenylate cyclase in the nervous system of *Octopus vulgaris*. Comp. Biochem. Physiol. Part B Comp. Biochem. *100*, 805–808. https://doi.org/10.1016/0305-0491(91)90294-N.

41. Erspamer, V. (1952). Identification of Octopamine as l-p-Hydroxyphenylethanolamine. Nature *169*, 375–376. https://doi.org/10.1038/169375b0.

42. Messenger, J.B. (1996). Neurotransmitters of cephalopods. Invert. Neurosci. *2*, 95–114. https://doi.org/10.1007/bf02214113.

43. Juorio, A.V., and Molinoff, P.B. (1974). The Normal Occurrence of Octopamine in Neural Tissues of the Octopus and Other Cephalopods. J. Neurochem. *22*, 271–280. https://doi.org/10.1111/j.1471-4159.1974.tb11590.x.

44. Styfhals, R.Z., Grygoriy; Hulselmans, Gert; Spanier, Katina I; Poovathingal, Suresh; Elagoz, Ali M; De Winter, Seppe; Deryckere, Astrid; Rajewsky, Nikolaus; Ponte, Giovanna; Fiorito, Graziano; Aerts, Stein; Seuntjens, Eve (2022). Cell type diversity in a developing octopus brain. Nat. Commun. *13*, 7392-NA. https://doi.org/10.1038/s41467-022-35198-1.

45. Songco-Casey, J.O., Coffing, G.C., Piscopo, D.M., Pungor, J.R., and Kern, A.K. (2022). Cell types and molecular architecture of the Octopus bimaculoides visual system. Curr. Biol. CB *32*, 5031-5044.e4. https://doi.org/10.1016/j.cub.2022.10.015.

46. Pungor, J.R. (2014). Characterization of the visual system of octopus bimaculoides.

47. Chrachri, A. (2020). Effect of FMRFamide on voltage-dependent currents in identified centrifugal neurons of the optic lobe of the cuttlefish, *Sepia officinalis*. Preprint, https://doi.org/10.1101/2020.09.29.318691 https://doi.org/10.1101/2020.09.29.318691.

48. Suzuki, H., Yamamoto, T., Nakagawa, M., and Uemura, H. (2002). Neuropeptide Y-immunoreactive neuronal system and colocalization with FMRFamide in the optic lobe and

peduncle complex of the octopus (Octopus vulgaris). Cell Tissue Res. *307*, 255–264. https://doi.org/10.1007/s00441-001-0492-9.

49. Young, J.Z. (1962). The Optic Lobes of Octopus vulgaris. Philos. Trans. R. Soc. Lond. B. Biol. Sci. *245*, 19–58. https://doi.org/10.1098/rstb.1962.0005.

50. Chin, G.J., Payza, K., Price, D.A., Greenberg, M.J., and Doble, K.E. (1994). Characterization and Solubilization of the FMRFamide Receptor of Squid. Biol. Bull. *187*, 185–199. https://doi.org/10.2307/1542241.

51. Chrachri, A., and Williamson, R. (2003). Modulation of spontaneous and evoked EPSCs and IPSCs in optic lobe neurons of cuttlefish *Sepia officinalis* by the neuropeptide FMRF-amide. Eur. J. Neurosci. *17*, 526–536. https://doi.org/10.1046/j.1460-9568.2003.02478.x.

52. Chrachri, A., Ödblom, M., and Williamson, R. (2000). G protein-mediated FMRFamidergic modulation of calcium influx in dissociated heart muscle cells from squid, *Loligo forbesii*. J. Physiol. *525*, 471–482. https://doi.org/10.1111/j.1469-7793.2000.00471.x.

53. Di Cosmo, A., and Di Cristo, C. (1998). Neuropeptidergic control of the optic gland of Octopus vulgaris: FMRF-amide and GnRH immunoreactivity. J. Comp. Neurol. *398*, 1–12. https://doi.org/10.1002/(sici)1096-9861(19980817)398:1<1::aid-cne1>3.0.co;2-5.

54. Henry, J., Zatylny, C., and Boucaud-Camou, E. (1999). Peptidergic control of egg-laying in the cephalopod Sepia officinalis: involvement of FMRFamide and FMRFamide-related peptides. Peptides *20*, 1061–1070. https://doi.org/10.1016/S0196-9781(99)00102-3.

55. Li, Y., Cao, Z., Li, H., Liu, H., Lü, Z., and Chi, C. (2018). Identification, Characterization, and Expression Analysis of a FMRFamide-Like Peptide Gene in the Common Chinese Cuttlefish (Sepiella japonica). Molecules *23*, 742. https://doi.org/10.3390/molecules23040742.

56. Loi, P.K., and Tublitz, N.J. (2000). Roles of glutamate and FMRFamide-related peptides at the chromatophore neuromuscular junction in the cuttlefish,Sepia officinalis. J. Comp. Neurol. *420*, 499–511. https://doi.org/10.1002/(SICI)1096-9861(20000515)420:4<499::AID-CNE7>3.0.CO;2-E.

57. Zhu, Y., Sun, L., Wu, J., Liu, H., Zheng, L., Lü, Z., and Chi, C. (2020). An FMRFamide Neuropeptide in Cuttlefish Sepia pharaonis: Identification, Characterization, and Potential Function. Molecules *25*, 1636. https://doi.org/10.3390/molecules25071636.

58. Mark, M., Rijli, F.M., and Chambon, P. (1997). Homeobox Genes in Embryogenesis and Pathogenesis. Pediatr. Res. *42*, 421–429. https://doi.org/10.1203/00006450-199710000-00001.

59. Duverger, O., and Morasso, M.I. (2008). Role of homeobox genes in the patterning, specification and differentiation of ectodermal appendages in mammals. J. Cell. Physiol. *216*, 337–346. https://doi.org/10.1002/jcp.21491.

60. Lee, P.N., Callaerts, P., de Couet, H.G., and Martindale, M.Q. (2003). Cephalopod Hox genes and the origin of morphological novelties. Nature *424*, 1061–1065. https://doi.org/10.1038/nature01872.

61. Tarazona, O.A., Lopez, D.H., Slota, L.A., and Cohn, M.J. (2019). Evolution of limb development in cephalopod mollusks. eLife *8*, e43828. https://doi.org/10.7554/eLife.43828.

62. Kawakami, K.S., Shigeru; Ozaki, Hidenori; Ikeda, Keiko (2000). Six family genes—structure and function as transcription factors and their roles in development. BioEssays News Rev. Mol. Cell. Dev. Biol. *22*, 616–626. https://doi.org/10.1002/1521-1878(200007)22:7<616::aid-bies4>3.3.co;2-i.

63. Kumar, J.P. (2008). The sine oculis homeobox (SIX) family of transcription factors as regulators of development and disease. Cell. Mol. Life Sci. CMLS *66*, 565–583. https://doi.org/10.1007/s00018-008-8335-4.

64. Weasner, B.P.; A., Jason; Kumar, Justin P. (2004). The Eye Specification Network in Drosophila. Proc. Indian Natl. Sci. Acad. Part B Biol. Sci. *B70*, 517–530.

65. Pasquale, E.B. (2005). Eph receptor signalling casts a wide net on cell behaviour. Nat. Rev. Mol. Cell Biol. *6*, 462–475. https://doi.org/10.1038/nrm1662.

66. Pasterkamp, R.J. (2012). Getting neural circuits into shape with semaphorins. Nat. Rev. Neurosci. *13*, 605–618. https://doi.org/10.1038/nrn3302.

67. Wilkinson, D.G. (2001). Multiple roles of eph receptors and ephrins in neural development. Nat. Rev. Neurosci. *2*, 155–164. https://doi.org/10.1038/35058515.

68. Xu, Q., Mellitzer, G., and Wilkinson, D.G. (2000). Roles of Eph receptors and ephrins in segmental patterning. Philos. Trans. R. Soc. B Biol. Sci. *355*, 993–1002.

69. Boycott, B.B. (1961). The Functional Organization of the Brain of the Cuttlefish Sepia officinalis. Proc. R. Soc. Lond. B Biol. Sci. *153*, 503–534. https://doi.org/10.1098/rspb.1961.0015.

70. Chichery, M.P., and Chichery, R. (1987). The anterior basal lobe and control of prey-capture in the cuttlefish (Sepia officinalis). Physiol. Behav. *40*, 329–336. https://doi.org/10.1016/0031-9384(87)90055-2.

71. Chichery, R., and chanelet, J. (1976). Motor and behavioural responses obtained by stimulation with chronic electrodes of the optic lobe ofSepia officinalis. Brain Res. *105*, 525–532. https://doi.org/10.1016/0006-8993(76)90598-9.

72. Zullo, L.S., Germán; Agnisola, Claudio; Flash, Tamar; Hochner, Binyamin (2009). Nonsomatotopic Organization of the Higher Motor Centers in Octopus. Curr. Biol. CB *19*, 1632–1636. https://doi.org/10.1016/j.cub.2009.07.067.

73. Shigeno, S., and Ragsdale, C.W. (2015). The gyri of the octopus vertical lobe have distinct neurochemical identities. J. Comp. Neurol. *523*, 1297–1317. https://doi.org/10.1002/cne.23755.

74. Buresi, A., Andouche, A., Navet, S., Bassaglia, Y., Bonnaud-Ponticelli, L., and Baratte, S. (2016). Nervous system development in cephalopods: How egg yolk-richness modifies the topology of the mediolateral patterning system. Dev. Biol. *415*, 143–156. https://doi.org/10.1016/j.ydbio.2016.04.027.

75. Endress, M., Zatylny-Gaudin, C., Leprince, J., Lefranc, B., Corre, E., Le Corguillé, G., Bernay, B., Leduc, A., Rangama, J., Mouret, L., et al. (2022). Structural and Functional Characterization of Orcokinin B-like Neuropeptides in the Cuttlefish (Sepia officinalis). Mar. Drugs *20*, 505. https://doi.org/10.3390/md20080505.

76. Pascual, N., Castresana, J., Valero, M.-L., Andreu, D., and Bellés, X. (2004). Orcokinins in insects and other invertebrates. Insect Biochem. Mol. Biol. *34*, 1141–1146. https://doi.org/10.1016/j.ibmb.2004.07.005.

77. Wang, P., Cui, Q., Zhang, Y., Wang, X., Huang, X., Li, X., Zhao, Q., Lei, G., Li, B., and Wei, W. (2021). A Review of Pedal Peptide/Orcokinin-type Neuropeptides. Curr. Protein Pept. Sci. *22*, 41–49. https://doi.org/10.2174/1389203721666201109112758.

78. Hobert, O., and Westphal, H. (2000). Functions of LIM-homeobox genes. Trends Genet. *16*, 75–83. https://doi.org/10.1016/S0168-9525(99)01883-1.

79. Albertin, C.B.; S., Oleg; Mitros, Therese; Wang, Z. Yan; Pungor, Judit R.;. Edsinger-Gonzales, Eric; Brenner, Sydney; Ragsdale, Clifton W.;. Rokhsar, Daniel S. (2015). The octopus genome and the evolution of cephalopod neural and morphological novelties. Nature *524*, 220–224. https://doi.org/10.1038/nature14668.

80. Gavriouchkina, D., Tan, Y., Ziadi-Künzli, F., Hasegawa, Y., Piovani, L., Zhang, L., Sugimoto, C., Luscombe, N., Marlétaz, F., and Rokhsar, D.S. (2022). A single-cell atlas of bobtail squid visual and nervous system highlights molecular principles of convergent evolution. Preprint, https://doi.org/10.1101/2022.05.26.490366 https://doi.org/10.1101/2022.05.26.490366.

81. Koizumi, M.S., Shuichi; Mizunami, Makoto; Tanaka, Nobuaki K. (2017). Calcium imaging method to visualize the spatial patterns of neural responses in the pygmy squid, Idiosepius paradoxus, central nervous system. J. Neurosci. Methods *294*, 67–71. https://doi.org/10.1016/j.jneumeth.2017.11.009.

82. Pungor, J.R., Allen, V.A., Songco-Casey, J.O., and Niell, C.M. (2023). Functional organization of visual responses in the octopus optic lobe. Curr. Biol. *33*, 2784-2793.e3. https://doi.org/10.1016/j.cub.2023.05.069.

83. Ahuja, N., Hwaun, E., Pungor, J.R., Rafiq, R., Nemes, S., Sakmar, T., Vogt, M.A., Grasse, B., Diaz Quiroz, J., Montague, T.G., et al. (2023). Creation of an albino squid line by CRISPR-Cas9 and its application for in vivo functional imaging of neural activity. Curr. Biol. *33*, 2774-2783.e5. https://doi.org/10.1016/j.cub.2023.05.066.

84. Crawford, K.Q., Juan Felipe Diaz; Koenig, Kristen M.;. Ahuja, Namrata; Albertin, Caroline B.;. Rosenthal, Joshua J.C. (2020). Highly Efficient Knockout of a Squid Pigmentation Gene. Curr. Biol. CB *30*, 3484-3490.e4. https://doi.org/10.1016/j.cub.2020.06.099.

85. Fiorito, G.A., Andrea; Basil, Jennifer A.;. Cole, Alison G.;. De Girolamo, Paolo; D'Angelo, Livia; Dickel, Ludovic; Gestal, Camino; Grasso, Frank W.;. Kuba, Michael J.;. Mark, Felix Christopher; Melillo, Daniela; Osorio, Daniel; Perkins, Kerry; Ponte, Giovanna; Shashar, Nadav; Smith, David D.;. Smith, Jane A.;. Andrews, Paul L.R. (2015). Guidelines for the Care and Welfare of Cephalopods in Research -A consensus based on an initiative by CephRes, FELASA and the Boyd Group. Lab. Anim. *49*, 1–90. https://doi.org/10.1177/0023677215580006.

CHAPTER V
CONCLUDING REMARKS

This dissertation dissects functional and molecular architecture of the octopus visual center – the optic lobes—and expands our knowledge regarding gene expression across the entire central nervous system in these animals. Our findings contribute to the growing field of cephalopod neuroscience by providing key resources as a foundation for future studies the anatomical, molecular, and functional underpinnings of neural circuits in this emerging model. In Chapter II, I contributed to the first optimization and application of two-photon calcium imaging in the octopus optic lobe, revealing functional organization of visually responsive units to light and dark spots of varying sizes. In Chapter III, I developed a single-cell molecular atlas of the octopus optic lobe by comprehensively analyzing RNA sequencing data and gene expression of top differentially expressed markers. By combining these two techniques, I further characterized the circuit underlying visual processing based on molecular signatures, delineating the previously identified cell types into sublaminar identities. In Chapter IV, I expanded our knowledge of the molecular architecture of the octopus central nervous system, identifying 20 lobes in this species and producing a resource outlining brain-wide gene expression for the first time in cephalopods. Together, this work characterizes the functional organization of the octopus optic lobe and the molecular architecture of the entire central nervous system, thereby facilitating our understanding of how other embodiments of advanced neural processing are achieved.

Longstanding questions about development, function, and evolution across the animal kingdom and, particularly, brain complexity, now feel more within reach due to technological advancements, such as sequencing and genetic manipulation, that have become more accessible over the last decade. For example, sequencing of the first cephalopod revealed genomic novelties, such as protocadherin expansion and active transposons, that may explain octopus "intelligence". Since then, several studies have applied RNA sequencing to further understand key molecular players involved in brain organization in these complex organisms[2–5]. For example, our investigation into the octopus visual system both confirmed expression of neurotransmitters previously identified to be present in the retina and optic lobe of octopuses as

well as characterized new immature neuronal subtypes that may give rise to these mature neuronal classes based both on sequencing data and on spatial expression patterns[2]. Despite the efforts here that progress our understanding of cephalopod brain complexity, there remains a significant gap in bridging molecular signatures with functional response properties at single-cell resolution – a technique that has the potential to transform the field of cephalopod neuroscience by revealing how circuits form and function with greater resolution. For example, while our work using calcium imaging revealed retinotopic organization as well as differential responses to light and dark spots[6], our approach to labeling units limits our ability to uncover functional diversity underlying that could be dissected if we had the ability to label individual cells or, better yet, target cells based on genes of interest. Lastly, our work in analyzing gene expression beyond the optic lobe revealed striking patterns in neuropeptides as well as ephrin and semaphoring signaling molecules across central brain structures. However, this resource could be enhanced by including either serial sagittal sections or accompanying segmentation data of a 3D brain. It is critical to continue investigating cell types in the octopus brain, using complementary techniques of morphology or synapse tracing, spatial transcriptomics at different developmental stages, and functional imaging to dissect neural circuits involved in complex behaviors; nevertheless, this thesis serves as a roadmap for such explorations.

References

1. Albertin, C.B.; S., Oleg; Mitros, Therese; Wang, Z. Yan; Pungor, Judit R.;. Edsinger-Gonzales, Eric; Brenner, Sydney; Ragsdale, Clifton W.;. Rokhsar, Daniel S. (2015). The octopus genome and the evolution of cephalopod neural and morphological novelties. Nature *524*, 220–224. https://doi.org/10.1038/nature14668.

2. Songco-Casey, J.O., Coffing, G.C., Piscopo, D.M., Pungor, J.R., and Kern, A.K. (2022). Cell types and molecular architecture of the Octopus bimaculoides visual system. Curr. Biol. CB *32*, 5031-5044.e4. https://doi.org/10.1016/j.cub.2022.10.015.

3. Styfhals, R.Z., Grygoriy; Hulselmans, Gert; Spanier, Katina I; Poovathingal, Suresh; Elagoz, Ali M; De Winter, Seppe; Deryckere, Astrid; Rajewsky, Nikolaus; Ponte, Giovanna; Fiorito, Graziano; Aerts, Stein; Seuntjens, Eve (2022). Cell type diversity in a developing octopus brain. Nat. Commun. *13*, 7392-NA. https://doi.org/10.1038/s41467-022-35198-1.

4. Duruz, J.S., Marta; Kaldun, Jenifer C; Al-Soudy, Al-Sayed; Lischer, Heidi E. L; van Geest, Geert; Nicholson, Pamela; Bruggmann, Rémy; Sprecher, Simon G. (2023). Molecular characterization of cell types in the squid Loligo vulgaris. eLife *12*, NA-NA. https://doi.org/10.7554/elife.80670.

5. Gavriouchkina, D., Tan, Y., Ziadi-Künzli, F., Hasegawa, Y., Piovani, L., Zhang, L., Sugimoto, C., Luscombe, N., Marlétaz, F., and Rokhsar, D.S. (2022). A single-cell atlas of bobtail squid visual and nervous system highlights molecular principles of convergent evolution. Preprint, https://doi.org/10.1101/2022.05.26.490366 https://doi.org/10.1101/2022.05.26.490366.

6. Pungor, J.R.A., V. Angelique; Songco-Casey, Jeremea O; Niell, Cristopher M. (2023). Functional organization of visual responses in the octopus optic lobe. Curr. Biol. CB *33*, 2784-2793.e3. https://doi.org/10.1016/j.cub.2023.05.069.